The Thesis Committee for Kenneth Stanley Bostwick
Certifies that this is the approved version of the following thesis:

Experimental Study of Impact Loading on Negative Stiffness Structures

APPROVED BY
SUPERVISING COMMITTEE:

Supervisor: _____
Carolyn C. Seepersad

Co-supervisor: _____
Michael R. Haberman

_____
Preston S. Wilson

Experimental Study of Impact Loading on Negative Stiffness Structures

by

Kenneth Stanley Bostwick, B.S.

Thesis

Presented to the Faculty of the Graduate School of

The University of Texas at Austin

in Partial Fulfillment

of the Requirements

for the Degree of

Master of Science in Engineering

The University of Texas at Austin

May 2015

Dedication

To Lyndsi and Linden, my pride and joy.

Acknowledgements

I would like to express my appreciation for all who participated in this thesis process; it has been a valuable learning experience. Like any life endeavor, there have been many who have contributed to the success and project completion, and I am grateful for every supporter.

Thank you to my three academic advisors, Dr. Carolyn Seepersad, Dr. Michael Haberman, and Dr. Preston Wilson. I appreciate the support that was given through advisement and brainstorming. I particularly am grateful for the trust they placed in me to share a part of their research and work.

A special thanks to others who provided support with testing and resources. Sergio Cortes and Dr. Desiderio Kovar gave valuable assistance for quasi-static testing. Thank you to Dixon Correa with whom I frequently collaborated and exchanged important results. Lastly, thank you to all my lab mates who kept the process light and enjoyable.

KENNETH STANLEY BOSTWICK

Abstract

Experimental Study of Impact Loading on Negative Stiffness Structures

Kenneth Stanley Bostwick, M.S.E.

The University of Texas at Austin, 2015

Supervisors: Carolyn C. Seepersad, Michael R. Haberman

This work outlines the design of a drop testing apparatus and the use of the apparatus to perform impact tests on negative stiffness honeycomb structures. Negative stiffness beams are non-linear spring elements that can be used to absorb energy. When prefabricated negative stiffness beams are arranged together in a periodic pattern they create an energy absorbing honeycomb material that can recover from large deformations. Negative stiffness honeycombs have been shown to function similarly to regular honeycombs during quasi-static loading, but are largely untested for impact loading. Two types of honeycomb designs—referred to as vertical and horizontal arrays—have been designed and fabricated to experimentally determine their performance when subjected to impact loading. The performance of each array is compared using finite element models (FEM), quasi-static tests, and drop tests. A drop test apparatus is constructed to perform the impact testing, by measuring the acceleration profile of a mass released from variable drop heights. Results indicate that vertical and horizontal honeycombs reduce accelerations by at least 85 percent when compared to impact without the presence of a honeycomb.

Table of Contents

List of Tables

List of Figures

Chapter 1: Introduction

1.1 MOTIVATION

Many engineering applications are faced with the need to absorb undesired impact accelerations and oscillatory vibrations. Unwanted machinery accelerations often cause undesirable manufacturing defects and poor part tolerances; similarly unwanted accelerations in devices or machines that interface with humans can result in negative health effects. Spring and damper elements are often utilized to address vibration isolation problems and reduce accelerations. Spring and damper elements can take many forms which are specific to each application. For example, car suspensions usually implement traditional metal springs and hydraulic damping pistons, whereas athletic helmets utilize air filled "pillows" that act as both spring and damping elements to reduce forces on the head during impact.

Although linear springs are typically used in suspension or shock absorbing systems, they have significant limitations as a result of undesirable tradeoffs between stiffness, transmitted force (or acceleration), and energy absorption. Springs with low stiffness provide a "soft feeling" but require very large displacements to absorb significant amounts of impact energy or to support high input forces. In contrast, springs with high stiffness often require very high input forces to absorb equivalent amounts of energy, resulting in very large transmitted forces and accelerations and potential damage or injury. An ideal system would have the capability to provide high levels of stiffness and impact energy absorption with limited transmitted force or acceleration. This behavior is achievable with non-linear negative stiffness (NS) elements, which show significant promise to absorb large amounts of energy when impact loaded, while still displaying high stiffness in the unloaded state [1].

Negative stiffness elements can be realized by employing transversely loaded buckled beams as passive non-linear springs. A NS buckled beam is a beam element which is loaded axially until the beam buckles or deforms into a curved state. Figure 1.1 displays a beam which is first buckled by axial force *P*. After the beam is buckled, the axial force *P* ideally becomes a rigid beam end constraint, and then the beam is loaded with a transverse force represented by F_t.

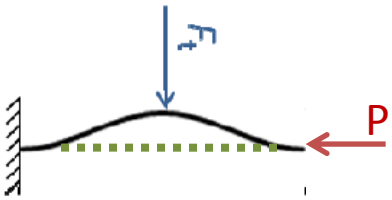

Figure 1.1: Illustration of bi-stable buckled beam with axial end constraint *P* and transverse load F_t. The green dotted line represents the axis of the beam before buckling occurs.

During transverse loading, a NS buckled beam exhibits different levels of stiffness, depending on the amount of transverse displacement. The response of the beam to transverse loading is captured by the force-displacement curve shown in Figure 1.2. Initially the beam has a positive stiffness (up to point 1), where for monotonically increasing transverse displacement, the transverse force responds by increasing. When the controlled displacement of the beam reaches point 1, the beam forces respond with a "snap-through," the force begins to decrease, and the beam deforms from the original buckled shape. The point 1, or initiation of NS beam "snap-through" occurs at the peak transverse force, also known as the NS beam force threshold. After beam "snap-through," the beam experiences negative stiffness as seen from point 1 to 3, where for increasing transverse displacement, the transverse force decreases. During the 1 to 3 phase, the beam displacement continues past the beam axis (see green line in Figure 1.1) which is

represented by point 2. When the transverse displacement reaches point 3, the NS beam approaches a second point of bi-stability and any additional displacement is again associated with positive stiffness.

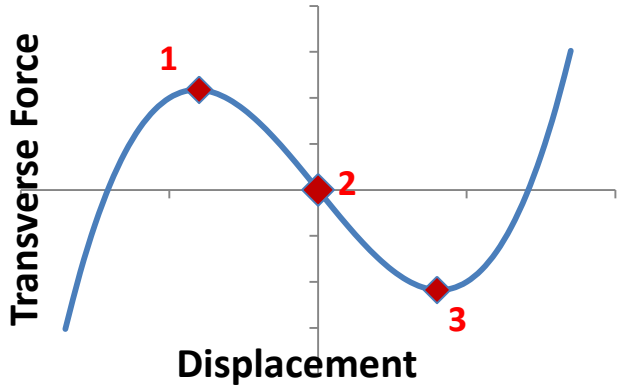

Figure 1.2: Illustration of NS beam element force-displacement plot. Point 1 represents beam "snap-through," point 2 corresponds with crossing beam midpoint, and point 3 represents lower stage stability.

In many applications, NS beams are used in parallel with a linear spring [2]. When a NS beam is used in parallel with an appropriately sized linear spring, the resultant force-displacement curve is slightly altered and the negative stiffness region is replaced by quasi-zero stiffness (i.e. a region of displacements with constant force levels) as a result of the added stiffness between the NS beam and positive stiffness linear spring. The resulting quasi-zero stiffness region seen in Figure 1.3 creates a constant force plateau where the area underneath the curve represents the energy absorbed by the NS beam and parallel linear spring. A longer quasi-zero stiffness region yields a higher amount of energy absorption.

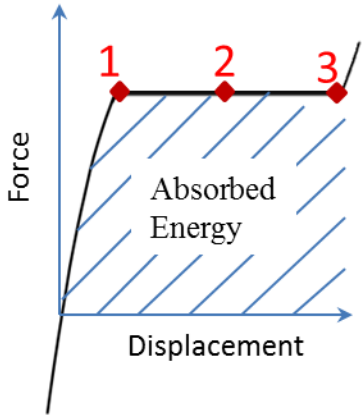

Figure 1.3: Illustration of force-displacement plot of NS beam in parallel with linear spring.

By manipulating beam geometry, NS beams can be designed to achieve specific force threshold values and displacement ranges at that force threshold and thus different beams can be tailored to absorb different amounts of energy. Using many NS beams in parallel and series can create a profile of energy absorbing capacities. One way to combine NS beams is into a honeycomb array as shown in Figure 1.4.

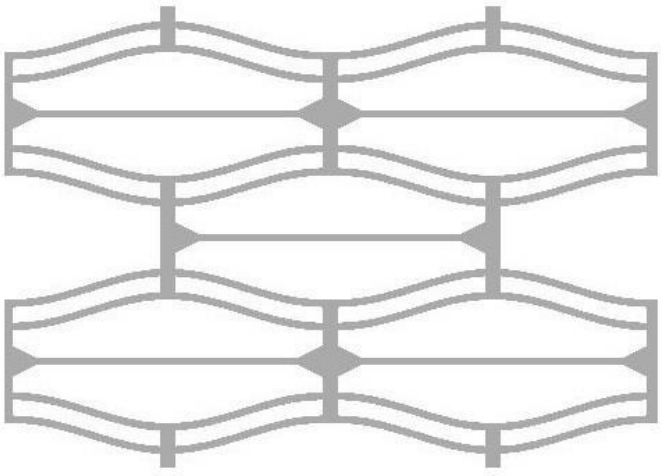

Figure 1.4: NS honeycomb array as implemented by Correa *et. al* [3].

While NS beam use is no longer an entirely novel concept [4], the use of many NS beams to construct a honeycomb lattice is very unique and thus-far an untested configuration for impact management. It is therefore of high interest to explore NS honeycomb structures under both quasi-static and dynamic loading conditions to achieve a better understanding of the capabilities of these types of honeycomb structures.

1.1.1 Honeycomb arrays of NS elements

Honeycomb arrays are advantageous in that they are generally lightweight and easily adaptable to most situations. Honeycomb structures can be composed from periodic unit cells that range from square to hexagonal with many combinations in between depending on the specific application.

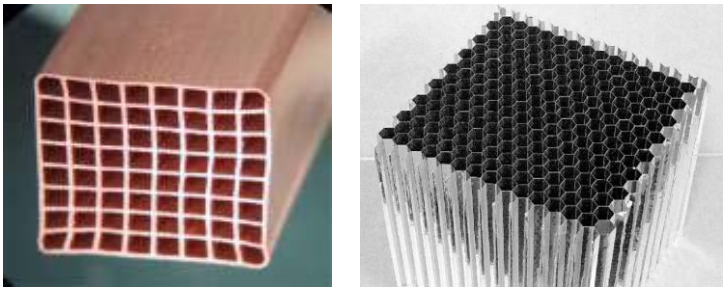

(a) (b)

Figure 1.5: Examples of honeycomb structures with a) square and b) hexagonal unit cells. Figures adapted from [5] and [6].

Honeycombs are extremely effective energy absorbers when plastically deformed [7]. The energy absorption capacity of a honeycomb is described by its elastic-plastic stress-strain relationship when subjected to compressive loading. Figure 1.5(a) displays the representative behavior of a honeycomb structure when subjected to a load that crushes the material. At low stress levels, the structure exhibits linear elasticity and a region of high stiffness as seen in the first image of 1.5(b). When stresses in solid

portions of the honeycomb structure reach the yield stress of the constituent material, they plastically deform and unit cells collapse shown in the second image of Figure 1.5(b). This collapse results in large deformations at nearly uniform stress levels. The plateau region indicated in Figure 1.5(a) is a result of this process propagating throughout the honeycomb. Once all of the unit cells have collapsed as in fourth image of Figure 1.5(b), the walls of the honeycomb are in contact and there is a rapid increase in stress with increasing imposed deformation. This region is known as densification.

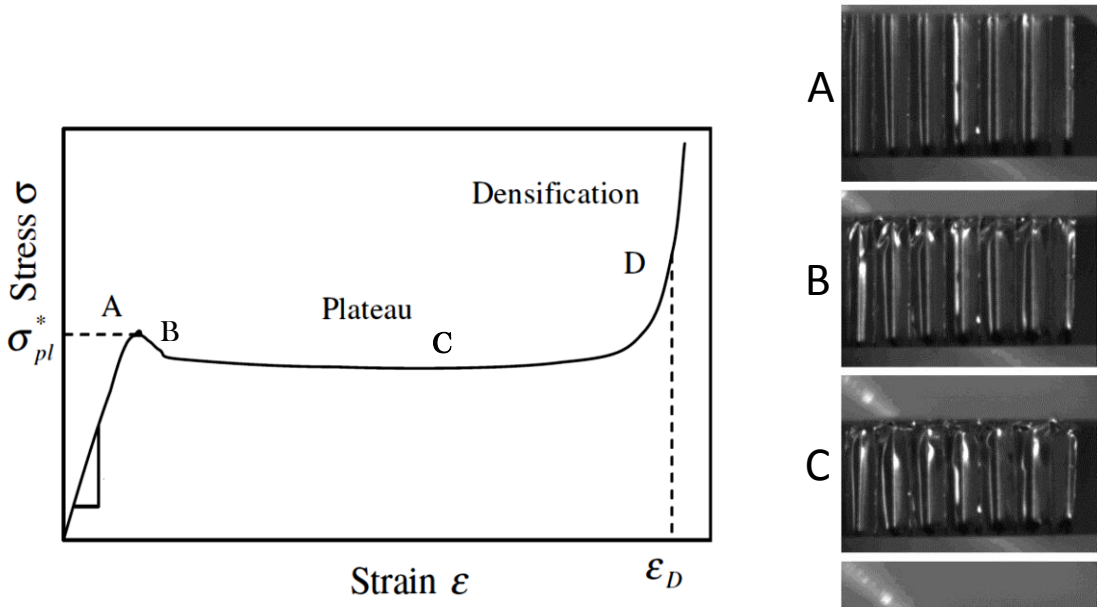

(a)

(b)

Figure 1.6: (a) Honeycomb relationship for stress-strain with (b) corresponding images at each stage of compression for a quasi-statically loaded honeycomb. Figures adapted from [8] and [9].

As seen in the illustration in Figure 1.6, solid materials and linear springs typically experience higher stress for similar strain as compared to honeycombs and are

more prone to yield without a significant plateau stress region. The extended plateau region is an advantage for honeycomb structures and enables them to be nearly-ideal impact absorbers because they absorb energy at relatively constant plateau stress. With a large constant stress region, the honeycomb is able to absorb a near maximum amount of energy for a specific force threshold, generally twice the amount a solid material can absorb [3].

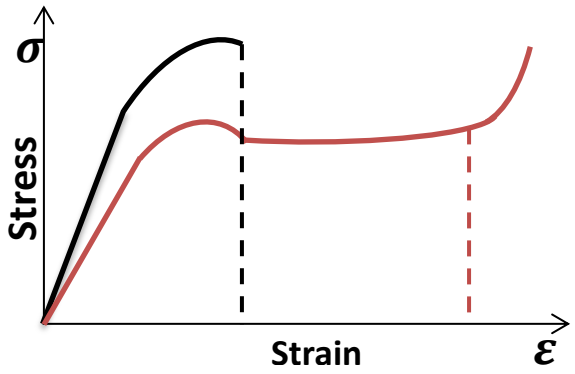

Figure 1.7: Comparative relationship between solid material or linear spring compression (black) and honeycomb compression (red).

All the above properties and advantages are inherent for any honeycomb structure including crushable foams, and various structural arrays. Unfortunately, the greatest limitation of a honeycomb structure is that once it has been crushed, it cannot be re-used. When a honeycomb enters the plateau region during impact, the cell walls plastically deform and that deformation cannot be recovered.

To utilize the positive properties of honeycomb elements in a more reusable form, Klatt *et. al* [3] introduced the idea of using negative stiffness beam elements collectively

as unit cells in honeycomb arrays. The advantage of incorporating NS beams into a honeycomb unit cell is the ability to have a "crushable" object that returns to its original shape and is readily reusable. NS beam elements enable high levels of initial stiffness, similar to the elastic deformation region for a regular honeycomb, followed by a nearly constant stress region in which the NS elements "snap through" due to localized buckling without experiencing permanent plastic deformation.

Correa *et. al* [3] have expanded the knowledge of NS honeycomb arrays by investigating the design space of NS honeycombs through a detailed investigation of analytical and finite element models and comparison with quasi-static experimental results. The work described in references [3] and [4] thus provide detailed information about high potential for absorbing mechanical energy using arrays of NS elements for use in applications like helmets and automotive bumpers. However, to date no experimental efforts have been made to evaluate the response of these structures when subjected to dynamic loading, which would be the primary application area for this unique structure. The work of this thesis therefore aims to address this gap in knowledge on the performance of NS honeycomb structures.

1.2 GOALS

Due to the positive engineering qualities of honeycomb structures, there is a large range of potential applications for honeycomb structures as impact-mitigating elements. With the relative ease of designing and manufacturing complicated geometric structures using additive manufacturing processes, the complicated geometry of NS beam elements can be incorporated into the honeycomb unit cell, and the honeycombs can be fabricated in either perfectly periodic or non-uniform arrangements. To target these applications,

however, it is important to understand the dynamic, high strain rate properties of NS honeycombs.

The purpose of this thesis is twofold:

1. The first and most pertinent goal was to investigate the general ability of NS honeycomb structures to mitigate impacts. The current understanding of NS honeycomb arrays is limited to performance under quasi-static loading conditions. While this knowledge is important, it does not speak fully to the capacity of NS honeycombs under realistic impact situations. Thus, dynamic testing of NS honeycomb arrays is necessary to understand their performance more fully. This goal has been accomplished by designing and building a drop test apparatus, and by using the apparatus to evaluate the honeycomb arrays under impacts. Performance of the NS honeycomb specimens is quantified by comparing the impact acceleration of a falling mass with and without the samples in place.
2. The second objective of this thesis was to develop and analyze the effectiveness of horizontal NS honeycomb arrays in addition to the vertical NS honeycomb arrays explored in complimentary research. The horizontal NS honeycomb array is intended to make the NS honeycombs more suitable for applications with limited vertical space. The effectiveness of the horizontal NS honeycomb array is compared to that of the vertical array geometry.

1.3 OVERVIEW

This thesis describes the research performed in pursuit of the two goals described in Section 1.2. The second chapter is reserved for further review of the science and

engineering associated with NS honeycomb elements. It presents a literature review that highlights NS elements, honeycomb structures, and strain rate effects. The third chapter introduces the design and functionality of the impact apparatus for dynamic honeycomb array testing. This chapter seeks to explain some of the intricacies of the testing apparatus design and its limitations. The fourth chapter presents the design of the horizontal NS honeycomb arrays and their comparison to the vertical arrays. Additionally this chapter further quantifies the comparison of design concepts through FE analysis. The fifth chapter expounds on the horizontal arrays and their performance under quasi-static loading in comparison to vertical arrays. The quasi-static or low strain rate comparison helps to set up the results of the dynamic testing. The sixth chapter provides a detailed summary and analysis of dynamic high strain-rate testing conducted on NS honeycomb. The final results quantify acceleration absorption capabilities of the two design concepts explored in this work. Finally, the seventh chapter concludes the work by summarizing the results and suggesting future work.

Chapter 2: Previous Work

2.1 NEGATIVE STIFFNESS BEAMS

2.1.1 Pre-compressed buckled beam

A buckled beam is a straight, slender structural element that has been loaded along its axis until it is no longer in static equilibrium without undergoing some transverse deformation [5]. When the axial load exceeds the buckling limit, the beam will exhibit some transverse curvature corresponding to a new, higher energy, equilibrium configuration. The specific buckled shape depends on the end-conditions of the beam (*i.e.* clamped, pinned, *etc.*) [10]. After buckling, the beam can be used as a spring element by placing transverse load F_t orthogonal to the initial buckling load P as seen in Figure 1.1.

The transversely loaded, displacement controlled, buckled beam undergoes three distinct deformation regions [11] which are shown visually in Figure 2.1. First, the beam maintains a buckled beam curve while the transverse displacement is less than the beam force threshold displacement, which is known as the first mode of beam buckling. Second, when the transverse displacement begins to exceed the force threshold displacement, the beam "snaps" and changes from a first mode buckled shape to a second mode buckled shape. For minimally buckled beams, the beam will continue in a second mode shape as seen in Figure 2.1(b). Third, as the transverse displacement extends beyond the negative stiffness region, the beam assumes another first mode buckled shape. This concept is further discussed detailed by Fulcher [1].

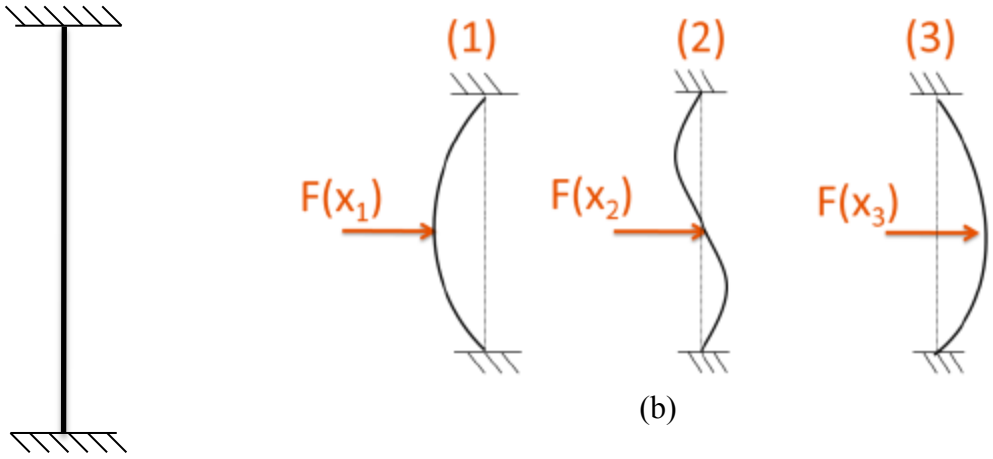

Figure 2.1: Illustration showing a (a) strait, slender beam prior to buckling and the (b) three bending modes of a buckled beam during transverse loading. Figure adapted from [1].

The bending modes of a pre-compressed buckled beam can be employed to assist in the energy absorbing process. When a beam is in either first or third position as identified in Figure 2.1(b), the beam is set in one of the bi-stable configurations. While in one of these stable configurations, the beam is stiff in the transverse direction. In contrast, after the transversely loaded beam has transitioned from first to second buckled mode, the beam exhibits negative stiffness. Negative stiffness (NS) is when an element offers decreasing resistance for an applied force as opposed to a positive stiffness element which offers increasing resistance for an applied force. In many cases NS elements can even assist the applied load. During the negative stiffness region of a buckled beam, the center of the beam passes through the original beam axis identified by position two in Figure 2.1(b). Each of the three deformation phases is labeled in the force-displacement diagram, Figure 2.2, where the NS region is clearly identified by the negative slope. The NS beam curve is shown compared to an unbuckled beam force-displacement plot in

Figure 2.2. The unbuckled beam has properties similar to a linear spring where the stiffness is always positive.

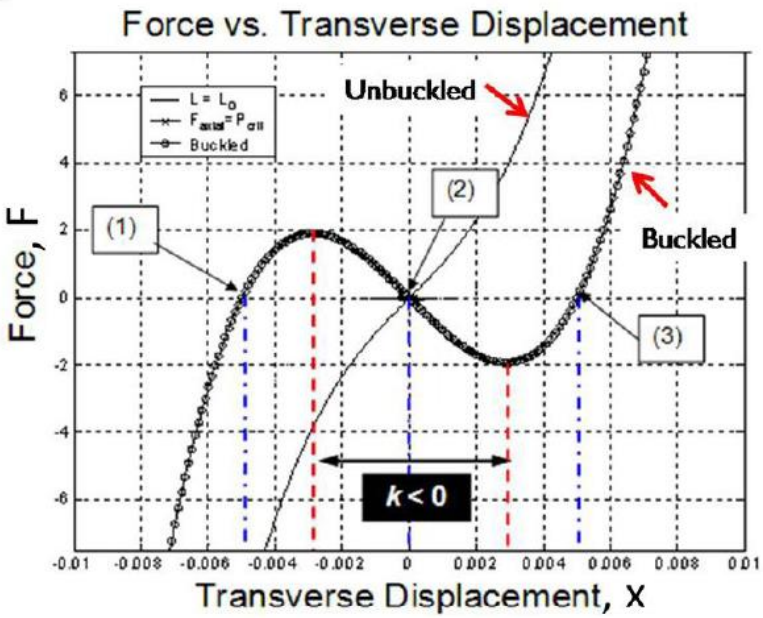

Figure 2.2: Comparison of linear (unbuckled) to non-linear (buckled) stiffness. Figure adapted from [2].

Engineering application of NS beams requires intuition of a beam's force threshold and full beam displacement, which can be found from the force-displacement plot. Previous authors have developed models that mimic the force displacement response of a pre-compressed NS beam. As introduced in the work of Albuzhev [11] and derived by Fulcher [1] for the pre-compressed beam, the transverse displacement u_y on the beam can be used to determine the corresponding transverse force F_t

$$F_t(u_y) = \frac{2\pi^4 EI}{l_0^3}\left[\left(1 - \frac{u_x}{u_{x,cr}}\right)u_y + \frac{A}{16I}u_y^3\right] \tag{2.1}$$

This mathematical model provides for easier augmentation of beam properties in order to tailor a NS beam for known input force for most efficient energy absorption.

2.1.2 Prefabricated curved beam

The ideal NS beam as has been discussed in Section 2.1.1 has good capabilities for transverse force mitigation, but it is very difficult to implement within a honeycomb application. A structure of this sort would require initial pre-compression followed by sufficient end force constraints during use and therefore be very impractical for most applications. For some time MEMS devices have used NS beams that are fabricated in a curved form as mechanical switching elements [4]. A prefabricated curved beam is manufactured in a shape resembling the curvature associated with the first mode of beam bending. Because the beam is fabricated in this way neither pre-compression nor end forces are necessary to maintain the shape of the beam when transverse loads are absent. However, rigid end conditions are still required to obtain the desirable transverse force-displacement behavior described in the Section 2.1.1.

Prefabricated curved beams behave similarly to pre-compressed NS beams in that they transition from one curved shape which resembles the first mode of bending to an opposite curved shape. However, the prefabricated beam differs from pre-compressed beams in that they are not necessarily bi-stable mechanisms because they are originally fabricated in a stable curved shape. The application of transverse force to prefabricated beams creates a similar force-displacement plot to Figure 2.2, but upon release of the transverse force, the beam "snaps-back" and returns to the original prefabricated curved shape without the necessity of a parallel linear spring as studied by Fulcher *et. al* [2]. Klatt *et. al* [3] investigated the effects of beam geometry on the prefabricated beam negative stiffness and "snap-back" response. The parameter Q introduced by Qiu *et. al*

represents the ratio of the curved beam height to its thickness, and was found to be very important in determining the presence of a NS region in the beam force-displacement plot [12]. For the geometry shown in Figure 2.3(a), the value of Q directly influences the constant force plateau value as seen in Figure 2.3(b).

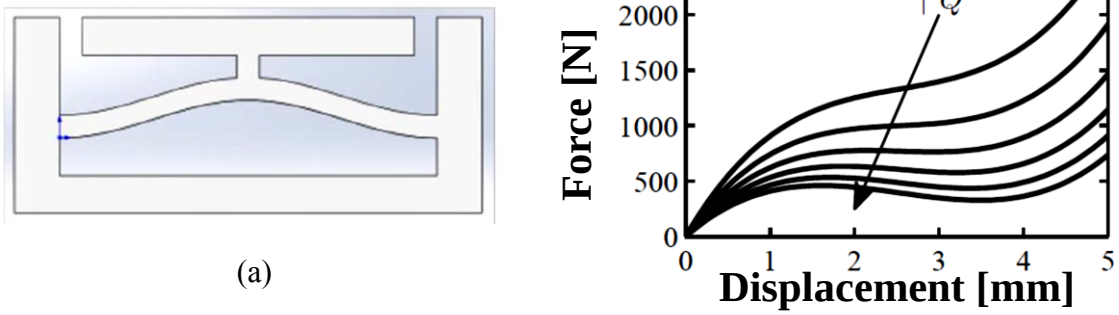

(a) (b)

Figure 2.3: (a) Design geometry of a curved NS beams used in testing. (b) The relationship force-displacement as related to Q = height/thickness. Figure adapted from [3].

As previously noted, constant boundary conditions are important to the success of the prefabricated curved beam during loading, which is similar to the importance of the axial buckling force for a pre-compressed beam. In the case where the beam end points are not sufficiently rigid, the force-displacement behavior of the bending beam is altered due to the change in beam length during compression. As the beam length increases during compression, the maximum force decreases, and the result is less efficient energy absorption. Klatt *et. al* [3] analyzed the effects of end conditions by comparing the forces seen experimentally during deflection of the curved beam compared to forces predicted by FEA. Figure 2.4 plots the discrepancy between model and experiment for both rigid

and free end conditions. One observes a marked difference in behavior between the models for rigid end conditions in both FE and experimental results.

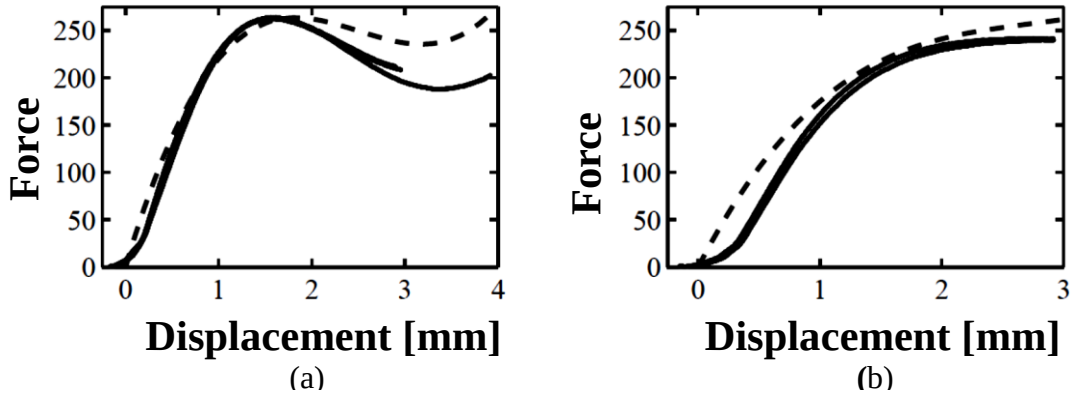

Figure 2.4: Force-displacement comparison for loading of prefabricated curved beam given (a) rigid end conditions and (b) free end conditions. Experimental results shown with solid lines and FE model results indicated by the dotted lines. Figure adapted from [3].

For prefabricated buckled beams, high levels of negative stiffness and force threshold can be difficult to achieve with a single beam because it twists into second mode buckling as illustrated in Figure 2.1(b). In order to obtain high levels of negative stiffness, it is necessary to restrict the second mode of beam bending. Qiu and others present the idea of using two pre-buckled beams in parallel that are connected at the midpoint by a thin orthogonal element [12-14]. Qiu *et al*. proved how the use of two concentric beams, which are coupled at the midpoint, provide for the ability to cancel the second mode and twisting mode while still maintaining snapback properties without an axial pre-stress [12]. Figure 2.5 is an illustration of the comparison between single beam and double beams which correspond with second and third mode bending respectively.

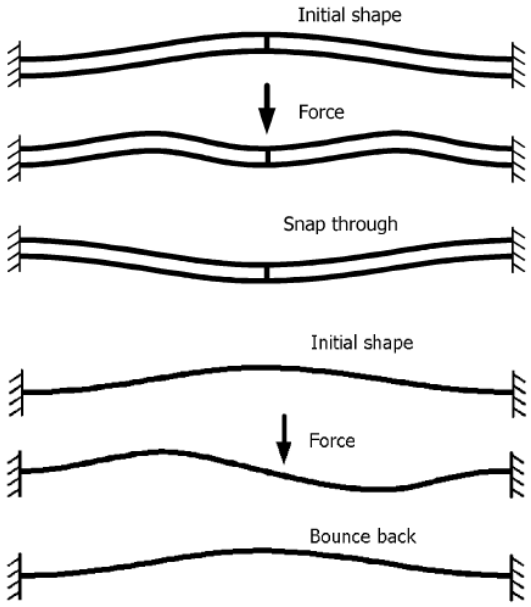

Figure 2.5: Representation of advantageous double beam concept. Figure adapted from [12].

For the case where the second bending mode is restricted, the NS beam will transition from first to third bending mode directly. In order to maintain this first-third-first mode transition, proper constraints are needed at both the beam midpoint and end points, or a second mode bended shape results and the beam force threshold will be decreased. With the double beam structure, the prefabricated beams can be designed to yield either bi-stable or mono-stable response according to the application need.

2.2 NEGATIVE STIFFNESS HONEYCOMB STRUCTURES

Honeycomb structures provide excellent capabilities for energy absorption during impact loading situations. As previously discussed in chapter 1, honeycomb elements are able to maintain a constant stress over a range of strain as a result of the collapsing elements within the honeycomb structure. The creation of a honeycomb structure using

mono-stable NS beam elements permits a design structure that has a nearly-constant stress plateau, as is the case for traditional honeycombs, but with the additional attribute of recovering from large deformations [15].

To test the capacity of NS honeycomb structures, Correa *et. al* [3] fabricated a NS honeycomb with a unit cell made of two double beam elements built together as seen in Figure 2.6(a) This unit cell was multiplied to create a full honeycomb structure as seen in Figure 2.6(b).

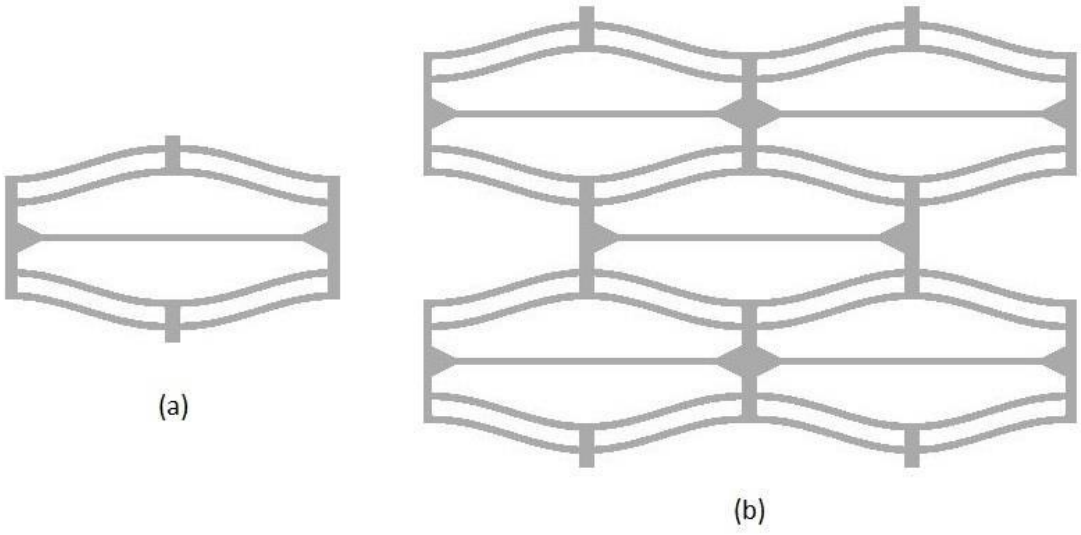

Figure 2.6: NS honeycomb structure. Figure adapted from [3].

Correa further expanded on the NS honeycomb design by outlining design guidelines for the beam elements. Utilizing the properties of NS beams, the NS honeycomb retains its initial shape until the input force reaches the force threshold of a row of cells. The force threshold can be tailored through the geometry of the beams in an individual unit cell. Once the force threshold for a row of cells is reached, the unit cells in that row will collapse as the beam elements snap into the alternate first-mode buckled position. Similarly, the rest of the honeycomb collapses row-by-row until *i*) the structure

fully densifies, *ii*) the applied load is removed, or *iii*) the energy of the loading mechanism is fully absorbed. Figure 2.7 shows FE results illustrating the snap through process of a NS honeycomb array.

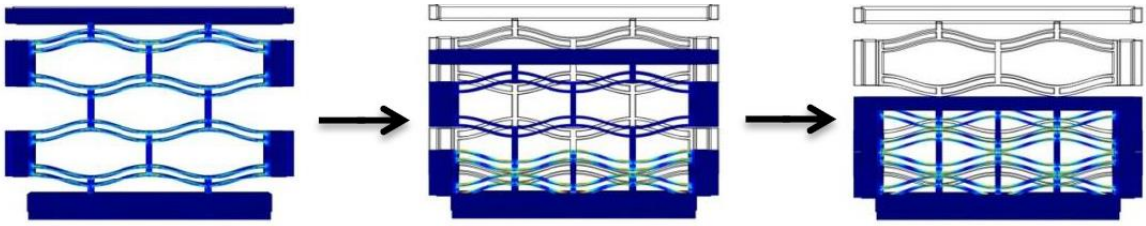

Figure 2.7: NS honeycomb structure during transverse displacement or compression. Figure adapted from [3].

Correa *et. al* also evaluated NS honeycomb performance by analyzing the force-displacement curves of the structure. As a NS honeycomb receives an input transverse force, the corresponding compression or displacement is measured. For honeycomb structures without NS elements, force-displacement analysis provides one curve reflecting only the compression of the honeycomb. Because properly designed NS honeycomb arrays are recoverable, the honeycomb experiences the full range of displacement twice, once during compression, and then again when the load is removed. This behavior is shown in the modeled and measured force-displacement plots in Figure 2.8 [3]. The full loading and unloading path shown in the experimental results, obtained under quasi-static displacement controlled loading, displays a significant hysteresis. The upper portion of the curves represents the honeycomb compression and the lower portion represents the unloading. Each peak represents the "snap-through" behavior of one layer of the NS honeycomb.

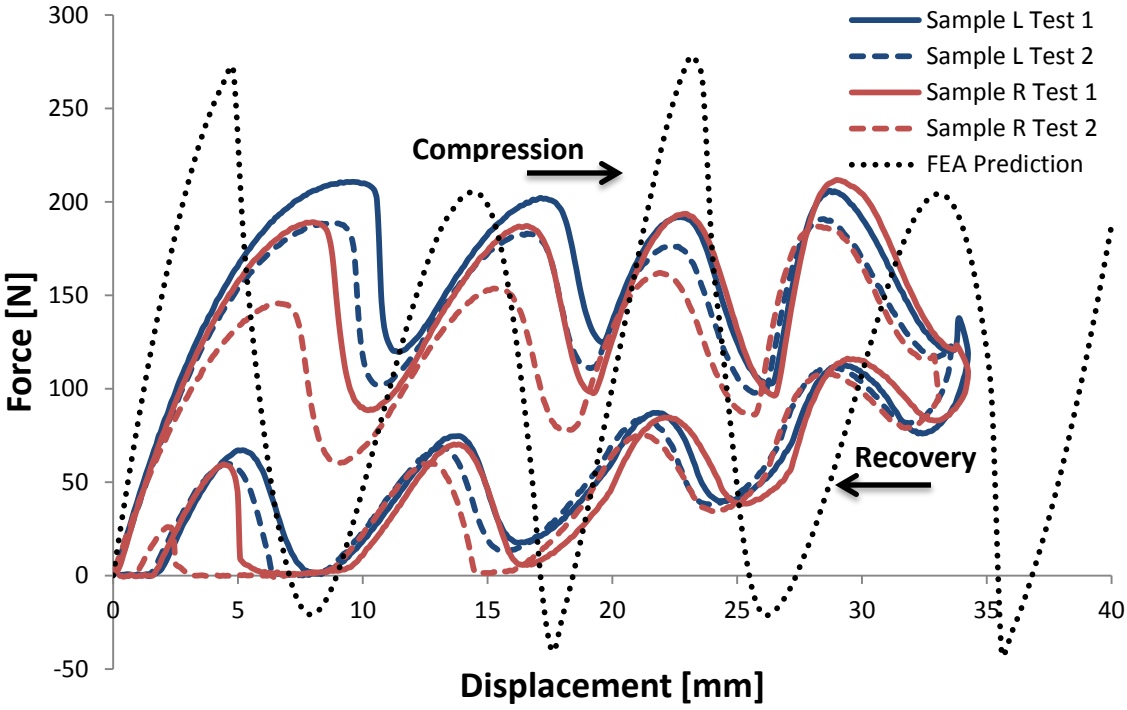

Figure 2.8: Experimental force-displacement data of NS honeycombs under quasi-static loading. Each data cycle represents compression and recovery. Figure adapted from [3].

Energy absorbed by any structure is the energy under the force-displacement curve upon loading and unloading. For honeycombs that crush un-recoverably, the energy absorbed is simply the area under the curve on the loading cycle. For recoverable NS honeycombs, energy absorption is calculated through both loading and unloading. The NS honeycomb net energy absorbed is the area of the force-displacement hysteresis. Results of the discussed NS honeycomb will be used in Section 5.2.3 for comparison purposes, and will not be discussed further in this chapter.

Force-displacement curves for honeycomb arrays are useful to evaluate the effectiveness of the array for both quasi-static and dynamic loading. Unfortunately, obtaining force-displacement curves for dynamic loading is difficult and quasi-static

loading does not fully quantify the energy absorptive capabilities of a NS honeycomb when subjected to impact loads, primarily due to strain-rate dependent materials properties, which will be discussed in Section 2.3.

2.3 BEAM STRAIN AND STRAIN RATE

2.3.1 Stress and strain

A negative stiffness element experiences deformations that lead to an overall strain on the element. Axial strain along the x-direction, ε_x, is defined as the gradient of the deformation in the x-direction, $\varepsilon_x = \partial u_x / \partial x$. For many engineering applications where uniaxial strain is observed this is often approximated as the ratio of the elongation of an infinitesimal element relative to the initial element length

$$\varepsilon_x \approx \frac{\Delta l}{l_0} \tag{2.2}$$

While this metric effectively captures the strain of a monolithic object, the strain experienced by the material at different locations within the NS honeycomb requires additional development. In general, the spatial dependence of strain in the NS honeycomb depends on the geometry and loading of a test piece and can only be accurately addressed using an appropriately benchmarked FE model. To approximate the strain at specific locations however, it is possible to develop simplified analytical models that help guide the design and analysis of NS honeycombs.

Euler-Bernoulli beam theory allows the approximation of the strain orthogonal to the transverse displacement at an arbitrary position along the thickness of a bending beam of constant rectangular cross-section [16]. For Euler-Bernoulli beam bending the simplified expression for the strain ε

$$\varepsilon = \frac{z}{\rho} \tag{2.3}$$

is the ratio of the distance, z, to the point of interest from the central axis of the beam relative to the radius of curvature, ρ, as shown in Figure 2.9 [17]. Maximum strain occurs on the exterior of the beam where z is equal to half of the beam thickness. In this case strain is considered tangential to the bended beam.

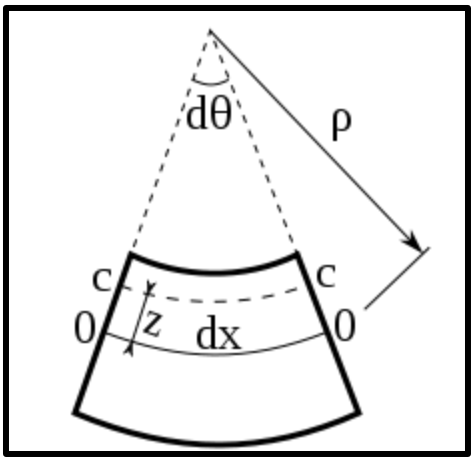

Figure 2.9: Illustration of beam in deformation and strain variables.

Strain is important to study due to the constitutive relationship between engineering stress σ and strain ε which is linearly related by material modulus of elasticity Y

$$\sigma = Y\varepsilon \tag{2.4}$$

An understanding of strain, in particular maximum strain that a beam element experiences during loading, allows the engineer to estimate the stresses experienced by the beam. The stress levels can then be compared to known elastic and ultimate strength limits of the materials used to fabricate a NS honeycomb, and give insight as to proper constraints when designing NS beam elements.

Using the basic intuition gained about strain within bending beams, these equations and knowledge can be applied to the double beam prefabricated NS elements.

For idealized beam deformation due to transverse loading, meaning no warping or shear modes, the Equations 2.3 and 2.4 can be utilized to estimate the maximum stress/strain that an NS element would experience during the snap-through process. During bending of beams with a low slenderness ratio, the distance z does not change, and thus the only the radius of curvature will be altered as the NS honeycomb deforms. As has been previously discussed, the beam transitions from first to third mode of bending. The radius of curvature in the "third mode" can be significantly less than that present in the "first mode," as indicated by Figure 2.10. Equation 2.3 predicts therefore that the strain will increase during this transition and that the maximum strain would occur during snap-through events.

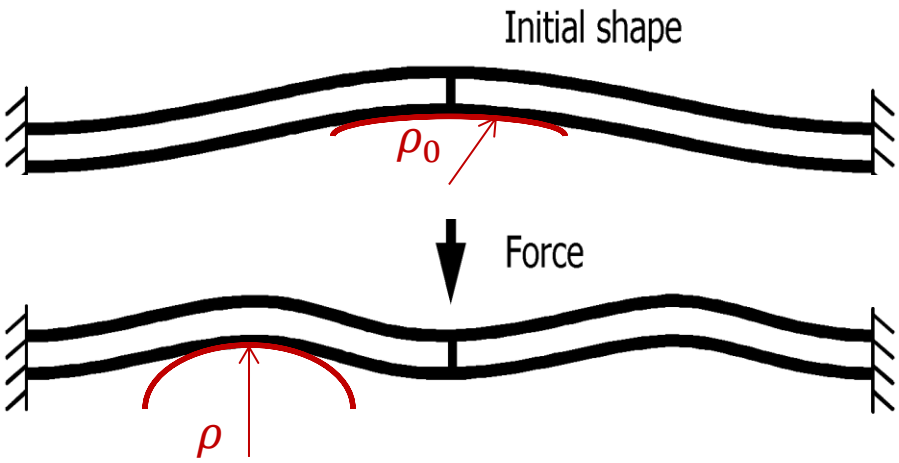

Figure 2.10: Illustration of the change in radius of curvature during beam deflection. Figure adapted from [12].

2.3.2 Strain Rate

Significant to the evaluation of stress a NS beam experiences during a snap through process is the rate at which the constitutive material is strained. The deformation rate in the material is a function of transverse velocity at the center NS beam when

subjected to a time-dependent transverse force. As the velocity increases so does the rate at which material deformation occurs. There are various degrees of strain rates, defined as $\dot{\varepsilon} = d\varepsilon/dt$ and having units of s^{-1}, between "high" ($> 10^4 s^{-1}$) and "quasi-static ($< 10^{-4} s^{-1}$) [18]. For this reason, the evaluation of the capacity of NS honeycombs to absorb energy must include tests in both quasi-static and high strain rates. The former has been evaluated by Correa and co-workers [15], while the latter provides insight on the response of a NS honeycomb under impulsive loading.

Various authors have developed strain rate formulations for a beam that is initially straight but then strained into a parabolic curve shape [19], [20]. The formulation of Symonds *et. al* provided in Equation 2.5 was applied for close to parabolic curves, similar to NS beams, with good agreement when compared to experimental bending [19] and thus the estimation is reasonable here. Equation 2.5 is the representation of strain rate $\dot{\varepsilon}$ as a function of the velocity vector of the bending beam which is approximated as the unidirectional initial input velocity V_0, the beam thickness h, and half beam length l

$$\dot{\varepsilon} = \left(\frac{\partial y}{\partial x}\right)\left(\frac{\partial v}{\partial x}\right) = \frac{hV_o\lambda}{16l^2} \tag{2.5}$$

In this expression, λ represents a dimensionless parameter defined by $\lambda = \frac{mV_0^2 l^2}{hM_0}$, where m is equal to the mass per unit length of the beam and $M_0 = \sigma_0 \frac{bh^2}{4}$, which is the static moment of the beam as a function of static stress σ_0, and beam width b and thickness h. From this strain rate form it can be seen that strain rate has a cubic relation to initial velocity. This expression therefore suggests that the velocity of the input force could be a major contributing variable to the performance of NS honeycombs.

2.3.3 Stress as a function of strain rate

As previously discussed, stress and strain are connected during any bending or deformation, which is particularly relevant during deflection of NS beam elements in

honeycombs. While the Hooke's law for a stress strain relationship is adequate for small deformations and low deformation rates, it is not always the most appropriate estimation. For the case of an impact, which generates elevated strain rates in the constitutive materials, the stress-strain relationship should incorporate strain rate effects. Symonds again provides a useful relationship for beam stress as a function of both static strain and strain rate for a bending beam which is similar to the form shown in other works

$$\frac{\sigma(\dot{\varepsilon})}{\sigma_0} = 1 + \left(\frac{\dot{\varepsilon}}{D}\right)^{\frac{1}{p}} \tag{2.6}$$

In this expression, σ_0 denotes the stress due to the static strain. The variable p is chosen as an odd integer and is usually related to the temperature of the beam during strain. For the purposes of this work and the materials used, a linear approximation, *i.e.* p = 1, is acceptable for measurements made at room temperature. The variable D is material constant which must be experimentally determined.

Symonds provides information on the strain rate effects of steel, pin-joint constrained buckled beams. Unfortunately, a large sampling of nylon selective laser sintering (SLS) pre-buckled beams under various strain rates would be needed to appropriately estimate the material constants required for correct implementation of Equation 2.6 for the beams tested in this work. However, the information implicit in this expression confirms intuition that high strain rate applications increase the stress of a bending beam for a given instantaneous strain level. Further, it provides a material property that should be identified for any material that one intends to employ in the fabrication of NS honeycombs.

2.3.4 Strain rate hardening

In addition to increase in stress as a result of the rate of deformation, stress in a material itself increases with increased strain rate. This is due to strain rate hardening

which is sometimes referred to as strain rate dependence. Referencing any number of introductory material properties texts, one can understand that strain is a relative displacement of particles as a result of a stress on a material. With an increased strain rate, more energy is imparted to the particles and they are displaced more readily than when subjected to quasi-static loading. The fundamental reason for the existence of strain rate hardening is the addition of flow stress placed on a material. Barlat *et. al* provide the following constitutive relationship for the effects of strain rate hardening [21], [22].

$$\Sigma(\dot{\varepsilon}) = \sigma(\varepsilon)(\dot{\varepsilon}/\dot{\varepsilon}_0)^m, \tag{2.8}$$

where Σ represents the flow stress. In this expression, the flow stress is a function of the quasi-static stress-strain response, $\sigma(\varepsilon)$, the and the ratio of the imposed strain rate, $\dot{\varepsilon}$, to some reference strain rate, $\dot{\varepsilon}_0$, and a strain rate sensitivity parameter m which is calculated from empirical data. The reference strain rate is usually imposed when generating the quasi-static strain curve. This relationship is reminiscent of the relationship provided in Equation 2.6 for bending stress as a function of strain rate. These two stresses can be combined with the normal static stress to create a stress strain relationship that will predict an increase in stress with increasing strain rate.

Both strain rate induced stresses are relevant to understand how honeycomb structures will respond to impulsive loads. Often higher amplitude impacts generate higher strain rates on both the collapsing elements and the honeycomb cell walls. For NS honeycomb cells, the NS beams will carry a majority of the bending stress, where the strain rate hardening mostly affects the cellular wall structure. However, the overall stress of a honeycomb during impact would result from a combination of the two stresses discussed in this section.

2.4 HONEYCOMB BEHAVIOR UNDER IMPACT

The theory of increased stress in honeycomb material due to increased strain rate is widely supported in the literature with various honeycomb tested structures comparing quasi-static and dynamic or impact loads [23], [6], [24]. For all cases, stresses experienced in impact loading scenarios are as much as two times higher than the equivalent quasi-static case. Figure 2.11 displays one example of such a stress loading case, where both peak stress and the honeycomb collapsing stress plateau are both higher under impact loading.

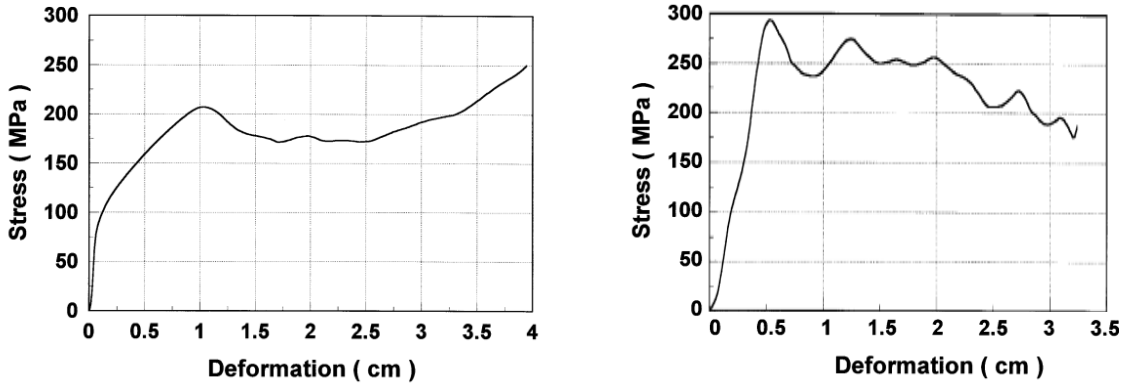

Figure 2.11: Aluminum honeycomb stress under static (a) and impact (b) loading test situations as presented by Baker [23].

Applying all of the understanding outlined in this chapter to the NS honeycomb structure, a few outcomes can be expected. First, NS honeycombs should be able to absorb nearly the same amount of energy under the impact loading scenario as traditional honeycomb structures. Second, NS honeycombs, like all honeycomb structures, will experience larger stresses during dynamic loading when compared to the values generated under quasi-static loading. This strain hardening could be a significant design factor for preventing honeycomb failure, accurately predicting force thresholds, and

ensuring that they are sufficient to receive an impact load. Third, NS honeycombs will be advantageous compared to regular honeycomb structures [23], [6], [24] because they are recoverable elements. All of these hypotheses are investigated in the following chapters.

Chapter 3: Impact Test Apparatus Design and Development

3.1 TESTING REQUIREMENTS

A 7.5 Joule impact test apparatus was constructed to test the dynamic behavior of NS honeycombs. The apparatus was constructed to measure the acceleration of an object as it impacts a NS honeycomb and the honeycomb is dynamically compressed. The impact apparatus is designed to release a weighted plate from various heights and record the accelerations of the plate as it impacts and compresses NS honeycomb specimens. The apparatus was constructed to satisfy the following simple requirements:

1) To record accelerations experienced during impact and compression of a test specimen of NS honeycomb,
2) To investigate the effect of variable loading situations (i.e., variable kinetic energy and speed), and
3) To provide repeatable loading conditions for all NS honeycomb test specimens considered in this work.

Impact testing can be accomplished with two different methods. First, impacts are often measured by accelerating a given test specimen into a static surface and recording the time history of the specimen's accelerations; this impact testing method is commonly used for testing manufactured and prepared parts ready for user implementation. Alternatively, impact measurements can be recorded by accelerating a known mass into a stationary test specimen. The impact test apparatus constructed in this work is designed using the latter approach of impact or drop testing. The advantage of this method is that it provides greater freedom for adjusting the geometry of the test specimen, as opposed to a test apparatus constructed for one type of test specimen.

3.2 CONSTRUCTION

The impact apparatus consists of three main components: *i*) the external frame, *ii*) the impact plate, and *iii*) electronics. Each component is described in further detail in the following Sections 3.2.1 – 3.2.3.

3.2.1 External frame

The test apparatus frame is constructed with one-inch-wide 80/20 extruded aluminum with supporting fasteners. The frame base is rectangular, with supporting feet that extend approximately 10 cm from the rectangular base for stabilization. Two vertical guideposts extend from the rectangular base approximately 65 cm upward. The two vertical guides are supported by eight 45° struts which connect the guides to the rectangular base. The extreme top of the vertical guides are reinforced for additional rigidity by one horizontal piece of 80/20 extruded aluminum. Basic external dimensions in centimeters and layout are shown in Figure 3.1.

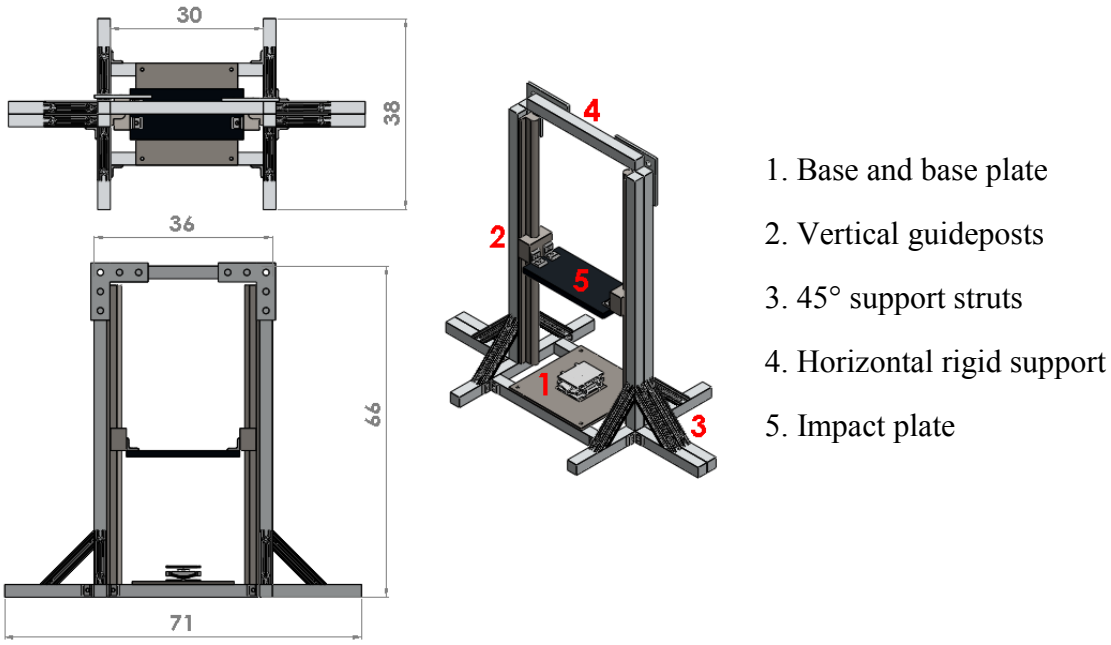

Figure 3.1: Impact apparatus frame and outer dimensions in centimeters. Key frame components are shown labeled to the right. The NS honeycomb sample is additional shown as a reference.

3.2.2 Impact plate and test specimen

To produce the necessary impact force on a test specimen, an impact plate is used. The rectangular impact plate is connected on two sides to the frame using lubricated rollers. Each ball roller slides along guided cylindrical rails that are rigidly fastened to the uprights of the frame.

Two different impact plates are used to accommodate a wide range of force thresholds of honeycomb specimens. The impact plates are made from machined polyethylene plastic. For lower force thresholds cases seen in horizontal array testing, a 600 g plate is used. This plate is gray in appearance as shown in the left panel of Figure 3.2. It has exterior dimensions of approximately 10 cm x 20 cm x 2 cm. For higher force thresholds seen by the vertical arrays, a 1800 g impact plate is used. This plate is white

and shown in the right panel of Figure 3.2. The exterior dimensions of the larger plate are approximately 15 cm x 20 cm x 5 cm.

Each test plate serves both as the force input and the measurement piece where accelerations data is collected using a accelerometer (PCB model 352-C03). The accelerometer was rigidly attached to the test plates using threaded attachment.

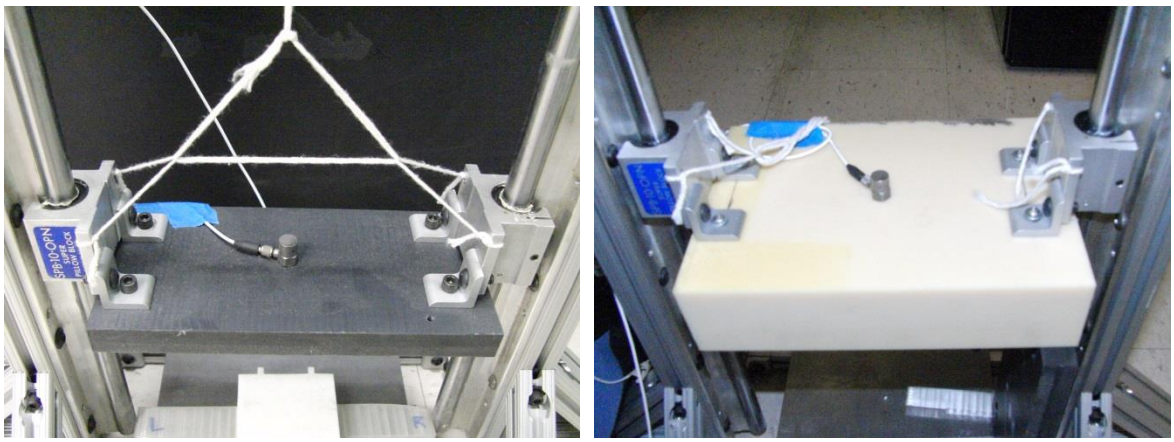

Figure 3.2: Impact plate masses connected attached to ball rollers. The gray impact plate was approximately one third (~600g) the mass of the white plate (~ 1800 g).

3.2.3 Electronics

The primary data output of the impact tests reported in this work is the time history of acceleration of the impact plate. Assuming that the impact plate moves in unison with the upper surface of the honeycomb test specimen during impact, the accelerations of the impact plate are assumed to be equal to the accelerations experienced by the top surface of the honeycomb specimen during dynamic testing. The acceleration coupling between test specimen and impact plate is valid if the impact waves are sufficiently long such that the wave and vibrational motion in the impact plate are deemed negligible, which is assumed in this work. Acceleration measurements are taken using the accelerometer which was screwed into place in the center of the top of the

impact plate. Voltages recorded by the accelerometer were acquired through a signal conditioner (PCB Mode number 482C) and into a National Instruments compact DAQ.

Table 3.1: Functional specifications for data acquisition components of test apparatus.

	Item #	Sensitivity	Measure Range	Freq Range
PCB Accelerometer	PCB 352C03	10 mV/g	±500 g	0.5 – 10kHz
PCB Signal Conditioner	PCB 482C		x0.1 – x200 Voltage Gain	0.5 – 100kHz
NI DAQ Card	NI 9234		±5 V	0.5 – 10MHz
NI DAQ	NI cDAQ 9178		±20 V	0 – 1MHz

Time acceleration plots are then recorded in a National Instruments LabView script created by the author.

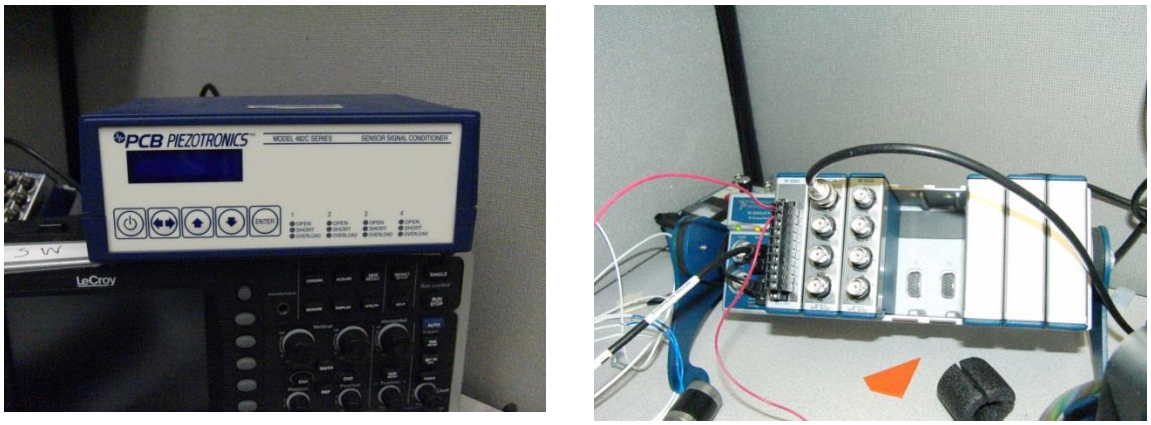

Figure 3.3: Impact testing electronics set up. For DAQ block diagram, reference Figure 6.1.

3.2.4 Experiment specific capabilities

Leveling

To ensure quality acceleration measurements, the test specimen needs to rest sufficiently horizontal and flat. To ensure a flat impact base, four leveling feet were added (two to the front and two to the rear) of the base as shown in Figure 3.4(b). Before each round of testing, the leveling feet are adjusted to raise or lower the corners of the apparatus to ensure the bottom plate is level as measured by a bullseye level.

Additionally, it is important to ensure that the impact plate is flat when it strikes the test specimen to reduce any twisting or lateral motions in the test piece. To prevent these unwanted motions, the vertical guideposts in Figure 3.1 were precision machined to have orthogonal faces. The addition of the 45° supports provided for added support and limitation of movement of the vertical guideposts.

(a)

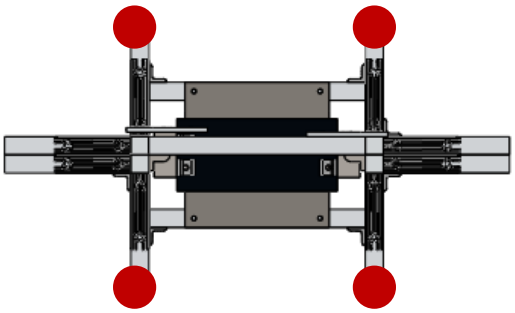

(b)

Figure 3.4: (a) Leveling feet with shock absorbing base. (b) Location of leveling feet (red dots) on the impact apparatus as seen from the top view

Specimen attachment

Preliminary trials of the impact apparatus revealed the necessity for a mechanism to limit the lateral movement of the test specimen on the bottom plate. The goal was to

constrain any lateral movement of the specimen while still allowing full functional compression and beam buckling. This was accomplished by constructing 3D printed clips (see Figure 3.5) to restrain the test specimen on the base plate. By consequence, the addition of the 3D printed clips limits the bounce back effect of the test specimen after initial impact of the impact plate, which provides for cleaner acceleration measurements.

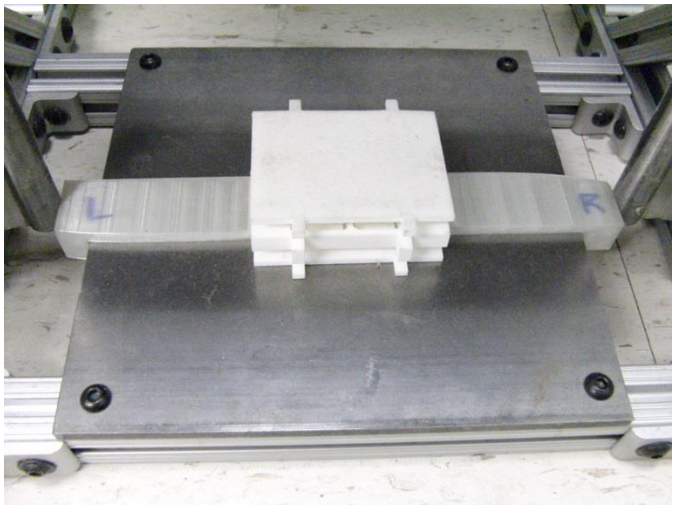

Figure 3.5: 3D printed specimen attachment method, showing 3D printed clips labeled "L" and "R."

Height control

The drop height of the impact plate is the main contributor to controlling the energy of the input, and thus is very important to regulate. Two movable aluminum L-brackets (see Figure 3.6) were added to the vertical guides to accommodate variable heights; the L-brackets are locked into place during testing to ensure consistent drop heights.

A smooth release is desired for the impact plate from various heights, but a desire to limit moving parts and vibrations of the impact plate made it difficult to add an additional mechanism to the apparatus. A string suspending system was selected to lift

the impact plate and then release it. The string was selected for simplicity of construction and minimal weight addition to the impact plate. The string is tied to the ball bearing rollers and then fed around a smooth circular cylinder at the top of the impact apparatus. The string is simply released by hand to start a test. Using this release method, acceleration profiles are found to be sufficiently consistent, but a more efficient releasing mechanism is a potential area for future work.

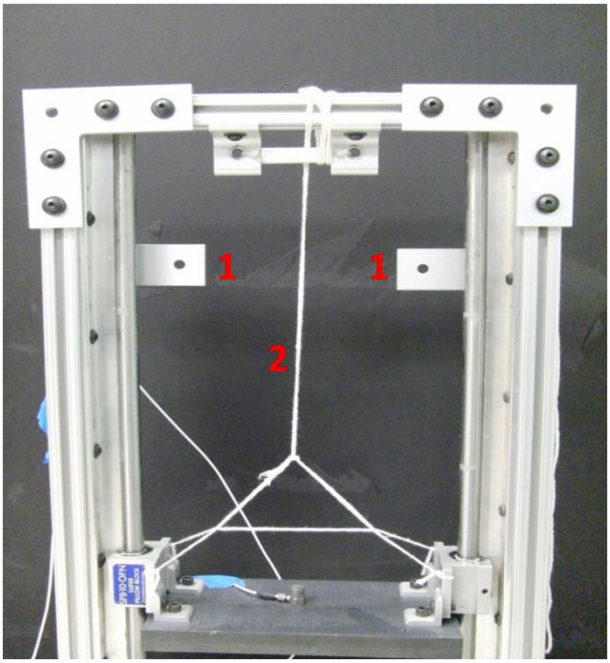

Figure 3.6: Image of 1) height control blocks and 2) lifting string of the impact apparatus.

3.3 TEST VALIDATION

The impact apparatus was constructed to provide a sufficiently-accurate means of testing the honeycomb arrays for acceleration response. The impact apparatus was certainly not constructed as a precision-machined mechanism, and by consequence it naturally has accuracy limitations. The behavior of the impact apparatus was characterized prior to testing the NS honeycomb arrays to better understand the

acceleration response. Low density crushable foam was tested as an experimental baseline. The impact apparatus was lifted to a 40 cm drop height and released to impact the stationary foam.

Recorded test data was organized into sets of acceleration measurements as shown in Figure 3.7. The first acceleration plot displayed in red represents the "input" acceleration, or recorded acceleration without the presence of a test specimen; the input acceleration lasts approximately 2 to 4 milliseconds. The following blue plots as seen in Figure 3.7 each represent a different trial recorded with the presence of the same test specimen. This method of data display is consistent throughout this work. The impact test for the experimental foam shows one peak lasting approximately 50 milliseconds, as seen in Figure 3.7 by the blue plots. The foam was tested for three trials with average max acceleration of 28.3g +/- 2.2g. Additionally the noise of the system was seen to be approximately +/- 0.1g of acceleration. This base result shows that the test apparatus construction and set-up is able to record peak accelerations of the NS honeycombs repeatedly with minimal noise.

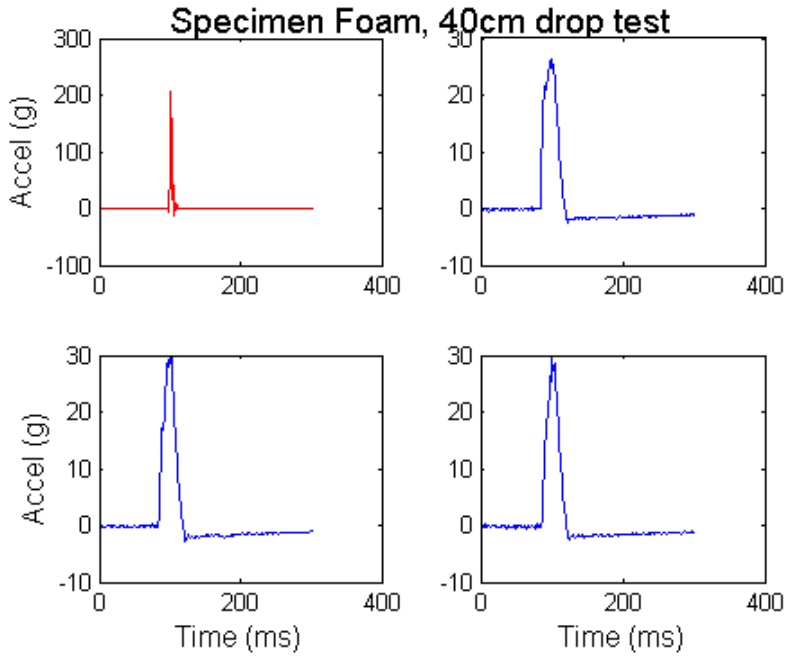

Figure 3.7: Experimental base test of a low density foam. Red represents the input acceleration, or recorded acceleration without the presence of the foam. Blue represents the acceleration recorded with the presence of the test foam.

The impact apparatus was used for dynamic testing of NS honeycombs as a means to accomplish the main goal of this thesis which is to better understand the impact capabilities of NS honeycombs. The second and supplementary goal to identify the effectiveness of different honeycomb geometries is introduced and discussed in Chapter 4.

Chapter 4: Honeycomb Array Modeling

4.1 HONEYCOMB ARRAY CONCEPTS

To satisfy the second goal outlined in Section 1.3, a unique honeycomb array concept was designed to complement the vertical array described in Section 2.2. An important opportunity for engineering development of honeycomb arrays is to decrease the vertical height of the honeycomb and the necessity for large amounts of vertical compression. With previously developed vertical designs, displacement provides a significant advantage with respect to energy absorption, since energy absorption is roughly determined by the product of force threshold and total displacement. The horizontal arrays described here were designed to absorb energy for applications with limited height and displacement requirements and where input force may be spread over larger areas.

4.1.1 Vertical vs. horizontal honeycomb arrays

One of the advantages of honeycomb structures is the ability to tailor their structure to meet design criteria. The addition of NS elements into a honeycomb array provides additional flexibility with respect to the force thresholds at which the beams collapse and the displacements that they undergo. Further, NS honeycomb structures have the added benefit of being able to recover from large deformations. The vertical and horizontal honeycomb structures discussed below represent two different ways to organize NS beams into a honeycomb structure.

A note on axis naming convention

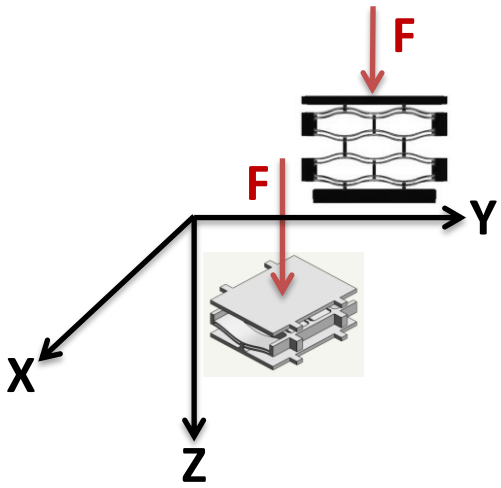

Figure 4.1: Input forces are assumed positive when anti-parallel with the *z*-axis. An example vertical honeycomb is shown in the upper-right as the black honeycomb and an example horizontal honeycomb is shown as the grey.

To aid in the comparison between designs, this work utilizes the coordinate axes directional conventions identified in Figure 4.1 where the positive *x*-direction is aligned with the normal to the page, the *y*-axis is horizontal, and the *z*-axis is vertical. Input forces for all honeycomb designs are assumed to be positive when anti-parallel with the *z*-axis.

Vertical honeycomb arrays

Vertical honeycomb designs are created by organizing arrays on the *y*-*z* plane. The work of Correa *et al.* [3] provided preliminary quasi-static experimental data demonstrating the capabilities of vertical NS honeycomb arrays to absorb large amounts of mechanical energy. Data from that work will be utilized in later chapters for comparison with the dynamic measurements provided in this thesis. One advantage of the vertical array is that NS beams can be designed to absorb increasing amounts of energy when the snap-through distance increases. Figure 4.2 shows one possible implementation

of the vertical honeycomb array concept. Specifics on the design of the vertical array pictured in Figure 4.2, can be found in the work of Correa *et al.* [3].

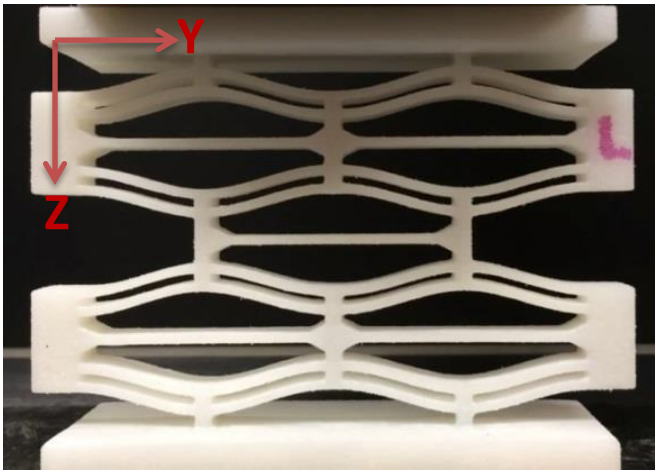

Figure 4.2: Vertical SLS honeycomb array following the design and testing reported by Correa [3].

Horizontal honeycomb arrays

A horizontal array is constructed by placing beams in the *x*-*y* plane, as shown in Figure 4.3. The main advantage of a horizontal array is the ability for a more compact construction in the *z*-direction. In contrast to the vertical array design, beams are not stacked but energy is distributed over a larger surface area. Where the vertical array absorbs energy by having a low force threshold and long force plateau, the horizontal array could absorb the same amount of energy, but with a higher force threshold and shorter displacement on the force plateau.

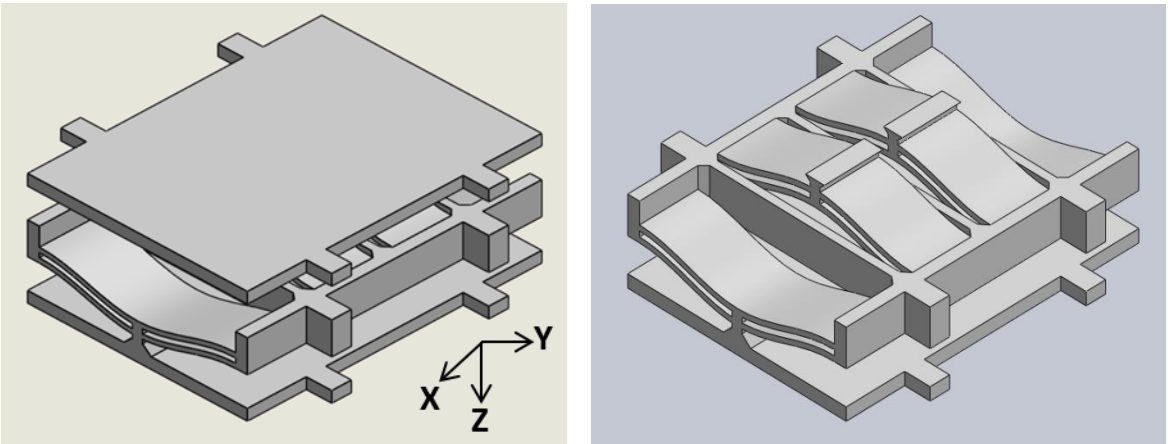

Figure 4.3: Horizontal honeycomb array unit cell design. The view on the right-hand side shows the top plate removed to expose the beams underneath.

By nature, a horizontal honeycomb design that distributes negative stiffness beams over a large area provides a greater ability to limit the necessary vertical displacement while maintaining the same capacity to absorb energy during impacts, at the cost of elevated force thresholds. As such beam stages are able to be nested together so the full throw of one beam stage can overlap the full throw of a second beam stage as shown in the side view image in Figure 4.5. This is not possible with a vertically stacked design, unless multiple vertical arrays are arranged in parallel.

Preliminary concepts were designed to arrange beams as closely as possible. The horizontal design objective was to utilize as much of a given surface area with negative stiffness elements organized in some manner that still allowed for effective force mitigation. In implementation, support components are needed between negative stiffness beams in any array, whether horizontal or vertical, in order to minimize displacements at the beam ends and thus generate beam buckling and snap through response. Using this

knowledge from previous vertical array designs [3], rigid horizontal supports are included in between beam elements in the horizontal array.

4.2 HORIZONTAL HONEYCOMB DEVELOPMENT

4.2.1 Unit design

The horizontal honeycomb design was created to best mimic the NS properties of the vertical design, but to absorb similar amounts of energy for smaller overall transverse displacements. The initial unit cell was designed as a collection of four prefabricated NS beam elements as shown in Figure 4.3.

Each beam element consists of a double beam structure which is consistent with previous work which observed that the double-beam structure resulted in much more reliable better snap through responses [4]. The beam curvature shape is governed by the equation

$$z(y) = \frac{u_0}{2}\left[1 - \cos\left(2\pi\frac{y}{L}\right)\right] \tag{4.1}$$

Each beam element is designed with the properties listed in Table 4.1 and illustrated in Figures 4.3 and 4.4.

Table 4.1: Horizontal unit cell beam design metrics. Note beam width is defined as out-of the plane or the extruded width.

Beam length	L	5 cm
Apex height	u_0	0.5 cm
Beam thickness	t	0.125 cm
Beam width	w	1.5 cm

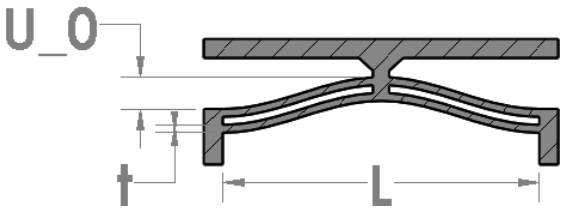

Figure 4.4: Horizontal unit cell beam design specifications.

Two Stage Design

The horizontal array beam elements are organized in two stages as shown in the top right image of Figure 4.5. The lower stage is composed of two "downward-facing" beams, where downward facing is defined as a NS beam structure whose apex is below the beam ends, and positioned in the outsides or first and fourth linear locations as identified in the bottom right image of Figure 4.5. The upper stage consists of two "upward-facing" beams, (identified as a beam whose apex is above its ends). The upper stage beams are positioned in the middle of the unit, or the second and third linear positions as defined in Figure 4.5.

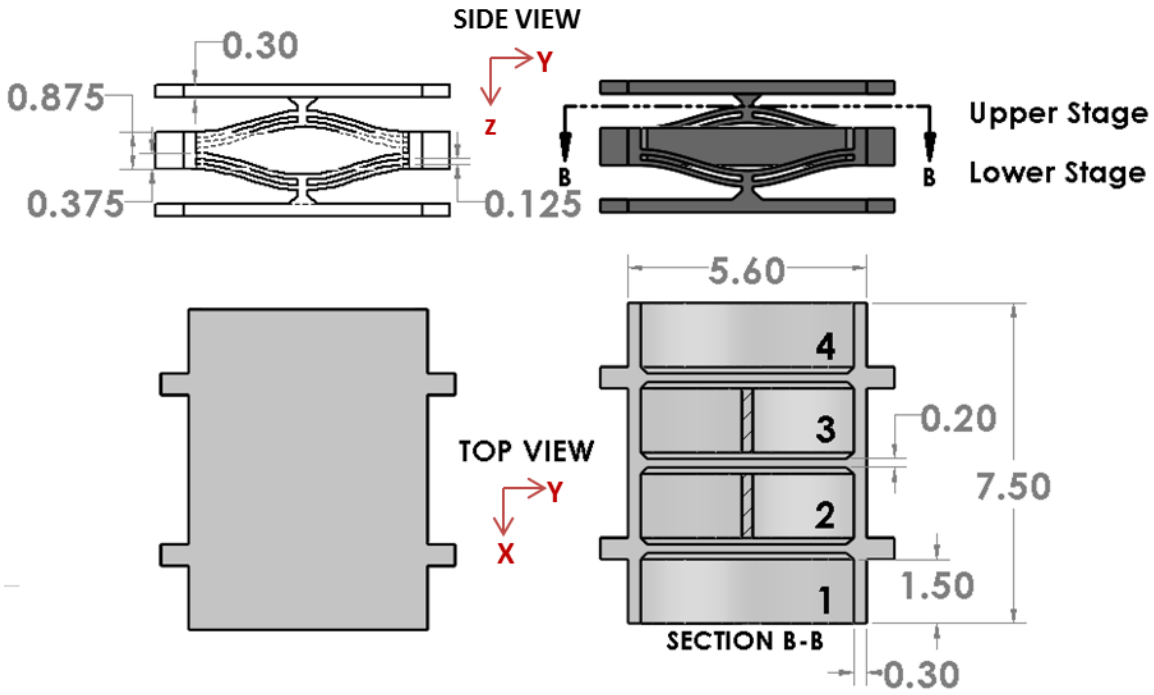

Figure 4.5: CAD drawings of the full unit cell design. The upper left image itemizes the linear positions of beam elements.

In between each beam element is a 0.20 cm horizontal support beam as shown in the bottom right image of Figure 4.5 that restricts lateral beam movement and maintains rigid beam endpoints. This improves the likelihood that NS behavior will be observed for a given beam configuration and thus that energy absorption efficiency will be maximized in the as-built geometry. The upper- and lower-stage beams were vertically nested for to minimize the total height of the unit cell. Assuming each beam stage fully snaps through, the beam stages overlap during the throw which is possible because of the horizontal honeycomb design.

4.2.2 Design concepts

To test the range of horizontal 2-D space with NS beam elements, the unit cell for the horizontal array is incorporated into four other geometric variations that can be

identified using appropriate matrix notation. Assuming the unit cell includes four beam elements in the orientation illustrated in Figure 4.1, the unit design would be considered the 1 x 1 matrix design. Additional horizontal honeycomb designs are constructed within a 2 x 2 matrix as shown in Figure 4.6. Table 4.2 lists the five horizontal honeycomb designs with brief explanations, and Figure 4.7 provides CAD models for each honeycomb design.

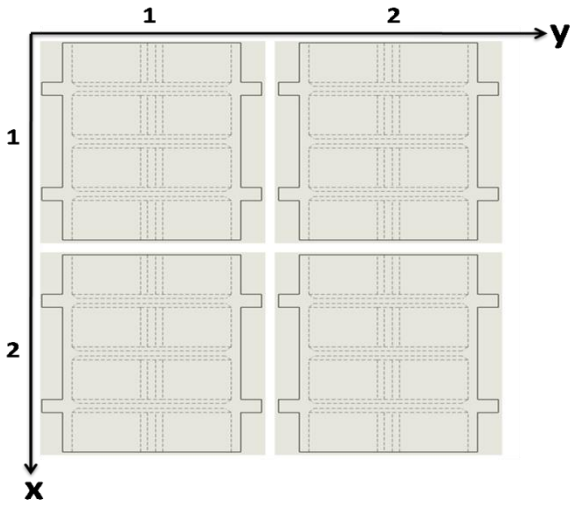

Figure 4.6: Matrix identification key.

Table 4.2: Brief explanation of horizontal honeycomb designs.

Unit design	1 x 1 matrix geometry
Side by side	2 x 1 matrix geometry containing two unit designs joined along the y axis. It consists of a total eight beams, four upper and four lower stage beams.
Back to back	1 x 2 matrix geometry containing two unit designs joined along the x axis. Has the same number of beams and unit cells as the 1 x 2 but the unit cells are joined at the beam ends.
Back to back flip	1 x 2 configuration with the same number and positioning of beam elements as back to back design, but the second unit cell in the 2 x 1 matrix position is flipped upside down.
Four units	A 2 x 2 combination of four unit cells. This geometric configuration has 16 total beam elements, eight in the upper stage and eight in the lower stage.

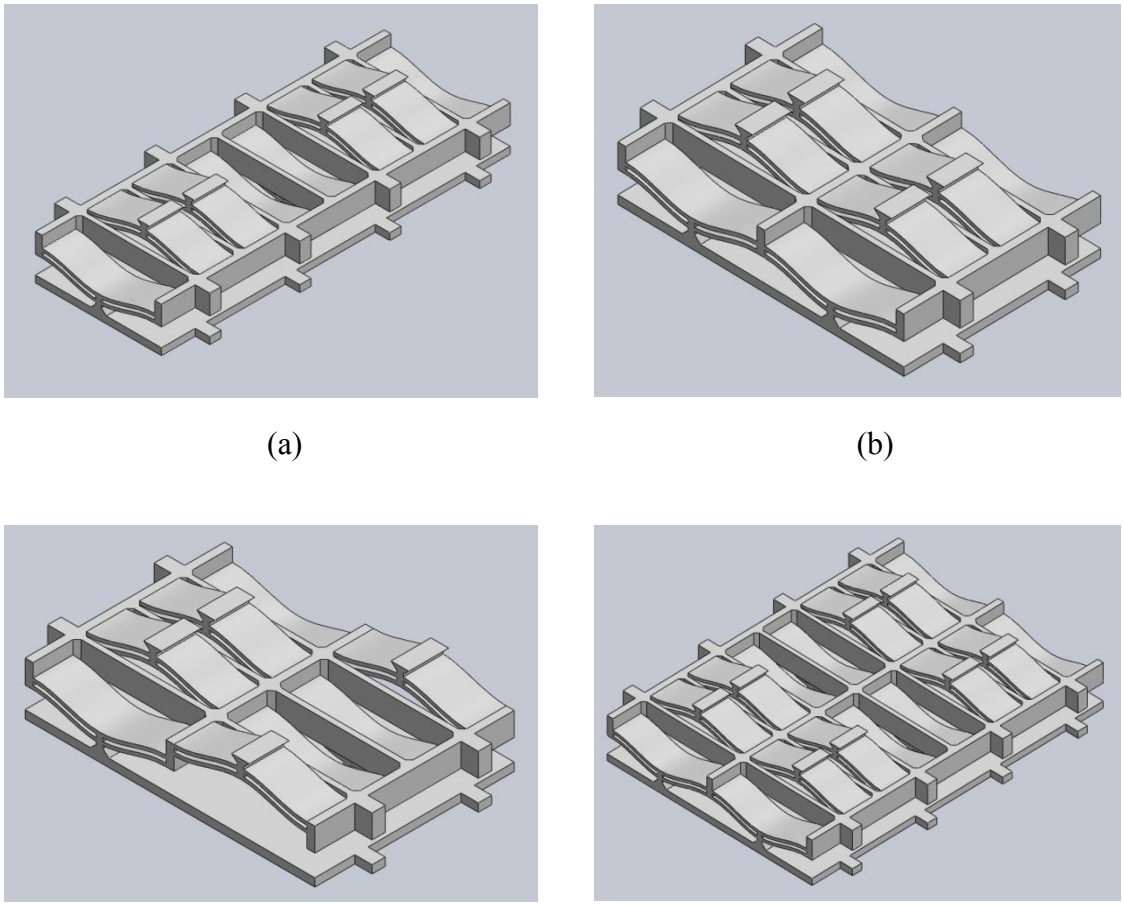

(a) (b)

(c) (d)

Figure 4.7: CAD renderings of various horizontal honeycomb designs: (a) side by side, (b) back to back, (c) back to back flip, (d) four units.

4.3 FINITE ELEMENT MODELING

For most engineering applications, it would be impractical to design a new honeycomb array and test the results to determine force thresholds and energy absorption capabilities. For this purpose both analytical and FE models are regularly used to estimate design effectiveness. This work once again mirrors and compares the efforts of Correa *et al* [3] by modeling the horizontal array design in FEA using Comsol Multiphysics 4.4.

The Comsol models were used to identify the force-displacement curves for the horizontal arrays.

4.3.1 Vertical array

The vertical array design shown in Figure 4.2 was analyzed with FE models that had reasonable agreement with quasi-static test results in the work of Correa *et al.* [3]. Figure 4.8 shows the force-displacement curve for the vertical honeycomb. The details of the FEM setup and analysis and shown further in the work of Correa [3].

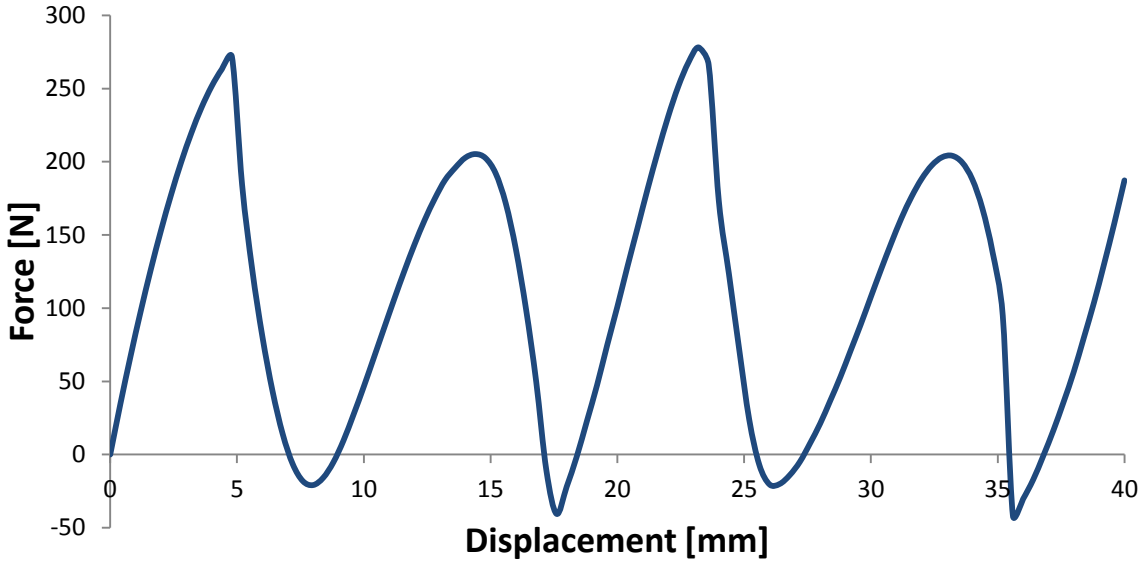

Figure 4.8: Force-displacement plot from FEA model of vertical honeycomb array. Figure adapted from [3].

4.3.2 Horizontal array

Finite element models of horizontal honeycombs were generated to provide an initial evaluation of their response. Two FE analyses are shown in this thesis; the unit design and the side by side design.

Finite element model setup

The FE models were created from geometries imported from Solidworks 2014. The models were provided minimal constraints to allow for the most accurate results. The two main constraints in the horizontal honeycomb FEA solution were first a rigid bottom boundary, simulating a massive flat surface for testing. Second, roller constraints were applied to the sides of the model to limit bulging of the model during beam deflection. The models were given a constant displacement input on the top face, opposite of the bottom rigid constraint. The top face was displaced thirteen millimeters, forcing the test piece to compress and beams to snap. Reference the appendix for full Comsol m-file output.

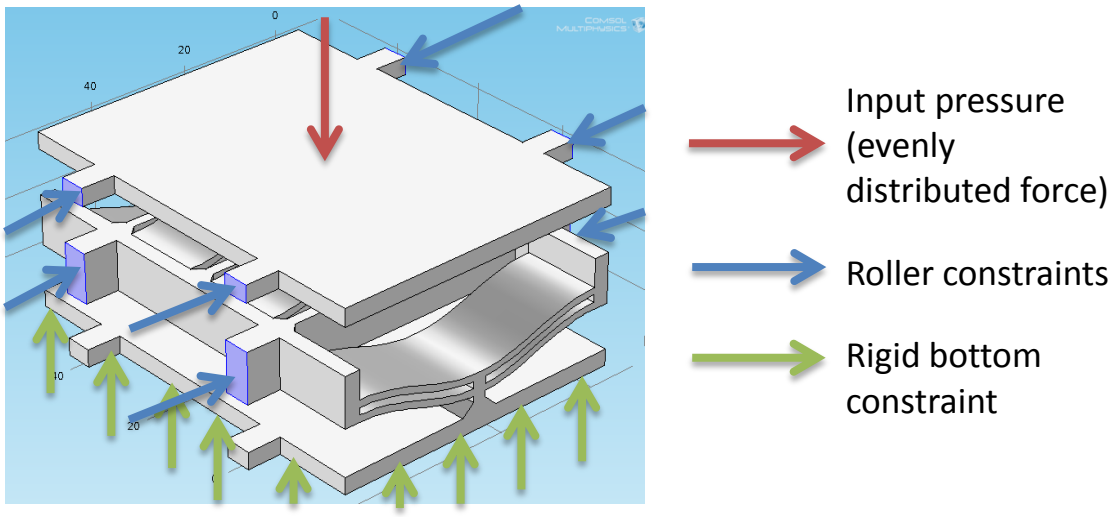

Figure 4.9: Horizontal array FE model constraints.

Quasi-static force-displacement response

With the boundary conditions described above, the Comsol equilibrium model was prescribed an input displacement and the force was monitored. The horizontal test design yielded force-displacement plots that contain two distinct peaks of unequal

magnitude. Each peak in the plot as seen in Figure 4.10 represents the snap through for one beam stage.

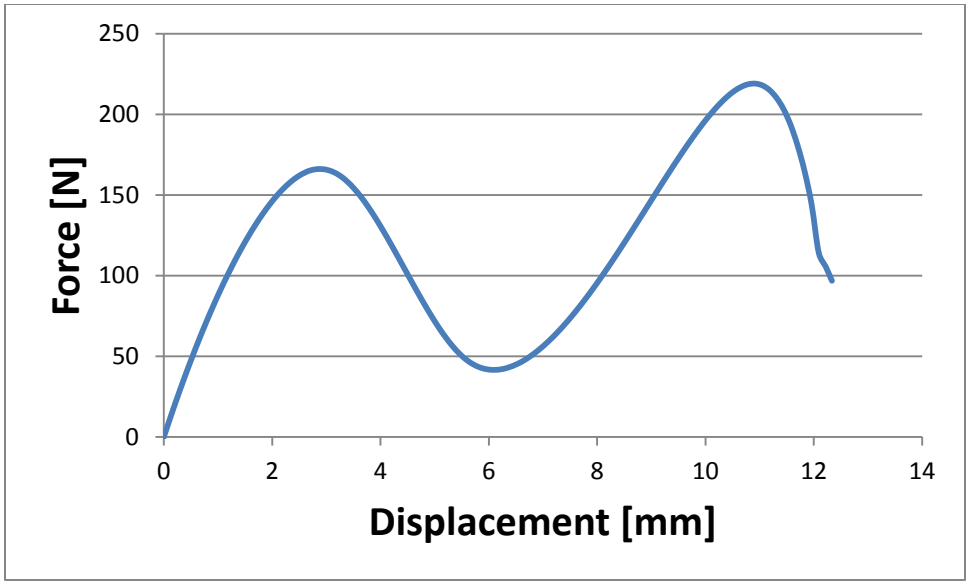

Figure 4.10: Force vs. displacement plot for FE model of horizontal unit cell.

An additional FEA study was conducted for the side-to-side horizontal design with the results shown in Figure 4.11. The FE analysis for the side-to-side design was prescribed the same boundary conditions as the unit cell model and was displaced the same compressional distance.

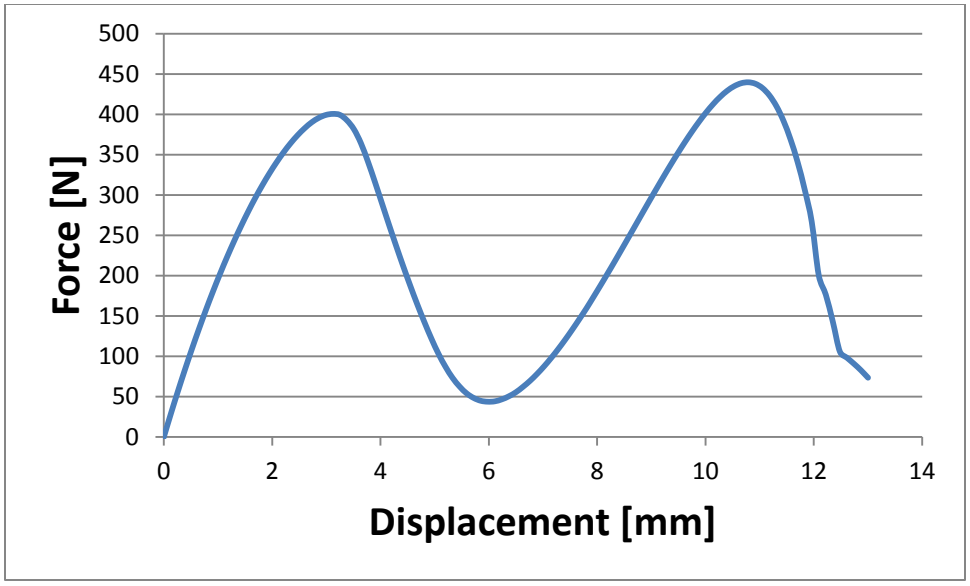

Figure 4.11: Force vs. displacement plot for side to side horizontal honeycomb design provided by FE analysis.

Similar to the unit cell FE analysis, this geometry provided two distinct peaks representing the force thresholds of each beam stage. Here the peaks, and thus the force thresholds, are approximately double that of the unit design. This result is expected because the side-by-side design has double the number of parallel beam elements as the unit design. Interestingly, the side to side design provided two peaks that are closer in magnitude, signifying that the beam stages are more closely matched. This is reasonable because the side to side design is larger and seemingly more rigid during compression.

4.3.4 Modeling challenges

Inherent in FE modeling are challenges with converging solutions when working with non-linear elements. NS beam elements are highly non-linear and usually difficult to model properly. This was the case for the horizontal honeycomb modeling.

Attempts were made to model all geometries shown in Figure 4.7 using Comsol 4.4. Unfortunately, most geometries (both 2 x 1 deviations, 2 x 2 geometry) did not

converge to a solution. Lack of convergence can result from numerous causes in any FE model. However, the large numbers of potential buckling events in the largely un-constrained three-dimensional models are likely to be the principal causes for difficulties in converging to a solution. Using similar FE models, Correa [3] demonstrated the capability of FE solvers to successfully predict the response of multiple pre-buckled beams. Unfortunately, his analysis was limited to vertical arrays which are well represented with 2D geometries. The horizontal array design introduces significant 3D motion. Figure 4.12 provides a good representation of 3D bending behavior observed during NS honeycomb compression. Noteworthy in Figure 4.12 are the twisting and bending of the vertical cell walls where the NS beam element endpoints are located. Certainly non-rigid end conditions change the nature of the NS beam buckling pattern.

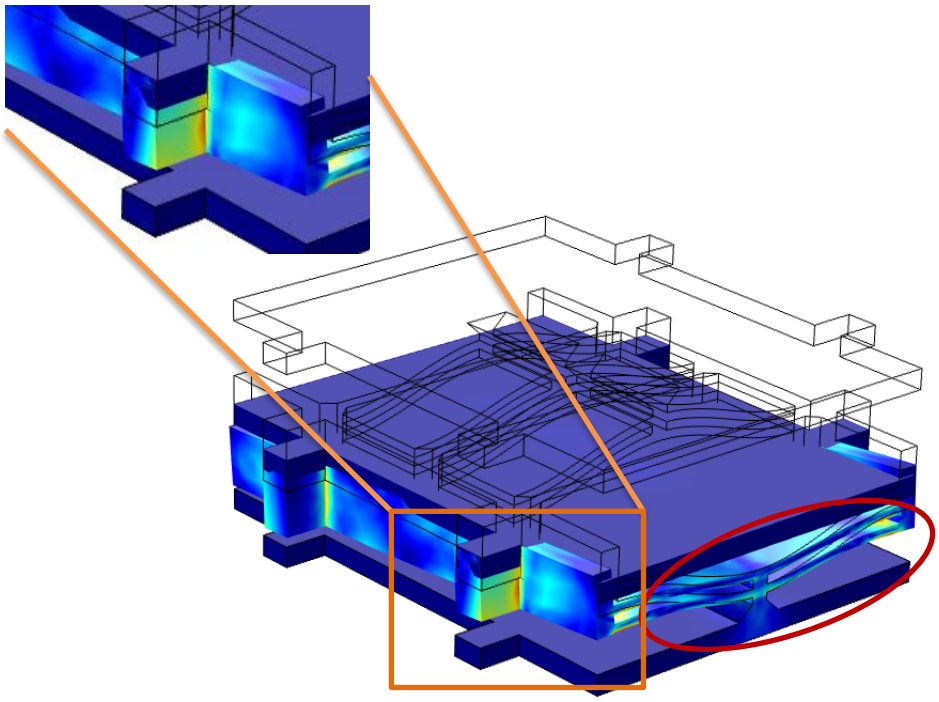

Figure 4.12: Horizontal unit array at full compression. This surface plot reflects the Von Mises stress. Note the anticipated NS beam deflection denoted by the red oval and the unwanted twisting and bending of the cell wall denoted by the orange rectangle. Note upward curling of cell wall punching through the top surface inside the orange rectangle.

Revised boundary conditions

To obtain a solution, idealized boundary conditions were added to the FE analysis. The boundary conditions aided in solution convergence but were determined not to result in large deviations between the models and actual boundary conditions.

The first idealized boundary condition was the addition of a roller constraint on the horizontal cell walls where the beam ends are constrained. Figure 4.9 displays the position of the added roller constraints with the blue shaded regions and blue arrows. The addition of roller constraints allowed for free motion in the *z*-direction but ensured no movement in the x-direction. The removal of a degree of freedom allowed for a less

complex FEM problem that was more readily solvable. It should be noted, however, that during testing of the actual system, visible displacement was observed in the *x*-direction.

The second idealized boundary condition was the lack of contact restraint between the top plate and beam end conditions. This is shown in Figure 4.12 where the buckled beam plates curl up and punch through the top plate at full compression. This is obviously a non-physical solution, but necessary to obtain an FE analysis.

Although the presence of these two idealized boundary conditions allowed for a convergent FE analysis, it is likely the force-displacement solutions are not completely accurate depictions of the horizontal honeycombs during compression. To investigate the accuracy of the FEA predications, they are compared with quasi-static testing results in Chapter 5. In addition, the false boundary conditions were only effective with the smaller horizontal array geometries (unit, side to side). The larger and thus more complex geometries were not able to be analyzed with the FEA solvers used in this work. For a more accurate FE analysis and better model for the horizontal arrays, a more robust solver is required.

Chapter 5: Low Strain-rate Measurements

To quantify the mechanical properties of honeycomb materials, test pieces are often subjected to quasi-static loading, or low strain-rate compression in this case, whereby a test piece's overall displacement versus compressive force relationship can be found in absence of rate dependence. Such a measured force-displacement curve provides information about the force threshold and energy absorption properties for a given a honeycomb structure. This low strain rate evaluation is equally applicable to NS honeycombs, for which compressive forces and overall displacements are also documented during unloading and recovery of the test piece. This chapter reports the results of quasi-static testing of both the vertical and horizontal arrays. Quasi-static testing of similar vertical arrays was also conducted by Correa *et al*. [15], and reported here for comparison purposes.

5.1 TESTING PROCESS

Quasi-static compression testing was conducted using a universal testing machine, (MTS Sintech 2G) which measures the reaction force of a sample when subjected to displacement-controlled loading. A horizontal NS specimen under test is shown in Figure 5.1. Each test specimen was placed on a flat solid surface and compressed by a large steel plate. The compression rate was fixed at 5 mm per minute for all tests reported herein.

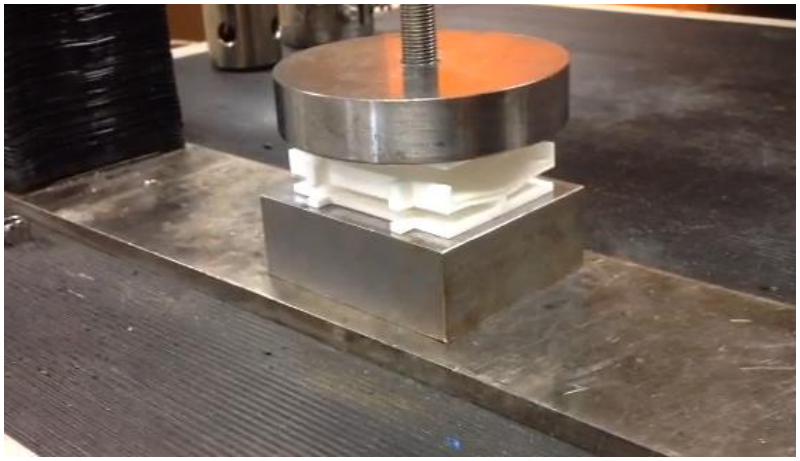

Figure 5.1: Quasi-static testing layout.

Honeycomb specimens were compressed until large exponential increases in force were observed, signifying that the beam elements had “bottomed out” and was beyond the usable range of the negative stiffness beam elements. The exact compression varied slightly for each test specimen, but all test pieces were compressed between 13 and 15 mm, and then were subsequently released at the same rate, 5 mm per minute.

In accordance with the estimation of Qui and co-workers [12] and previous understanding of prefabricated buckled beams, large force maxima were expected in the measured force-displacement curves, where each peak represents the force threshold for a honeycomb row. The number of beam peaks was expected to correspond to the number of NS honeycomb rows, four for the vertical honeycomb and two for the horizontal honeycomb. Similarly, force maxima were expected during honeycomb recovery at approximately the same displacement values as the peaks observed during loading. However, the amplitudes of the decompression force peaks were expected to be lower as a result of stress relaxation within the material.

5.2 FORCE VS. DISPLACEMENT CURVES

5.2.1 Vertical Honeycomb Array

Vertical negative stiffness honeycomb elements were previously quasi-statically tested and reported in the work of Correa *et. al* [15]. A portion of those findings are shown here, for comparison with the present work. Correa used the vertical honeycomb array shown in Figure 5.2, with the vertical array organized in four stages, where each stage contained two double beam NS elements in parallel. Two different specimens were tested quasi-statically, and Correa's force-displacement diagrams are shown in Figure 5.3. Four force maxima, which correspond to the peak forces or force threshold for each stage of the vertical array, are visible.

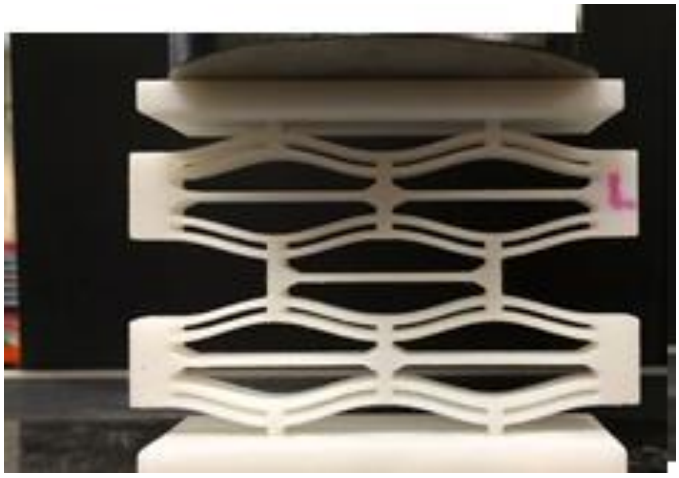

Figure 5.2: Vertical honeycomb design, Figure adapted from [15].

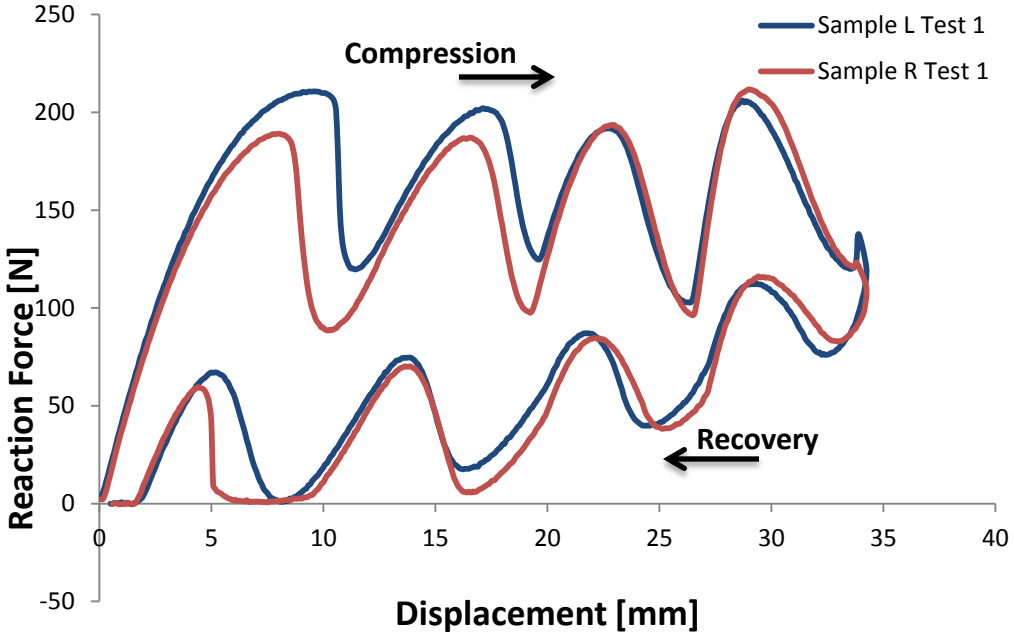

Figure 5.3: Force vs displacement measurements for Correa's vertical array design of Figure 5.2. Data from two samples, denoted as L and R, was included to show repeatability. Figure adapted from [15].

5.2.2 Horizontal Honeycomb Array

To build upon the findings of the vertical array concept, the newly designed horizontal honeycombs of the present work were tested quasi-statically under the same conditions as used by Correa [10].

Unit Cell

The horizontal unit cell originally shown in Figure 4.3 (and repeated here in Figure 5.4 for convenience) was tested for one cycle of compression and recovery. Since the horizontal honeycomb includes two rows of NS elements, the force-displacement plot was expected to include two force maxima in the loading path. The force-displacement plot seen in Figure 5.5 confirmed this assumption with two distinct peaks representing the force thresholds of each parallel beam stage.

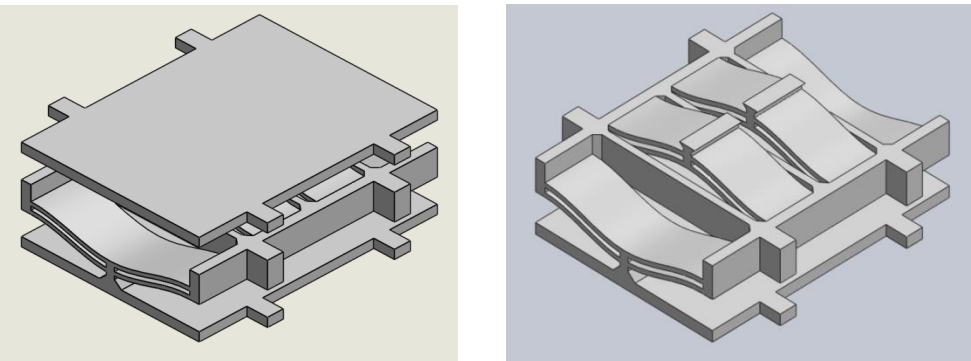

Figure 5.4: Horizontal honeycomb unit cell design.

In contrast to the vertical honeycomb design, the horizontal honeycomb's force-displacement results in Figure 5.5 show two peaks that differ significantly in amplitude. The deviation in force amplitude is likely a result of the manufacturing process or inadequate design geometry. While some deviation was expected due to manufacturing inconsistency, it is more likely that the peak forces differ because the horizontal honeycomb was not adequately constrained at the beam endpoints, which results in changes in beam geometry during loading. Chapter 4 discussed some of the twisting motion and rotational forces that resulted during compression of the horizontal honeycomb. The FE model effectively predicted un-equal force thresholds between the two beam stages but was not accurate as to the magnitude of the force thresholds. The amplitude seen during quasi-static testing are much lower than FEA predicted results, which is most likely the result of non-ideal weak beam constraints.

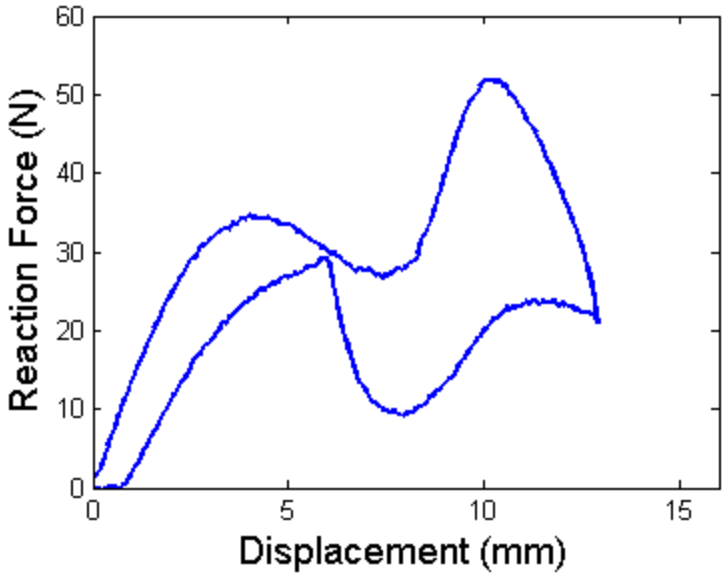

Figure 5.5: Force-displacement results of quasi-static testing for horizontal unit cell honeycomb design of Figure 5.4.

Additional horizontal honeycomb geometries

To add to the knowledge gained from quasi-static testing of the horizontal honeycomb unit design, the four other geometries described in Chapter 4 were tested for comparison between NS beam layouts. Results for each horizontal honeycomb design are similar to the unit cell of Figures. 5.4 and 5.5. It is noted that each force-displacement curve displayed two distinct force peaks and force thresholds differed depending on geometry and NS beam configurations. Figure 5.5 displays the results for each geometry.

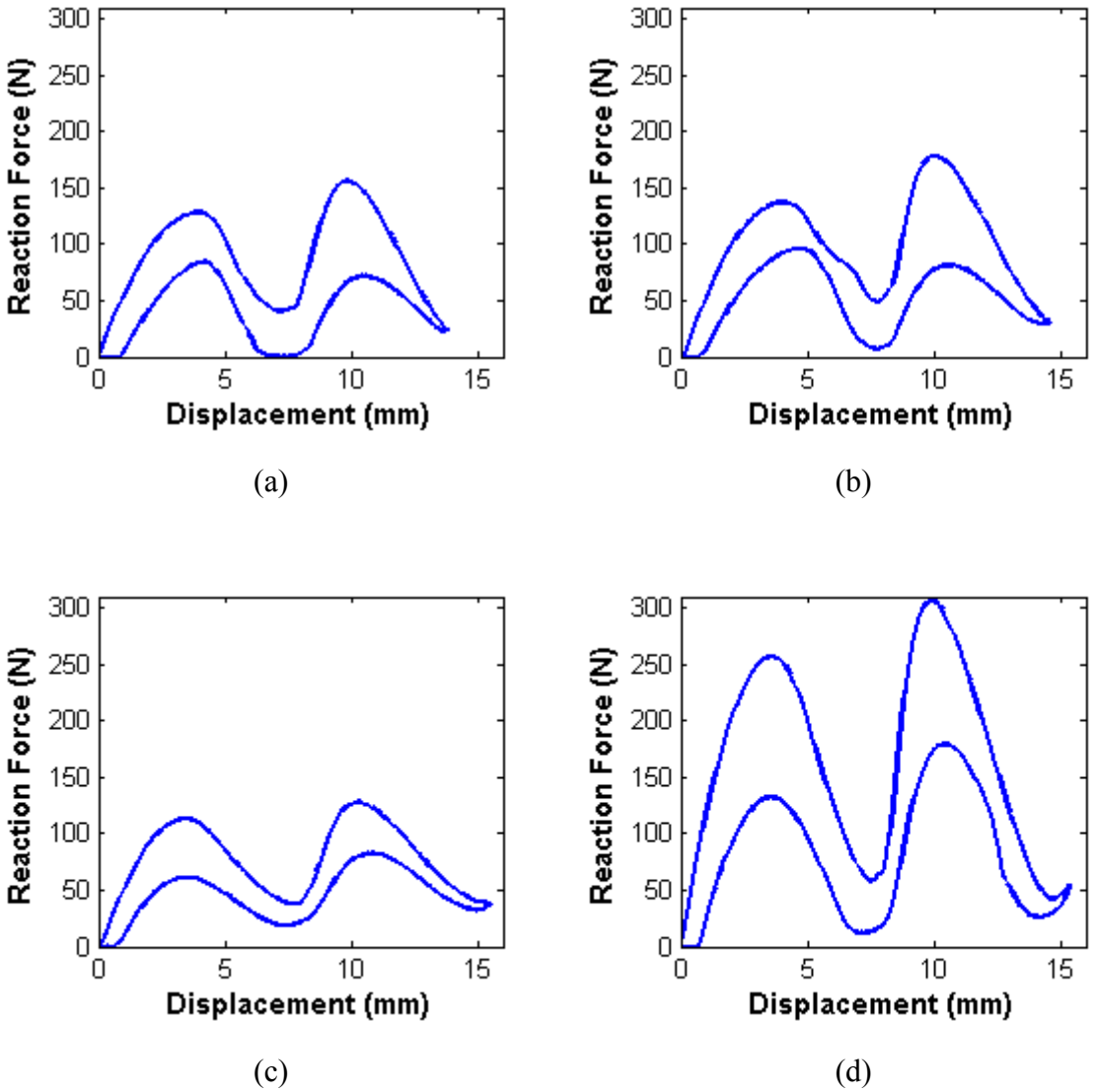

Figure 5.6: Force-displacement curves measured during quasi-static testing of various horizontal honeycomb designs: (a) side-to-side, (b) back-to-back, (c) back-to-back flip, (d) four units.

The quasi-static testing of various horizontal honeycomb geometries leads to better understanding of some of the interesting results seen for the unit cell. Each honeycomb geometry clearly showed two force maxima, signifying that the design generated NS beam snap through of each of the two stages as expected. Considering just

the number of beam elements, the geometries seen in Figure 5.6(a), (b), and (c) were expected to exhibit equivalent peak forces. Indeed, the peak forces observed during quasi-static loading of these different geometries were similar in magnitude though some deviations are apparent. These deviations are likely a result of variation of the effective end constraints of each distinct geometry. The cell walls (which are also the beam ends) noticeably twisted and deformed during testing which decreased the effectiveness of the honeycombs because it changed the NS beam properties. The back-to-back geometry seen in Figure 5.6(b) had the least cell wall deflection by nature of honeycomb design, thus the force thresholds were higher. All horizontal honeycomb geometries displayed two peak forces of slightly differing magnitude. With larger geometries and higher numbers of NS beam elements, the difference in amplitude decreased as seen in Figure 5.6(d). The deviation in force maxima is informative for future design work and the importance of cell wall integrity in NS honeycombs.

5.2.3 Energy absorption and model effectiveness

Negative stiffness honeycomb effectiveness is measured by the ability to absorb or reduce impact energy. The force-displacement diagram can be used to assess the energy absorbed by the honeycomb, where the total energy absorbed is represented by the area between the compression and recovery of the negative stiffness element, or as seen in the force-displacement plots, the upper and lower curves. Hence, the area between the compression and release curves was summed for each statically tested design. The total energy absorption and absorption per NS beam for the horizontal array (Figure 5.6) is shown in Table 5.1, along with the results from the vertical array as found by Correa *et al.* [3], included for comparison.

Table 5.1: Calculated energy absorption from quasi-static testing of vertical and horizontal honeycombs. Vertical array data reproduced from [3].

		Energy Absorbed (J)	Energy Absorbed per NS beam
Horizontal Arrays	Unit	0.41	0.125
	Side to side	1.23	0.154
	Back to back	1.46	0.183
	Back to back flip	1.20	0.150
	Four unit	2.52	0.158
Vertical Arrays	Correa 1	3.26	0.408
	Correa 2	3.52	0.440

Energy absorption and volume displacement

For many applications non-linear NS springs are needed to function in small spaces, thus generally speaking small NS honeycombs with large energy absorption are desired. Accordingly, the metric of total volume was devised in this work to provide a crude comparison of the various NS honeycombs. Total volume means the volume measured by the bounding dimensions of an element at rest.

The various horizontal designs were compared using the metric of energy absorption and total volume. In addition the design elements were compared to the results of previous vertical designs, which are represented by the blue symbols in Figure 5.7.

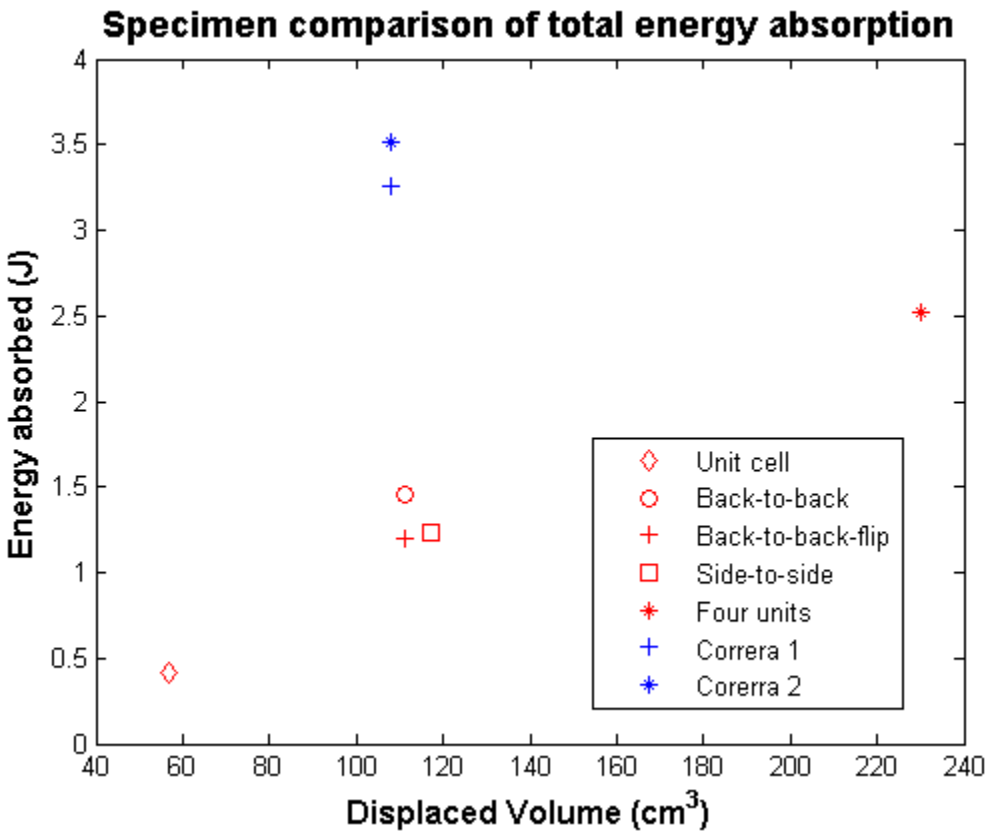

Figure 5.7: Comparison of energy absorption versus volume displaced for various vertical and horizontal honeycomb geometries.

Two conclusions can be drawn from the results of Table 5.1 and Figure 5.7. First, the vertical honeycomb specimens tested by Correa *et. al* are more volumetrically-efficient energy absorbers. The horizontal honeycombs were designed to mirror the properties of the vertical honeycombs, but they show poorer performance. This is likely due to weak beam end constraints which led to lower beam force thresholds and this reduced energy absorption for the same amount of imposed displacement. Additional test data and improved honeycomb designs are needed to fully optimize honeycomb design. The quasi-static testing results here support observations in previous chapters of the importance of rigid beam end constraints for efficient energy absorption. Second, the

results seen in Figure 5.7 highlight potential relationships for energy absorption as a function of volume. The five designs that are plotted in red in Figure 5.7 exhibit a nearly linear relationship between energy absorption and volume. This result provides potential for appropriate mathematical models to be created for future NS honeycomb design work, where honeycomb designs can be tailored according to dimensional design constraints.

Chapter 6: Impact Testing: High Strain-rate Analysis

Although NS honeycombs exhibit promising energy absorption behavior when evaluated at low strain rates, high strain rate analysis of these types of structures has not yet been explored. It is obvious that for any practical application, NS honeycombs would be required to perform well under high strain rate applications, such as impact. To address this deficiency, impact tests were performed to investigate the mechanical behvior of NS honeycombs subjected to high strain rate loading.

6.1 Description of Impact Testing

The objective of impact testing was to provide experimental data on the dynamic performance of NS honeycombs. This was achieved by measuring the acceleration reduction of a falling plate as it impacts a honeycomb test specimen, compared to a benchmark case of a falling plate impacting an uncovered base plate.

6.1.1 Data recording

To measure acceleration, a PCB model 352-C03 three-axis accelerometer was used. The accelerometer was connected by stud to the top of the impact plate as seen in Figure 6.1. The signal generated by the accelerometer was sent through a PCB model 482C signal conditioner and into a NI cDAQ-9178 compact data acquisition system. The PCB accelerometer had an operating voltage output range of +/- 5 V with a sensitivity of 10 mV/g, and the compact DAQ also had a measurement input voltage range of +/- 5 V. This combination allowed for a measurement range of +/- 500 g of acceleration.

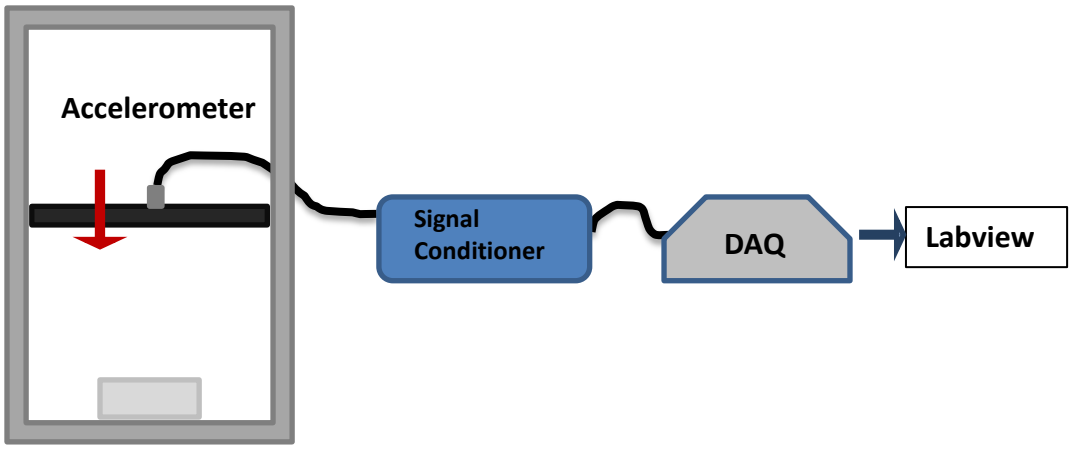

Figure 6.1: Illustration of the drop test set-up.

The acceleration data was collected and recorded using a simple Labview script written by the author. The user interface and Labview virtual instrument (VI) front panel is illustrated in Figure 6.2. Data was collected at a rate of 1000 Hz for five seconds. The data acquisition was manually triggered and a time history of acceleration of the falling plate was recorded. The Labview interface provided a simple plot of acceleration versus time, and each plot was saved for post-processing.

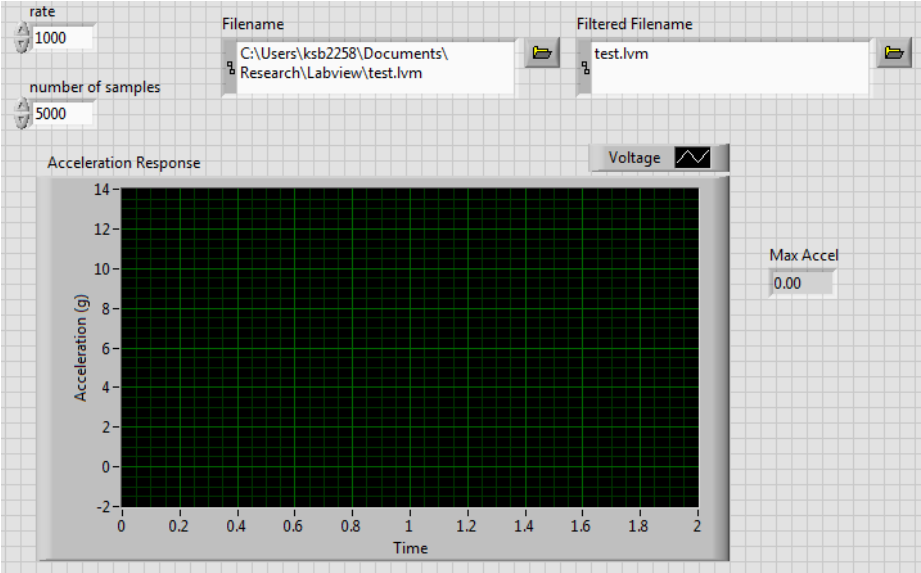

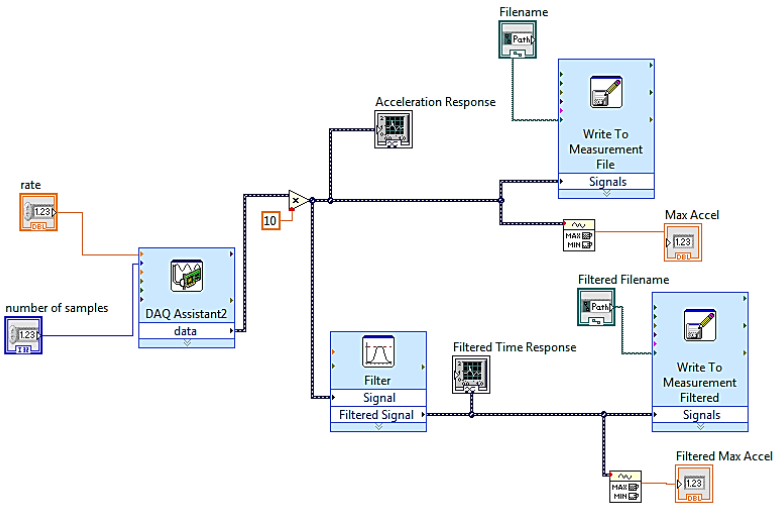

Labview VI process

1. Data acquisition
    a. 1000 Hz
    b. 5 seconds
2. 10x multiplier accounting for signal conditioner 1/10 reduction
3. Low pass filtering (< 1kHz) [The filtered data was not used, and is not reported in this thesis]
4. Accel data plot for both unfiltered and filtered response
5. Data saving

Figure 6.2: LabView VI wiring diagram for impact data collection.

6.1.2 Test procedure

The impact test was designed to accelerate an impact plate into a stationary NS honeycomb. The impact plate was accelerated to different velocities by dropping the impact plate from different test heights. Two test groups were considered: (1) the vertical

honeycomb, and (2) the horizontal honeycomb. Tests were conducted by dropping the impact plate from three predetermined heights of 20, 30, and 40 cm. The following test procedure was followed for all cases.

Pre testing

1. The impact plate was first dropped from a height of 20, 30, and 40 cm without the presence of a test specimen. Three accelerations were recorded for each height and the average maximum acceleration served as the benchmark value.

Testing

2. A test specimen was placed on the base plate and secured using the 3-D printed attachment pieces. The impact plate was raised to 20 cm and dropped by manually releasing the string. Electronic triggering was not used.
3. Acceleration measurements were taken from before impact plate release until after acceleration response, including initial test piece impact and rebounding. For all cases, five seconds of test data was gathered.
4. This process was repeated five times for one test piece.
5. The test piece was repositioned and the process was repeated for 30 cm release height.
6. The process was repeated for 40 cm release height.

Testing groups

7. For consistency in data, one test piece was used for all three impact heights for both the vertical and honeycomb array.
8. Due to the difference in force thresholds for the honeycomb designs, two different impact plates (of different mass) were used for the horizontal and vertical arrays.

The smaller mass plate (~600g) was used for the horizontal arrays and the larger mass plate (~1800g) was used for the vertical array.

6.2 Data Analysis

The primary goal of impact testing was to evaluate the capability of the NS honeycombs to mitigate force transmitted to a system in high strain rate applications. To accomplish that goal it was sufficient to analyze the peak accelerations for each drop test. Peak accelerations were collected by recording the time history of acceleration with and without a test specimen and finding the maximum of each. Additionally, initial impact (not including secondary impacts resulting from rebound) was the focus of the drop testing; thus, only initial impact and recovery is plotted in the acceleration plots. The acceleration plots are shown below in Figures 6.3 - 6.8 where the red plots represent the benchmark acceleration recorded by dropping the impact plate directly on to the bottom plate without a NS honeycomb test specimen. Each of the blue plots represents one of the five drop tests conducted for a NS honeycomb test specimen, conducted according to the procedure described previously in this section. Not the large difference in scale between the red and blue plots for Figures 6.3 - 6.8.

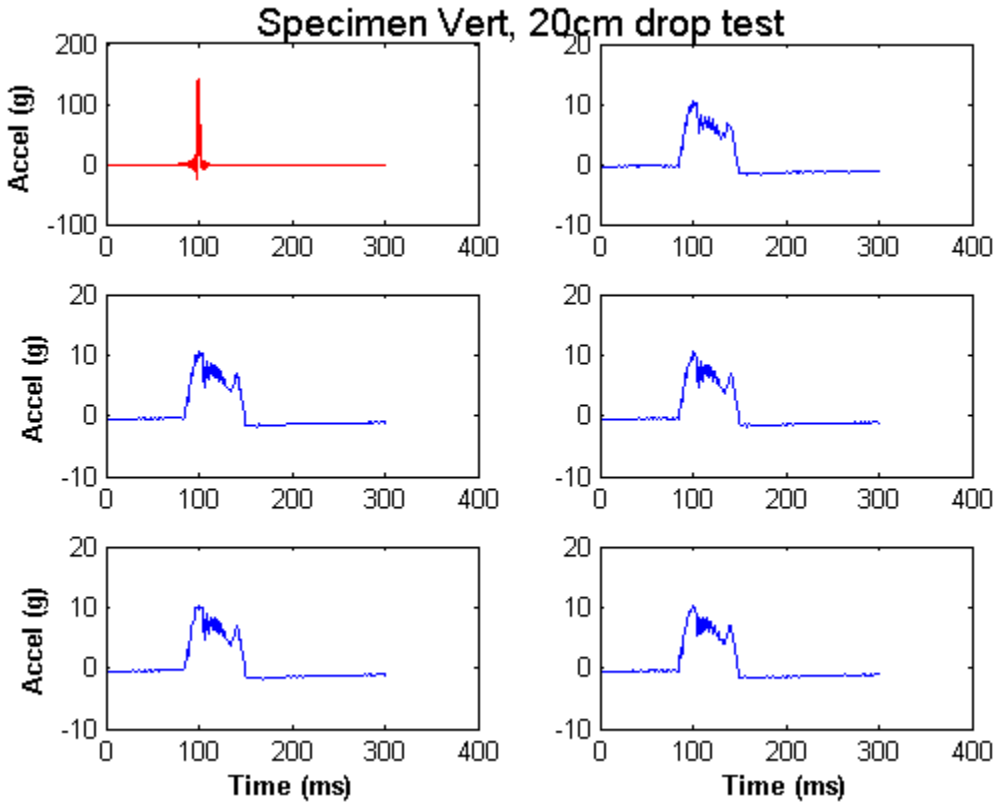

Figure 6.3: Benchmark acceleration of the impact plate without a NS honeycomb test specimen (red) and acceleration of the impact plate with a NS honeycomb test specimen (blue) for a 20 cm drop test of the vertical honeycomb test piece illustrated in Figure 4.2. The five blue plots illustrate repetitions of identical testing conditions.

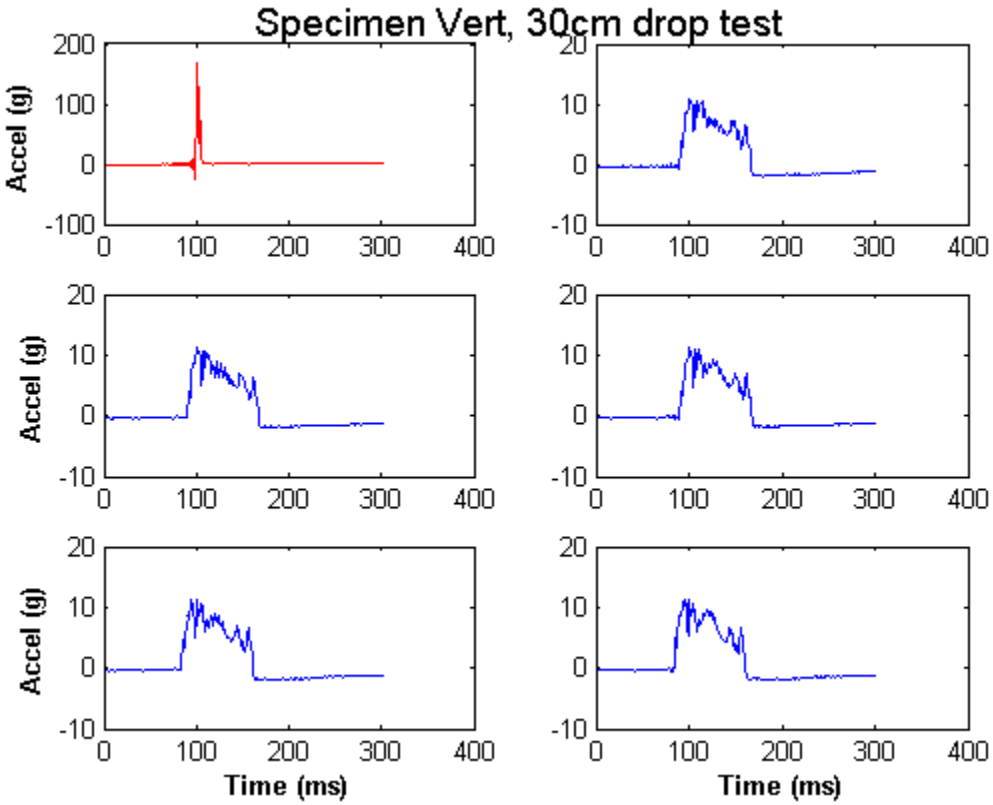

Figure 6.4: Benchmark acceleration of the impact plate without a NS honeycomb test specimen (red) and acceleration of the impact plate with a NS honeycomb test specimen (blue) for a 30 cm drop test of the vertical honeycomb test piece illustrated in Figure 4.2. The five blue plots illustrate repetitions of identical testing conditions.

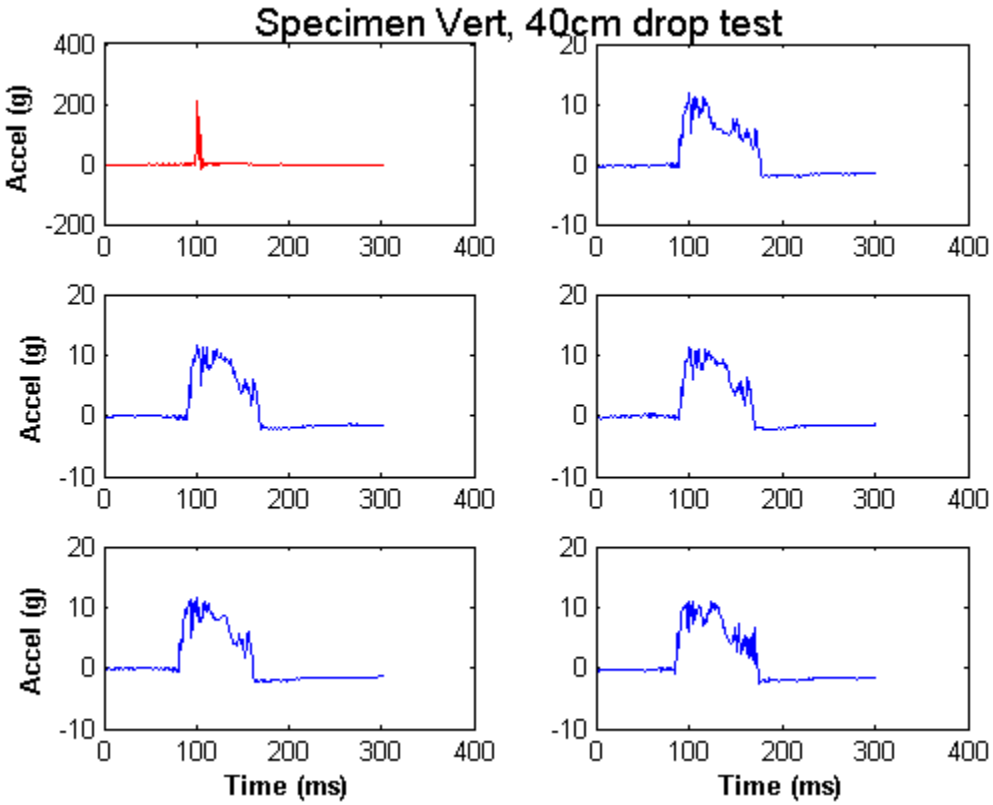

Figure 6.5: Benchmark acceleration of the impact plate without a NS honeycomb test specimen (red) and acceleration of the impact plate with a NS honeycomb test specimen (blue) for a 40 cm drop test of the vertical honeycomb test piece illustrated in Figure 4.2. The five blue plots illustrate repetitions of identical testing conditions.

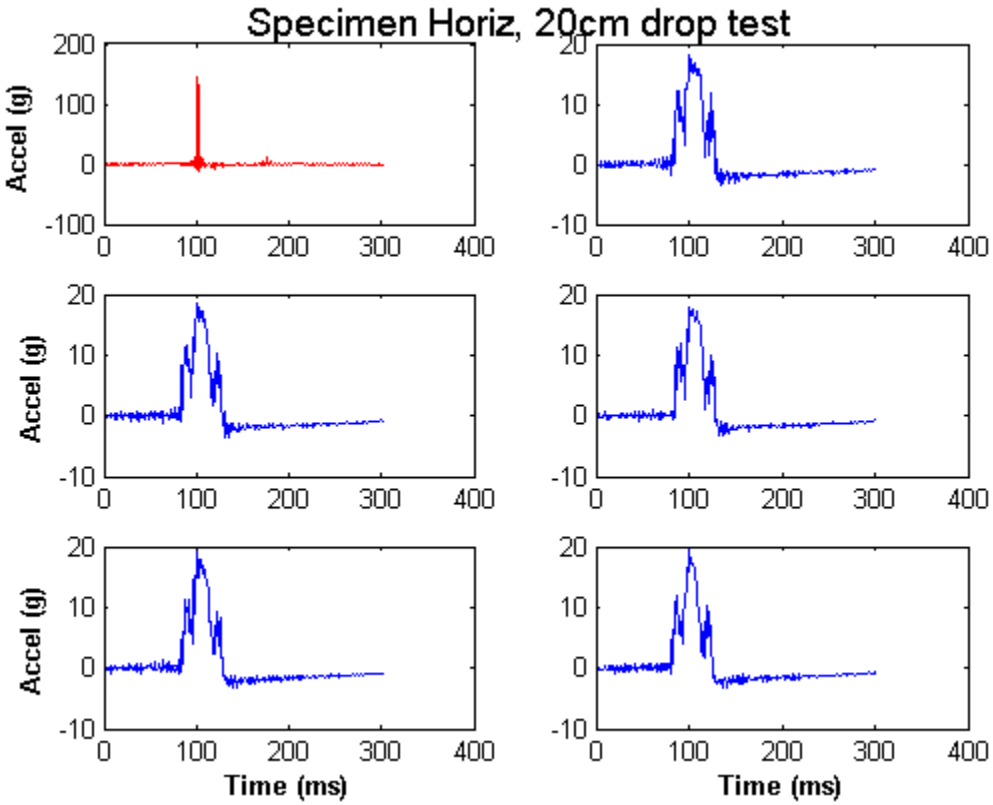

Figure 6.6: Benchmark acceleration of the impact plate without a NS honeycomb test specimen (red) and acceleration of the impact plate with a NS honeycomb test specimen (blue) for a 20 cm drop test of the horizontal honeycomb test piece illustrated in Figure 4.3. The five blue plots illustrate repetitions of identical testing conditions.

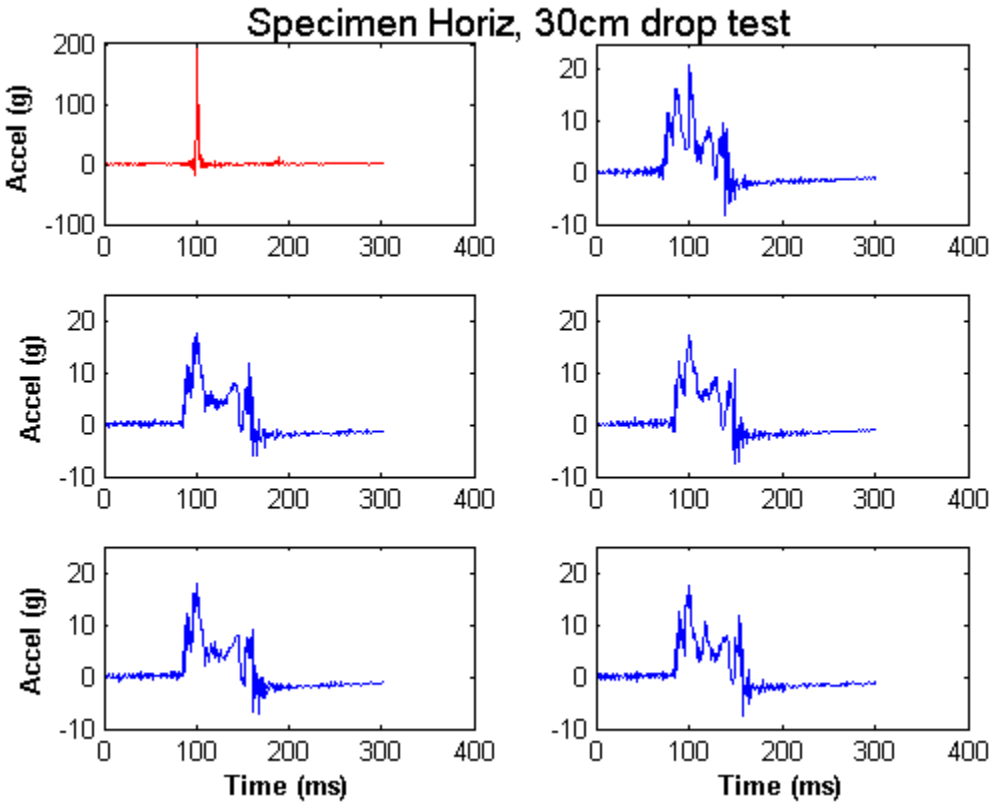

Figure 6.7: Benchmark acceleration of the impact plate without a NS honeycomb test specimen (red) and acceleration of the impact plate with a NS honeycomb test specimen (blue) for a 30 cm drop test of the horizontal honeycomb test piece illustrated in Figure 4.3. The five blue plots illustrate repetitions of identical testing conditions.

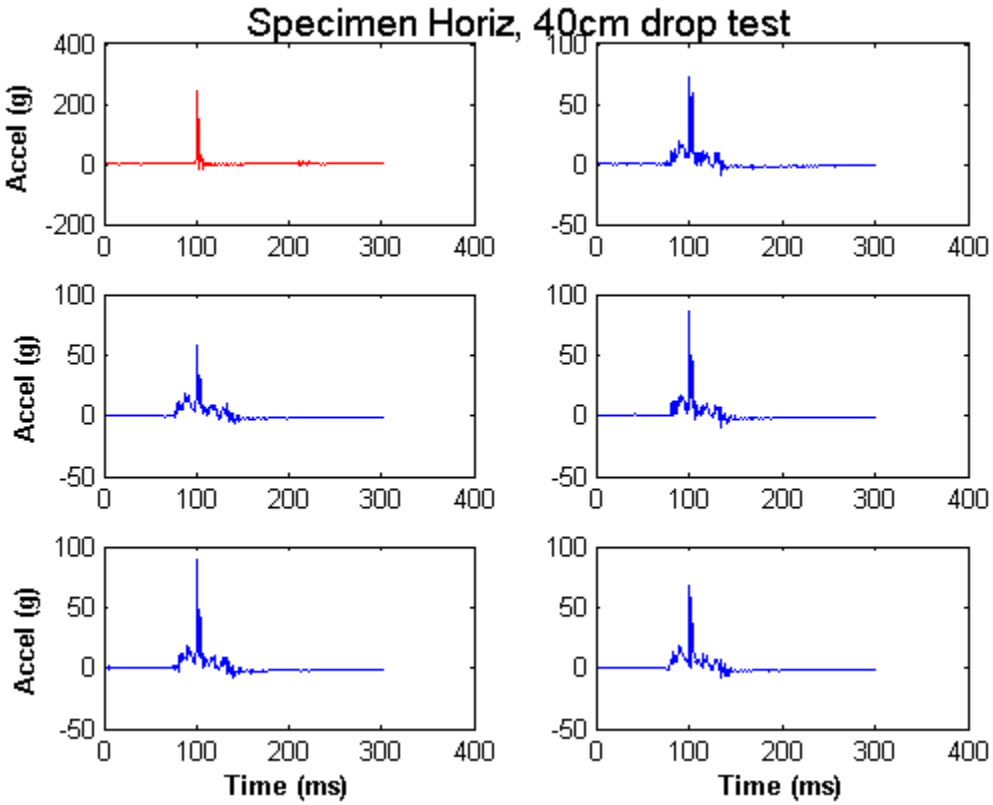

Figure 6.8: Benchmark acceleration of the impact plate without a NS honeycomb test specimen (red) and acceleration of the impact plate with a NS honeycomb test specimen (blue) for a 40 cm drop test of the horizontal honeycomb test piece illustrated in Figure 4.3. The five blue plots illustrate repetitions of identical testing conditions.

6.3 DATA ANALYSIS

6.3.1 High speed camera comparison

A high-speed camera was used to help assess the measured acceleration data collected on each of the test specimens. Selected images showing the complete range of motion show points of initial impact, beam snap through, and beam snap back. The stages of deformation captured by the high-speed camera are reflected in the recorded

acceleration data. Namely, peak accelerations occurred at approximately the same times as the honeycomb layers were visually observed to collapse (or recover). This behavior is reminiscent of the behavior observed in the quasi-static force-displacement testing.

Table 6.1: Phases during compression of vertical and horizontal honeycomb impact test.

	40 cm Vertical	30 cm Horizontal	
1	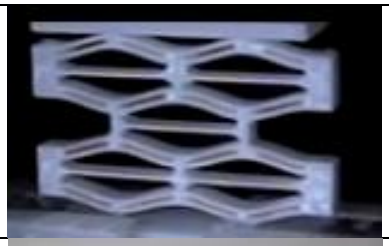		Test piece immediately prior to impact.
2			Test piece at first stage snap-through or peak acceleration.
3			Test piece at second stage snap-through or peak acceleration.
4			Test piece at third stage snap-through or peak acceleration.
5			Test piece at first stage snap-back.

Table 6.1 (continued)

6			Test piece at second stage snap-back.
7			Test piece at third stage snap-back.

Table 6.1 steps through the impact process for both the 40 cm vertical and 30 cm horizontal honeycombs. Each image displayed in Table 6.1 corresponds to acceleration peaks recorded in Figures 6.9 and 6.10 for the vertical and horizontal honeycomb tests, respectively.

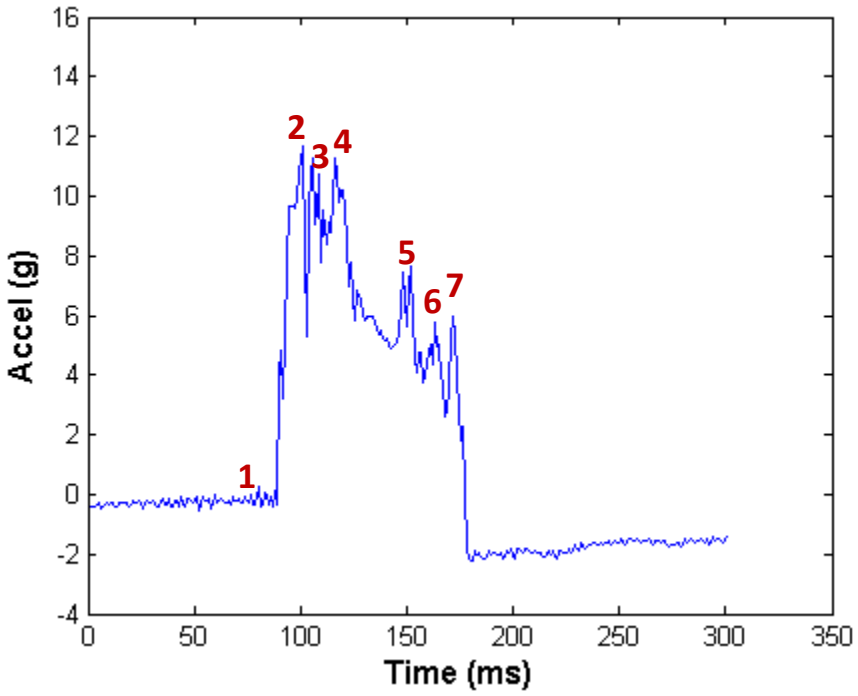

Figure 6.9: Acceleration versus time plot for 40 cm impact test of vertical honeycomb, with numbers corresponding to the stages illustrated in Table 6.1.

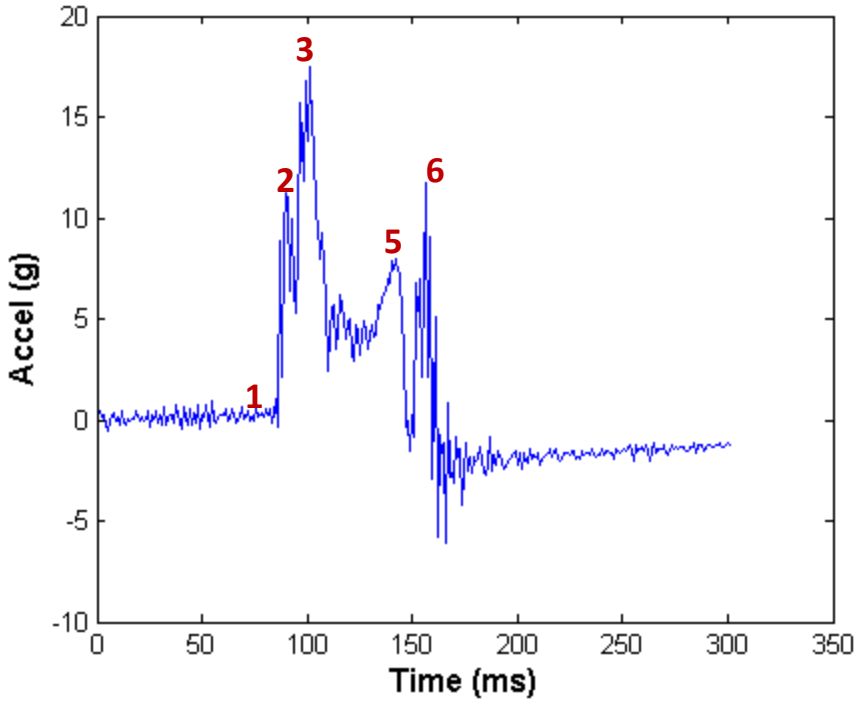

Figure 6.10: Acceleration versus time plot for 30cm impact test of horizontal honeycomb.

The analysis of high-speed camera images simultaneously with the acceleration data indicates that the peaks in the acceleration plot match important snap-through and recovery stages. For both the vertical and horizontal testing results, the recovery acceleration peaks exhibited lower amplitudes than the snap-through acceleration peaks. This can be viewed as a positive confirmation that the honeycomb designs removed some of the energy of the impact plate during impact. The peak acceleration ratios between snap-through and recovery (reference Figure 6.9) seem to be consistent, insinuating that each collapsed honeycomb stage participated equally in the energy absorption process.

6.3.2 Acceleration Threshold

The vertical and horizontal NS honeycombs were tested with a variety of different starting heights for the impact plate, to provide varying amounts of compression for the

honeycombs. Increasing compression causes an increasing number of NS honeycomb rows to "snap through." Table 6.2 explains briefly the effect of different starting heights on the behavior of the vertical NS honeycomb.

Table 6.2: Impact testing NS stage response results for various test heights. The number of stages noted for each figuration denotes the number of NS beam stages that "snapped through" during impact.

	20 cm	30 cm	40 cm
Vertical	1 stage	2 stages	3 stages
Horizontal	1 stage	2 stages	Bottom out

Although each impact height yielded varying amounts of honeycomb compression, the peak accelerations caused by the honeycombs remained consistent. This result of the impact testing is attributed to the plateau stress region in a honeycomb stress strain curve. The consistent peak accelerations observed for different inputs illustrates that the force threshold of the honeycomb is capped, until the compression exceeds the capacity of the honeycomb, which can be referred to as "bottoming out." The consistent peak acceleration of the falling mass for various inputs can be seen in Figures 6.12 and 6.13. The constant stress region of the honeycombs can also be interpreted as an acceleration threshold, meaning under usable conditions the accelerations imposed by the NS honeycomb will not exceed a certain value. The acceleration threshold values are visually represented in Figures 6.12 and 6.13 by green dashed lines.

None of the vertical honeycomb tests exceeded the energy absorption capacity as seen in Figure 6.12. Each test trial as seen in Figures 6.3 - 6.5 showed honeycomb compression below the compression limit and thus the energy threshold was never

exceeded. Conversely, the horizontal honeycomb testing results showed the effects of "bottoming out" for the 40 cm drop test as shown in Figure 6.13. For this case the honeycomb compressed fully, absorbing a portion of the impact energy, but the remaining energy was transferred through the honeycomb unaltered which caused a large acceleration spike. For a more detailed analysis of the "bottoming out" response, reference the acceleration plots shown in Figure 6.8.

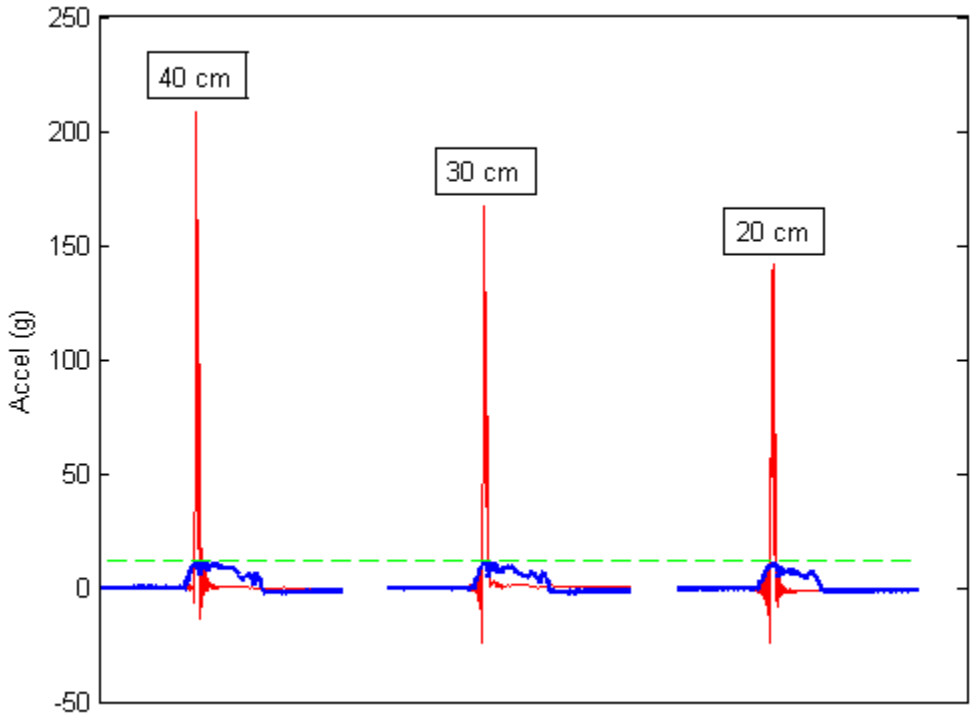

Figure 6.12: Vertical honeycomb accelerations (blue) compared to benchmark accelerations (red) for three heights. Peak accelerations imposed by the honeycomb are shown to be consistent as compared using the green dashed line.

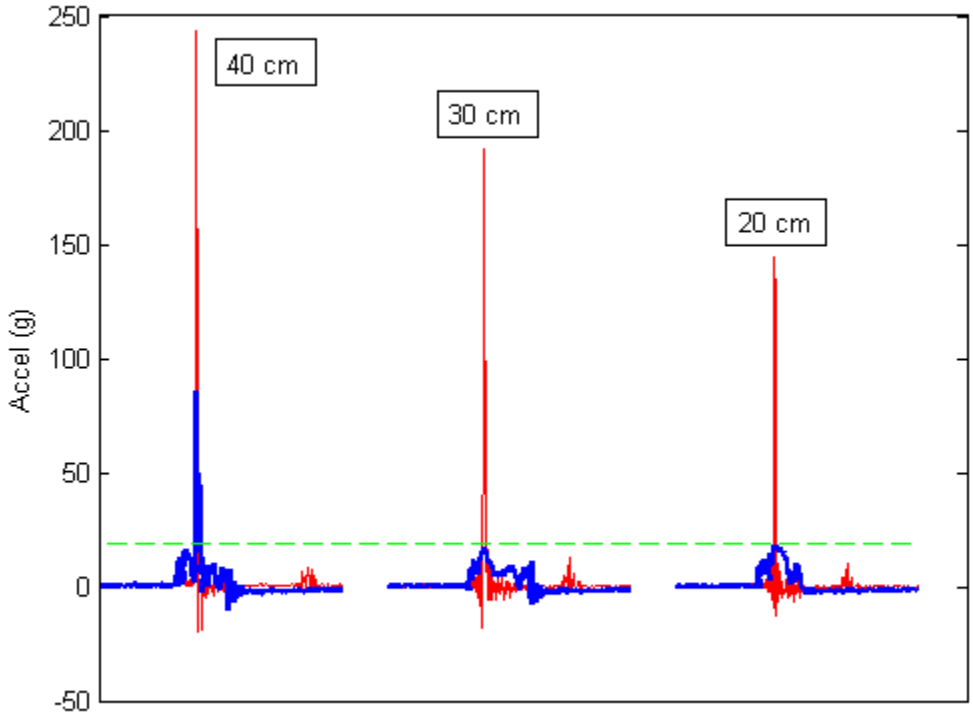

Figure 6.13: Horizontal honeycomb accelerations (blue) compared to benchmark accelerations (red) for three heights. Peak accelerations imposed by the honeycomb are shown to be consistent as compared using the green dashed line. Notice a large increase in acceleration for the 40 cm input, resulting from the "bottoming out" phenomenon.

6.3.3 Honeycomb recoverability

The main advantage of a NS honeycomb over a traditional honeycomb for impact applications is the recoverability of the NS honeycomb and its consistency over time. To measure the NS honeycomb design for consistency, five impact measurements were recorded for each design and each input height (20, 30, 40 cm), as plotted in Figures 6.3 - 6.8 and recorded in Tables 6.3 and 6.4. The maximum accelerations of the impact plate

for both the vertical and horizontal honeycomb tests were extremely consistent over each repetition. The only exception is the 40 cm horizontal honeycomb testing. This exception is a result of the "bottoming out" phenomenon during impact testing, which damaged the honeycomb.

Table 6.3: Vertical honeycomb impact test accelerations and calculations.

Specimen	Height (cm)	Peak Accel (g)	Avg Accel (g)	% of Input	% Input Avg
Benchmark	40	141.88			
Benchmark	40	143.04			
Benchmark	40	130.38	**138.44**		
Vert	40	10.49		7.57	
Vert	40	10.53		7.61	
Vert	40	10.51		7.59	
Vert	40	10.44		7.54	
Vert	40	10.29	**10.45**	7.44	**7.55**
Benchmark	30	160.34			
Benchmark	30	187.88			
Benchmark	30	167.21	**171.81**		
Vert	30	10.93		6.36	
Vert	30	11.35		6.61	
Vert	30	11.39		6.63	
Vert	30	11.27		6.56	
Vert	30	11.41	**11.27**	6.64	**6.56**
Benchmark	20	168.03			
Benchmark	20	220.59			
Benchmark	20	207.89	**198.84**		
Vert	20	11.68		5.88	
Vert	20	11.47		5.77	
Vert	20	11.35		5.71	
Vert	20	11.59		5.83	
Vert	20	11.06	**11.43**	5.56	**5.75**

Table 6.4: Horizontal honeycomb impact test accelerations and calculations.

Specimen	Height (cm)	Peak Accel (g)	Avg Accel (g)	% of Input	% Input Avg
Benchmark	40	243.12			
Benchmark	40	216.65			
Benchmark	40	228.54	**229.44**		
Horiz	40	72.68		31.68	
Horiz	40	57.84		25.21	
Horiz	40	85.75		37.38	
Horiz	40	89.82		39.15	
Horiz	40	68.52	**74.92**	29.87	**32.66**
Benchmark	30	191.55			
Benchmark	30	189.65			
Benchmark	30	169.22	**183.48**		
Horiz	30	21.02		11.46	
Horiz	30	17.46		9.52	
Horiz	30	16.97		9.25	
Horiz	30	17.84		9.72	
Horiz	30	17.34	**17.12**	9.45	**9.88**
Benchmark	20	144.73			
Benchmark	20	183.12			
Benchmark	20	177.32	**168.39**		
Horiz	20	18.27		10.85	
Horiz	20	18.51		11	
Horiz	20	17.82		10.58	
Horiz	20	19.19		11.4	
Horiz	20	19.37	**18.64**	11.51	**11.07**

Tables 6.3 and 6.4 also document the percent of the benchmark acceleration recorded by the honeycomb designs. Excluding accelerations recorded during "bottoming

out," both NS honeycomb designs reduced benchmark accelerations by at least 80 percent.

For a good comparison of high acceleration inputs on NS beam elements, the acceleration reduction seen in the work of Fulcher *et al.*, is useful to review the results provided in reference [2]. Direct comparison of results is not possible because the work of Fulcher was dedicated to the development of NS beam elements not necessarily as a part of honeycomb arrays. Fulcher reported an unfiltered reduction of more than 90 percent which is shown in Figure 6.14.

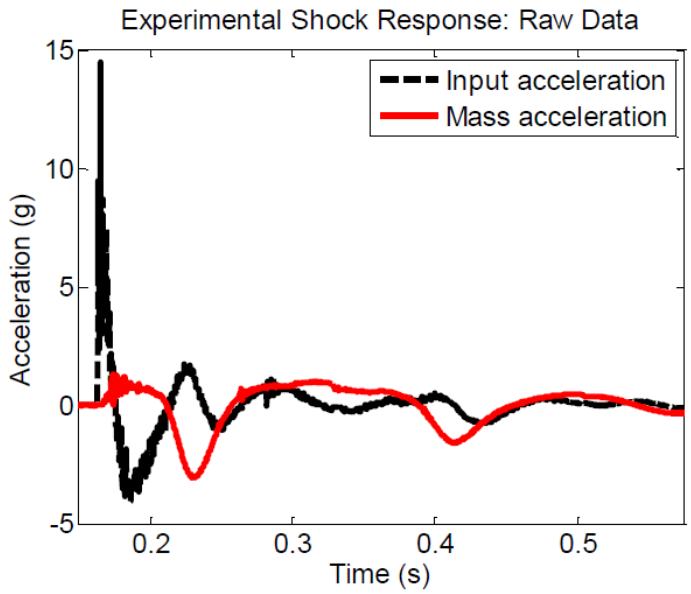

Figure 6.14: Acceleration reduction for NS beam system as shown by Fulcher [2].

The input accelerations seen in this work are much higher than those utilized in Fulcher's work, but the relative acceleration reduction is very similar, suggesting that the NS beam elements perform as designed for impact loads even in honeycomb configurations.

Chapter 7: Conclusion

7.1 SUMMARY

The research presented in this thesis is dedicated to the further analysis and evaluation of negative stiffness honeycombs by expanding the understanding of impact loading capabilities. Negative stiffness honeycombs are a relatively unexplored engineering technology that implements negative stiffness elements in the form of curved beams as unit cells in a periodic honeycomb matrix. Prefabricated negative stiffness beams function as passive non-linear spring elements and are excellent alternatives to active spring-damper systems. When multiple negative stiffness beams are combined in a matrix or honeycomb, the combined product is a very efficient, recoverable energy absorber. Negative stiffness honeycombs can be easily tunable to remain rigid under low stress conditions, and designed to collapse at an optimal stress threshold providing for long plateau stress regions for a large range of strain. Contrary to most sacrificial honeycombs, the "snap-back" nature of negative stiffness honeycombs enables recovery and reusability of the honeycomb after impact.

Much of the previous research conducted on negative stiffness elements and negative stiffness honeycombs was discussed in Chapter 2. Most applications of negative stiffness elements use precompressed buckled beams. Precompressed beams have been shown to provide significant force mitigation, but it is challenging to implement in honeycomb configurations. The prefabricated curved beam was developed to mirror the behavior of precompressed beams and remain simple to use in honeycombs. Relevant to honeycomb applications, prefabricated curved beams are heavily affected by end conditions and require rigid end constraints for optimal energy absorption. When the prefabricated beams are organized into a honeycomb matrix, the beams function as a set

of parallel and series elements; all beams in one row work in parallel and "snap-through" uniformly at one force threshold, and beams stacked in series increase the honeycomb displacement for the constant force threshold. Honeycomb effectiveness can be determined by calculating the energy absorption which is represented by the area under the force-displacement curve. In previous research, the negative stiffness honeycomb design was tested quasi-statically for comparison between analytical models, finite element analysis, and experimental data.

In addition to quasi-static analysis, impact response of honeycombs is necessary for better understanding of honeycomb effectiveness. Negative stiffness honeycombs respond differently under impact loads due to elevated strain rates and strain hardening effects. Increased strain rate loading and strain hardening both contribute to elevated stress in honeycombs. To evaluate the response of honeycombs under high strain rate impacts, an impact rig was constructed and used for drop testing.

Chapter 3 focused on the construction and specifics of the drop testing impact apparatus, which was constructed from an aluminum frame, with two vertical guide posts on which a polyethylene impact plate was able to move vertically. Data recording was implemented using PCB accelerometers and a LabView DAQ system. The impact apparatus enabled multiple types of honeycombs to be tested from multiple heights.

The honeycomb models used for static and impact testing were presented in Chapter 4. Vertical and horizontal honeycomb arrays were identified. The horizontal honeycomb unit design and its design metrics were introduced in this work; whereas the vertical honeycomb was an adaptation from the work of previous authors. Multiple horizontal honeycomb designs made from various configurations of the horizontal unit design were presented. The results of FEA modeling of the horizontal honeycomb were compared to the vertical honeycomb FEA results of previous work. The two models

predicted similar force-displacement properties but different expected force thresholds. FEA modeling limitations of honeycomb compression of the horizontal honeycomb were discussed.

Chapter 5 discussed the results of quasi-static testing for the vertical and horizontal honeycombs. The vertical honeycombs were tested in previous work, and the results were briefly shown for comparison with the horizontal honeycomb. As predicted by FEA analysis, the horizontal honeycombs were shown to have lower force thresholds than the vertical honeycomb and less efficient energy absorption. The quasi-static testing results were compared relative to volumetric displacement.

The most important contributions of this work are the impact testing results, which were shown in Chapter 6. Both the vertical and horizontal honeycomb designs were tested for impact response using the impact testing apparatus. The honeycombs were tested at three different drop heights for acceleration response over time, and peak accelerations were used for honeycomb comparison. Varying layers of compression were seen by the honeycombs for different input heights; for the largest test input height, the vertical honeycomb collapsed three layers and the horizontal honeycomb "bottomed-out." Analysis of peak accelerations exhibited by the honeycombs revealed an acceleration threshold for each honeycomb design. All honeycomb peak accelerations remained below the acceleration threshold with the exception of horizontal honeycombs that "bottomed-out." Many drop tests were conducted and the honeycombs remained very consistent. On average honeycombs reduced input acceleration by approximately 90 percent, which was consistent with previous findings on precompressed negative stiffness beams.

7.2 FUTURE WORK

The findings presented in this thesis provide an improved understanding of negative stiffness honeycombs, but there are lingering questions as to the honeycombs' full capacity. Knowledge of negative stiffness honeycombs could be advanced in three areas.

First, a better capacity for FEA modeling of negative stiffness honeycombs is very important to the future application of honeycombs. It is impractical to expect to build working prototypes for every honeycomb application because this process is tedious and expensive. FEA modeling is effective in many engineering fields for fast and inexpensive model analysis, and could provide critical support to the development of negative stiffness honeycomb design. Of course FEA models need to be accurate representations of physical models in order to replace physical prototypes during the design process. As shown in Chapter 4, FEA modeling of negative stiffness beam deflection often deviates from physical models. A better understanding of beam end constraints and beam buckling and twisting motion can help model accuracy, but the implementation of FEA modeling in this thesis is not sufficiently accurate to be a reliable model replacement.

Second, honeycomb modeling can be expanded by understanding the relationship between volume and energy absorption for negative stiffness honeycombs. Static analysis of the two honeycomb types as shown in Chapter 5 alluded to a linear relationship between honeycomb volume and observed energy absorption. The data collected in this thesis certainly do not encompass a large enough design space to identify any mathematical model relating build volume and energy absorption, but further testing of different design configurations could lead to predictable relationships. Testing could be

expanded to both multiple vertical and horizontal designs as well as new honeycomb designs that combine the two structures.

Third, more developed impact testing of honeycombs would be helpful to more fully understand the effects of high strain rate impacts. The impact test results found in this work report upon the relative effectiveness of a honeycomb during impact loading compared to impacts without the presence of a honeycomb. While the accelerations recorded show good potential for energy absorption under impact loads, force-displacement analysis would be better. Future impact testing should implement displacement measurements of honeycomb compression and load cell measurements of force at the base of the honeycomb during impact in order to obtain force information as a function of honeycomb compression, leading directly to force-displacement plots and energy absorption calculations. With force-displacement diagrams during impact, direct comparisons can be made to quasi-static loading and change in energy absorption for different impact velocities.

Appendix

A. COMSOL M-FILE

```
function out = model
%
% four_point_balanced_V3.m
%
% Model exported on May 4 2015, 16:19 by COMSOL 4.4.0.195.

import com.comsol.model.*
import com.comsol.model.util.*

model = ModelUtil.create('Model');

model.modelPath('Z:\Documents\Thesis\COMSOL');

model.modelNode.create('mod1');

model.geom.create('geom1', 3);

model.mesh.create('mesh1', 'geom1');

model.physics.create('solid', 'SolidMechanics', 'geom1');

model.geom('geom1').lengthUnit('mm');
model.geom('geom1').feature.create('imp1', 'Import');
model.geom('geom1').feature('imp1').set('filename',
'\\austin.utexas.edu\disk\engrstu\me\ksb2258\Documents\Thesis\COMSOL\fo
ur_point_balanced_V3.IGS');
model.geom('geom1').feature('imp1').importData;
model.geom('geom1').run;

model.material.create('mat1');
model.material('mat1').name('Acrylic plastic');
model.material('mat1').set('family', 'custom');
model.material('mat1').set('lighting', 'phong');
model.material('mat1').set('fresnel', 0.5);
model.material('mat1').set('roughness', 0.1);
model.material('mat1').set('specular', 'custom');
model.material('mat1').set('customspecular', [0.9803921568627451
0.9803921568627451 0.9803921568627451]);
model.material('mat1').set('diffuse', 'custom');
model.material('mat1').set('customdiffuse', [0.39215686274509803
0.7843137254901961 0.39215686274509803]);
model.material('mat1').set('ambient', 'custom');
```

```
model.material('mat1').set('customambient', [0.39215686274509803
0.7843137254901961 0.39215686274509803]);
model.material('mat1').set('shininess', 1000);
model.material('mat1').propertyGroup('def').set('thermalexpansioncoeffi
cient', '7.0e-5[1/K]');
model.material('mat1').propertyGroup('def').set('heatcapacity',
'1470[J/(kg*K)]');
model.material('mat1').propertyGroup('def').set('density',
'1190[kg/m^3]');
model.material('mat1').propertyGroup('def').set('thermalconductivity',
'0.18[W/(m*K)]');
model.material('mat1').propertyGroup.create('Enu', 'Young''s modulus
and Poisson''s ratio');
model.material('mat1').propertyGroup('Enu').set('poissonsratio',
'0.35');
model.material('mat1').propertyGroup('Enu').set('youngsmodulus',
'3.2e9[Pa]');
model.material('mat1').set('family', 'custom');
model.material('mat1').set('lighting', 'phong');
model.material('mat1').set('fresnel', 0.5);
model.material('mat1').set('roughness', 0.1);
model.material('mat1').set('specular', 'custom');
model.material('mat1').set('customspecular', [0.9803921568627451
0.9803921568627451 0.9803921568627451]);
model.material('mat1').set('diffuse', 'custom');
model.material('mat1').set('customdiffuse', [0.39215686274509803
0.7843137254901961 0.39215686274509803]);
model.material('mat1').set('ambient', 'custom');
model.material('mat1').set('customambient', [0.39215686274509803
0.7843137254901961 0.39215686274509803]);
model.material('mat1').set('shininess', 1000);

model.mesh('mesh1').feature.create('ftet1', 'FreeTet');
model.mesh('mesh1').run;

model.physics('solid').feature.create('fix1', 'Fixed', 2);
model.physics('solid').feature('fix1').selection.set([24]);
model.physics('solid').feature.create('disp1', 'Displacement3', 3);
model.physics('solid').feature.remove('disp1');
model.physics('solid').feature.create('disp1', 'Displacement2', 2);
model.physics('solid').feature('disp1').selection.set([2]);
model.physics('solid').feature('disp1').set('Direction', 2, '1');
model.physics('solid').feature('disp1').set('U0', 2, '.015');

model.study.create('std1');
model.study('std1').feature.create('stat', 'Stationary');
model.study('std1').feature('stat').activate('solid', true);

model.sol.create('sol1');
model.sol('sol1').study('std1');
model.sol('sol1').feature.create('st1', 'StudyStep');
model.sol('sol1').feature('st1').set('study', 'std1');
```

```
model.sol('sol1').feature('st1').set('studystep', 'stat');
model.sol('sol1').feature.create('v1', 'Variables');
model.sol('sol1').feature('v1').set('control', 'stat');
model.sol('sol1').feature.create('s1', 'Stationary');
model.sol('sol1').feature('s1').feature.create('fc1', 'FullyCoupled');
model.sol('sol1').feature('s1').feature.remove('fcDef');
model.sol('sol1').attach('std1');

model.result.create('pg1', 3);
model.result('pg1').set('data', 'dset1');
model.result('pg1').feature.create('surf1', 'Surface');
model.result('pg1').feature('surf1').set('expr', {'solid.mises'});
model.result('pg1').name('Stress (solid)');
model.result('pg1').feature('surf1').feature.create('def', 'Deform');
model.result('pg1').feature('surf1').feature('def').set('expr', {'u'
'v' 'w'});
model.result('pg1').feature('surf1').feature('def').set('descr',
'Displacement field (Material)');

model.name('four_point_balanced_V3.mph');

model.sol('sol1').study('std1');
model.sol('sol1').feature.remove('s1');
model.sol('sol1').feature.remove('v1');
model.sol('sol1').feature.remove('st1');
model.sol('sol1').feature.create('st1', 'StudyStep');
model.sol('sol1').feature('st1').set('study', 'std1');
model.sol('sol1').feature('st1').set('studystep', 'stat');
model.sol('sol1').feature.create('v1', 'Variables');
model.sol('sol1').feature('v1').set('control', 'stat');
model.sol('sol1').feature.create('s1', 'Stationary');
model.sol('sol1').feature('s1').feature.create('fc1', 'FullyCoupled');
model.sol('sol1').feature('s1').feature.remove('fcDef');
model.sol('sol1').attach('std1');
model.sol('sol1').runAll;

model.result('pg1').run;

model.param.set('D', '0.016 [m]');
model.param.set('ND', '0');

model.physics('solid').feature('disp1').set('U0', 2, 'ND*D');

model.study('std1').feature('stat').set('useparam', 'on');
model.study('std1').feature('stat').setIndex('pname', 'D', 0);
model.study('std1').feature('stat').setIndex('plistarr', '', 0);
model.study('std1').feature('stat').setIndex('pname', 'D', 0);
model.study('std1').feature('stat').setIndex('plistarr', '', 0);
model.study('std1').feature('stat').setIndex('pname', 'ND', 0);
model.study('std1').feature('stat').setIndex('plistarr',
'range(0,0.01,1)', 0);
```

```
model.sol('sol1').study('std1');
model.sol('sol1').feature.remove('s1');
model.sol('sol1').feature.remove('v1');
model.sol('sol1').feature.remove('st1');
model.sol('sol1').feature.create('st1', 'StudyStep');
model.sol('sol1').feature('st1').set('study', 'std1');
model.sol('sol1').feature('st1').set('studystep', 'stat');
model.sol('sol1').feature.create('v1', 'Variables');
model.sol('sol1').feature('v1').set('control', 'stat');
model.sol('sol1').feature.create('s1', 'Stationary');
model.sol('sol1').feature('s1').feature.create('p1', 'Parametric');
model.sol('sol1').feature('s1').feature.remove('pDef');
model.sol('sol1').feature('s1').feature('p1').set('control', 'stat');
model.sol('sol1').feature('s1').set('control', 'stat');
model.sol('sol1').feature('s1').feature.create('fc1', 'FullyCoupled');
model.sol('sol1').feature('s1').feature.remove('fcDef');
model.sol('sol1').attach('std1');

model.study('std1').feature('stat').set('geometricNonlinearity', 'on');

model.sol('sol1').study('std1');
model.sol('sol1').feature.remove('s1');
model.sol('sol1').feature.remove('v1');
model.sol('sol1').feature.remove('st1');
model.sol('sol1').feature.create('st1', 'StudyStep');
model.sol('sol1').feature('st1').set('study', 'std1');
model.sol('sol1').feature('st1').set('studystep', 'stat');
model.sol('sol1').feature.create('v1', 'Variables');
model.sol('sol1').feature('v1').set('control', 'stat');
model.sol('sol1').feature.create('s1', 'Stationary');
model.sol('sol1').feature('s1').feature.create('p1', 'Parametric');
model.sol('sol1').feature('s1').feature.remove('pDef');
model.sol('sol1').feature('s1').feature('p1').set('control', 'stat');
model.sol('sol1').feature('s1').set('control', 'stat');
model.sol('sol1').feature('s1').feature.create('fc1', 'FullyCoupled');
model.sol('sol1').feature('s1').feature.remove('fcDef');
model.sol('sol1').attach('std1');

model.physics('solid').feature.create('roll1', 'Roller', 2);
model.physics('solid').feature('roll1').selection.set([9 13 17 21 153
154 155 156]);

model.material.create('mat2');
model.material.remove('mat1');
model.material.remove('mat2');
model.material.create('mat1');
model.material('mat1').propertyGroup('def').set('youngsmodulus',
{'1.4e9'});
model.material('mat1').propertyGroup('def').set('poissonsratio',
{'.33'});
model.material('mat1').propertyGroup('def').set('density', {'1040'});
```

```
model.sol('sol1').study('std1');
model.sol('sol1').feature.remove('s1');
model.sol('sol1').feature.remove('v1');
model.sol('sol1').feature.remove('st1');
model.sol('sol1').feature.create('st1', 'StudyStep');
model.sol('sol1').feature('st1').set('study', 'std1');
model.sol('sol1').feature('st1').set('studystep', 'stat');
model.sol('sol1').feature.create('v1', 'Variables');
model.sol('sol1').feature('v1').set('control', 'stat');
model.sol('sol1').feature.create('s1', 'Stationary');
model.sol('sol1').feature('s1').feature.create('p1', 'Parametric');
model.sol('sol1').feature('s1').feature.remove('pDef');
model.sol('sol1').feature('s1').feature('p1').set('control', 'stat');
model.sol('sol1').feature('s1').set('control', 'stat');
model.sol('sol1').feature('s1').feature.create('fc1', 'FullyCoupled');
model.sol('sol1').feature('s1').feature.remove('fcDef');
model.sol('sol1').attach('std1');
model.sol('sol1').runAll;

model.result('pg1').run;
model.result('pg1').run;
model.result('pg1').run;
model.result('pg1').run;
model.result('pg1').run;
model.result('pg1').run;
model.result.report.create('rpt1', 'Report');
model.result.report('rpt1').set('level', 'complete');
model.result.report('rpt1').feature.create('tp1', 'TitlePage');
model.result.report('rpt1').feature.create('toc1', 'TableOfContents');
model.result.report('rpt1').feature.create('sec1', 'Section');
model.result.report('rpt1').feature('sec1').set('source', 'custom');
model.result.report('rpt1').feature('sec1').set('heading', 'Global
Definitions');
model.result.report('rpt1').feature('sec1').feature.create('sec1',
'Section');
model.result.report('rpt1').feature('sec1').feature('sec1').set('source
', 'firstchild');
model.result.report('rpt1').feature('sec1').feature('sec1').set('headin
g', 'Parameters');
model.result.report('rpt1').feature('sec1').feature('sec1').feature.cre
ate('param1', 'Parameter');
model.result.report('rpt1').feature.create('sec2', 'Section');
model.result.report('rpt1').feature('sec2').set('source', 'custom');
model.result.report('rpt1').feature('sec2').set('heading', 'Model 1
(mod1)');
model.result.report('rpt1').feature('sec2').feature.create('sec1',
'Section');
model.result.report('rpt1').feature('sec2').feature('sec1').set('source
', 'custom');
model.result.report('rpt1').feature('sec2').feature('sec1').set('headin
g', 'Definitions');
```

```
model.result.report('rpt1').feature('sec2').feature('sec1').feature.cre
ate('sec1', 'Section');
model.result.report('rpt1').feature('sec2').feature('sec1').feature('se
c1').set('source', 'custom');
model.result.report('rpt1').feature('sec2').feature('sec1').feature('se
c1').set('heading', 'Coordinate Systems');
model.result.report('rpt1').feature('sec2').feature('sec1').feature('se
c1').feature.create('sec1', 'Section');
model.result.report('rpt1').feature('sec2').feature('sec1').feature('se
c1').feature('sec1').set('source', 'firstchild');
model.result.report('rpt1').feature('sec2').feature('sec1').feature('se
c1').feature('sec1').set('heading', 'Boundary System 1');
model.result.report('rpt1').feature('sec2').feature('sec1').feature('se
c1').feature('sec1').feature.create('csys1', 'CoordinateSystem');
model.result.report('rpt1').feature('sec2').feature('sec1').feature('se
c1').feature('sec1').feature('csys1').set('noderef', 'sys1');
model.result.report('rpt1').feature('sec2').feature.create('sec2',
'Section');
model.result.report('rpt1').feature('sec2').feature('sec2').set('source
', 'firstchild');
model.result.report('rpt1').feature('sec2').feature('sec2').set('headin
g', 'Geometry 1');
model.result.report('rpt1').feature('sec2').feature('sec2').feature.cre
ate('geom1', 'Geometry');
model.result.report('rpt1').feature('sec2').feature('sec2').feature('ge
om1').set('noderef', 'geom1');
model.result.report('rpt1').feature('sec2').feature.create('sec3',
'Section');
model.result.report('rpt1').feature('sec2').feature('sec3').set('source
', 'custom');
model.result.report('rpt1').feature('sec2').feature('sec3').set('headin
g', 'Materials');
model.result.report('rpt1').feature('sec2').feature('sec3').feature.cre
ate('sec1', 'Section');
model.result.report('rpt1').feature('sec2').feature('sec3').feature('se
c1').set('source', 'firstchild');
model.result.report('rpt1').feature('sec2').feature('sec3').feature('se
c1').set('heading', 'Material 1');
model.result.report('rpt1').feature('sec2').feature('sec3').feature('se
c1').feature.create('mat1', 'Material');
model.result.report('rpt1').feature('sec2').feature('sec3').feature('se
c1').feature('mat1').set('noderef', 'mat1');
model.result.report('rpt1').feature('sec2').feature.create('sec4',
'Section');
model.result.report('rpt1').feature('sec2').feature('sec4').set('source
', 'custom');
model.result.report('rpt1').feature('sec2').feature('sec4').set('headin
g', 'Solid Mechanics (solid)');
model.result.report('rpt1').feature('sec2').feature('sec4').feature.cre
ate('phys1', 'Physics');
model.result.report('rpt1').feature('sec2').feature('sec4').feature('ph
ys1').set('noderef', 'solid');
```

```
model.result.report('rpt1').feature('sec2').feature.create('sec5',
'Section');
model.result.report('rpt1').feature('sec2').feature('sec5').set('source
', 'firstchild');
model.result.report('rpt1').feature('sec2').feature('sec5').set('headin
g', 'Mesh 1');
model.result.report('rpt1').feature('sec2').feature('sec5').feature.cre
ate('mesh1', 'Mesh');
model.result.report('rpt1').feature('sec2').feature('sec5').feature('me
sh1').set('noderef', 'mesh1');
model.result.report('rpt1').feature.create('sec3', 'Section');
model.result.report('rpt1').feature('sec3').set('source', 'custom');
model.result.report('rpt1').feature('sec3').set('heading', 'Study 1');
model.result.report('rpt1').feature('sec3').feature.create('std1',
'Study');
model.result.report('rpt1').feature('sec3').feature('std1').set('nodere
f', 'std1');
model.result.report('rpt1').feature('sec3').feature.create('sec1',
'Section');
model.result.report('rpt1').feature('sec3').feature('sec1').set('source
', 'custom');
model.result.report('rpt1').feature('sec3').feature('sec1').set('headin
g', 'Solver Configurations');
model.result.report('rpt1').feature('sec3').feature('sec1').feature.cre
ate('sec1', 'Section');
model.result.report('rpt1').feature('sec3').feature('sec1').feature('se
c1').set('source', 'firstchild');
model.result.report('rpt1').feature('sec3').feature('sec1').feature('se
c1').set('heading', 'Solver 1');
model.result.report('rpt1').feature('sec3').feature('sec1').feature('se
c1').feature.create('sol1', 'Solver');
model.result.report('rpt1').feature('sec3').feature('sec1').feature('se
c1').feature('sol1').set('noderef', 'sol1');
model.result.report('rpt1').feature.create('sec4', 'Section');
model.result.report('rpt1').feature('sec4').set('source', 'custom');
model.result.report('rpt1').feature('sec4').set('heading', 'Results');
model.result.report('rpt1').feature('sec4').feature.create('sec1',
'Section');
model.result.report('rpt1').feature('sec4').feature('sec1').set('source
', 'custom');
model.result.report('rpt1').feature('sec4').feature('sec1').set('headin
g', 'Data Sets');
model.result.report('rpt1').feature('sec4').feature('sec1').feature.cre
ate('sec1', 'Section');
model.result.report('rpt1').feature('sec4').feature('sec1').feature('se
c1').set('source', 'firstchild');
model.result.report('rpt1').feature('sec4').feature('sec1').feature('se
c1').set('heading', 'Solution 1');
model.result.report('rpt1').feature('sec4').feature('sec1').feature('se
c1').feature.create('dset1', 'DataSet');
model.result.report('rpt1').feature('sec4').feature('sec1').feature('se
c1').feature('dset1').set('noderef', 'dset1');
```

```
model.result.report('rpt1').feature('sec4').feature.create('sec2',
'Section');
model.result.report('rpt1').feature('sec4').feature('sec2').set('source
', 'custom');
model.result.report('rpt1').feature('sec4').feature('sec2').set('headin
g', 'Plot Groups');
model.result.report('rpt1').feature('sec4').feature('sec2').feature.cre
ate('sec1', 'Section');
model.result.report('rpt1').feature('sec4').feature('sec2').feature('se
c1').set('source', 'firstchild');
model.result.report('rpt1').feature('sec4').feature('sec2').feature('se
c1').set('heading', 'Stress (solid)');
model.result.report('rpt1').feature('sec4').feature('sec2').feature('se
c1').feature.create('pg1', 'PlotGroup');
model.result.report('rpt1').feature('sec4').feature('sec2').feature('se
c1').feature('pg1').set('noderef', 'pg1');
model.result.report.remove('rpt1');
model.result.dataset.create('dset2', 'Solution');
model.result.dataset.remove('dset2');
model.result.create('pg2', 'PlotGroup1D');
model.result('pg2').run;
model.result('pg2').feature.create('lngr1', 'LineGraph');
model.result('pg2').feature('lngr1').set('data', 'dset1');
model.result('pg2').run;
model.result.remove('pg2');
model.result('pg1').run;
model.result('pg1').run;
model.result('pg1').run;

model.name('four_point_balanced_V3.mph');

model.result('pg1').run;

model.physics('solid').feature('roll1').selection.set([1 5 9 13 151 152
153 154]);

model.sol('sol1').study('std1');
model.sol('sol1').feature.remove('s1');
model.sol('sol1').feature.remove('v1');
model.sol('sol1').feature.remove('st1');
model.sol('sol1').feature.create('st1', 'StudyStep');
model.sol('sol1').feature('st1').set('study', 'std1');
model.sol('sol1').feature('st1').set('studystep', 'stat');
model.sol('sol1').feature.create('v1', 'Variables');
model.sol('sol1').feature('v1').set('control', 'stat');
model.sol('sol1').feature.create('s1', 'Stationary');
model.sol('sol1').feature('s1').feature.create('p1', 'Parametric');
model.sol('sol1').feature('s1').feature.remove('pDef');
model.sol('sol1').feature('s1').feature('p1').set('control', 'stat');
model.sol('sol1').feature('s1').set('control', 'stat');
model.sol('sol1').feature('s1').feature.create('fc1', 'FullyCoupled');
model.sol('sol1').feature('s1').feature.remove('fcDef');
```

```
model.sol('sol1').attach('std1');

model.name('four_point_balanced_V3.mph');

model.sol('sol1').study('std1');
model.sol('sol1').feature.remove('s1');
model.sol('sol1').feature.remove('v1');
model.sol('sol1').feature.remove('st1');
model.sol('sol1').feature.create('st1', 'StudyStep');
model.sol('sol1').feature('st1').set('study', 'std1');
model.sol('sol1').feature('st1').set('studystep', 'stat');
model.sol('sol1').feature.create('v1', 'Variables');
model.sol('sol1').feature('v1').set('control', 'stat');
model.sol('sol1').feature.create('s1', 'Stationary');
model.sol('sol1').feature('s1').feature.create('p1', 'Parametric');
model.sol('sol1').feature('s1').feature.remove('pDef');
model.sol('sol1').feature('s1').feature('p1').set('control', 'stat');
model.sol('sol1').feature('s1').set('control', 'stat');
model.sol('sol1').feature('s1').feature.create('fc1', 'FullyCoupled');
model.sol('sol1').feature('s1').feature.remove('fcDef');
model.sol('sol1').attach('std1');

model.result.numerical.create('int1', 'IntSurface');
model.result.numerical('int1').selection.set([2]);
model.result.numerical('int1').set('expr', 'solid.RFy');
model.result.numerical('int1').set('descr', 'Reaction force, y
component');
model.result.table.create('tbl1', 'Table');
model.result.table('tbl1').comments('Surface Integration 1
(solid.RFy)');
model.result.numerical('int1').set('table', 'tbl1');
model.result.numerical('int1').setResult;
model.result.create('pg2', 1);
model.result('pg2').set('data', 'none');
model.result('pg2').feature.create('tblp1', 'Table');
model.result('pg2').feature('tblp1').set('table', 'tbl1');
model.result('pg2').run;
model.result('pg1').run;
model.result('pg1').run;

model.geom('geom1').feature.remove('imp1');
model.geom('geom1').feature.create('imp1', 'Import');
model.geom('geom1').feature('imp1').set('filename',
'\\austin.utexas.edu\disk\engrstu\me\ksb2258\Documents\Thesis\COMSOL\fo
ur_point_balanced_V3.IGS');
model.geom('geom1').feature('imp1').set('unit', 'source');
model.geom('geom1').feature('imp1').importData;
model.geom('geom1').run;

model.physics('solid').feature('fix1').selection.set([2]);
model.physics('solid').feature('disp1').selection.set([24]);
```

```
model.physics('solid').feature('roll1').selection.set([9 13 17 21 153
154 155 156]);

model.param.set('D', '-0.016 [m]');

model.mesh('mesh1').run;

model.sol.remove('sol1');
model.sol.create('sol1');
model.sol('sol1').study('std1');
model.sol('sol1').feature.create('st1', 'StudyStep');
model.sol('sol1').feature('st1').set('study', 'std1');
model.sol('sol1').feature('st1').set('studystep', 'stat');
model.sol('sol1').feature.create('v1', 'Variables');
model.sol('sol1').feature('v1').set('control', 'stat');
model.sol('sol1').feature.create('s1', 'Stationary');
model.sol('sol1').feature('s1').feature.create('p1', 'Parametric');
model.sol('sol1').feature('s1').feature.remove('pDef');
model.sol('sol1').feature('s1').feature('p1').set('control', 'stat');
model.sol('sol1').feature('s1').set('control', 'stat');
model.sol('sol1').feature('s1').feature.create('fc1', 'FullyCoupled');
model.sol('sol1').feature('s1').feature.remove('fcDef');
model.sol('sol1').attach('std1');

model.result.create('pg3', 3);
model.result('pg3').set('data', 'dset1');
model.result('pg3').feature.create('surf1', 'Surface');
model.result('pg3').feature('surf1').set('expr', {'solid.mises'});
model.result('pg3').name('Stress (solid)');
model.result('pg3').feature('surf1').feature.create('def', 'Deform');
model.result('pg3').feature('surf1').feature('def').set('scaleactive',
true);
model.result('pg3').feature('surf1').feature('def').set('scale', '1');
model.result('pg3').feature('surf1').feature('def').set('expr', {'u'
'v' 'w'});
model.result('pg3').feature('surf1').feature('def').set('descr',
'Displacement field (Material)');
model.result.numerical.create('int1', 'IntSurface');
model.result.numerical('int1').selection.set([24]);
model.result.table.create('tbl2', 'Table');
model.result.table('tbl2').comments('Surface Integration 1
(solid.disp)');
model.result.numerical('int1').set('table', 'tbl2');
model.result.numerical('int1').setResult;
model.result.create('pg4', 1);
model.result('pg4').set('data', 'none');
model.result('pg4').feature.create('tblp1', 'Table');
model.result('pg4').feature('tblp1').set('table', 'tbl2');
model.result('pg4').run;
model.result('pg2').run;
model.result('pg3').run;
model.result('pg2').run;
```

```
model.result('pg4').run;
model.result('pg4').run;
model.result.remove('pg4');
model.result('pg2').run;
model.result('pg2').run;
model.result('pg3').run;
model.result('pg2').run;
model.result('pg3').run;

model.name('four_point_balanced_V3.mph');

model.result('pg3').run;
model.result('pg2').run;

model.name('four_point_balanced_V3.mph');

model.result('pg2').run;

model.param.set('D', '-0.013 [m]');

model.sol('sol1').updateSolution;

model.result('pg3').run;
model.result('pg2').run;
model.result('pg2').run;
model.result('pg2').run;
model.result('pg2').run;

model.name('four_point_balanced_V3.mph');

model.result('pg2').run;
model.result('pg2').run;
model.result('pg2').run;
model.result('pg3').run;
model.result('pg3').run;
model.result('pg3').set('allowtableupdate', false);
model.result('pg3').set('title', 'ND(96)=0.94875 Surface: von Mises
stress (N/m<sup>2</sup>)');
model.result('pg3').feature('surf1').set('rangeunit', 'N/m^2');
model.result('pg3').feature('surf1').set('rangecolormin',
6.930233436572695);
model.result('pg3').feature('surf1').set('rangecolormax',
1.225720492312875E8);
model.result('pg3').feature('surf1').set('rangecoloractive', 'off');
model.result('pg3').feature('surf1').set('rangedatamin',
6.930233436572695);
model.result('pg3').feature('surf1').set('rangedatamax',
1.225720492312875E8);
model.result('pg3').feature('surf1').set('rangedataactive', 'off');
model.result('pg3').feature('surf1').set('rangeactualminmax',
[6.930233436572695 1.225720492312875E8]);
```

```
model.result('pg3').set('renderdatacached', false);
model.result('pg3').set('allowtableupdate', true);
model.result('pg3').set('renderdatacached', true);
model.result.export.create('img1', 'Image2D');
model.result.export('img1').set('unit', 'px');
model.result.export('img1').set('height', '600');
model.result.export('img1').set('width', '800');
model.result.export('img1').set('lockratio', 'off');
model.result.export('img1').set('resolution', '96');
model.result.export('img1').set('size', 'manual');
model.result.export('img1').set('antialias', 'on');
model.result.export('img1').set('title', 'on');
model.result.export('img1').set('legend', 'on');
model.result.export('img1').set('logo', 'on');
model.result.export('img1').set('options', 'off');
model.result.export('img1').set('fontsize', '9');
model.result.export('img1').set('customcolor', [1 1 1]);
model.result.export('img1').set('background', 'color');
model.result.export('img1').set('qualitylevel', '92');
model.result.export('img1').set('qualityactive', 'off');
model.result.export('img1').set('imagetype', 'png');
model.result.export('img1').set('axes', 'on');
model.result.export.remove('img1');
model.result('pg2').run;
model.result('pg3').run;
model.result('pg3').run;
model.result('pg3').run;
model.result('pg3').run;
model.result('pg3').set('allowtableupdate', false);
model.result('pg3').set('title', 'ND(96)=0.94875 Surface: von Mises
stress (N/m<sup>2</sup>)');
model.result('pg3').feature('surf1').set('rangeunit', 'N/m^2');
model.result('pg3').feature('surf1').set('rangecolormin',
6.930233436572695);
model.result('pg3').feature('surf1').set('rangecolormax',
1.225720492312875E8);
model.result('pg3').feature('surf1').set('rangecoloractive', 'off');
model.result('pg3').feature('surf1').set('rangedatamin',
6.930233436572695);
model.result('pg3').feature('surf1').set('rangedatamax',
1.225720492312875E8);
model.result('pg3').feature('surf1').set('rangedataactive', 'off');
model.result('pg3').feature('surf1').set('rangeactualminmax',
[6.930233436572695 1.225720492312875E8]);
model.result('pg3').set('renderdatacached', false);
model.result('pg3').set('allowtableupdate', true);
model.result('pg3').set('renderdatacached', true);
model.result('pg3').run;
model.result.export.create('img1', 'Image2D');
model.result.export('img1').set('unit', 'px');
model.result.export('img1').set('height', '600');
model.result.export('img1').set('width', '800');
model.result.export('img1').set('lockratio', 'off');
```

```
model.result.export('img1').set('resolution', '96');
model.result.export('img1').set('size', 'manual');
model.result.export('img1').set('antialias', 'on');
model.result.export('img1').set('title', 'on');
model.result.export('img1').set('legend', 'on');
model.result.export('img1').set('logo', 'on');
model.result.export('img1').set('options', 'off');
model.result.export('img1').set('fontsize', '9');
model.result.export('img1').set('customcolor', [1 1 1]);
model.result.export('img1').set('background', 'color');
model.result.export('img1').set('qualitylevel', '92');
model.result.export('img1').set('qualityactive', 'off');
model.result.export('img1').set('imagetype', 'png');
model.result.export('img1').set('axes', 'on');
model.result.export.remove('img1');
model.result('pg3').run;
model.result('pg3').run;
model.result('pg3').run;
model.result('pg2').run;
model.result('pg3').run;
model.result('pg3').run;
model.result('pg3').run;
model.result('pg3').run;
model.result('pg3').set('edgecolor', 'yellow');
model.result('pg3').set('allowtableupdate', false);
model.result('pg3').set('title', 'ND(96)=0.94875 Surface: von Mises
stress (N/m<sup>2</sup>)');
model.result('pg3').feature('surf1').set('rangeunit', 'N/m^2');
model.result('pg3').feature('surf1').set('rangecolormin',
6.930233436572695);
model.result('pg3').feature('surf1').set('rangecolormax',
1.225720492312875E8);
model.result('pg3').feature('surf1').set('rangecoloractive', 'off');
model.result('pg3').feature('surf1').set('rangedatamin',
6.930233436572695);
model.result('pg3').feature('surf1').set('rangedatamax',
1.225720492312875E8);
model.result('pg3').feature('surf1').set('rangedataactive', 'off');
model.result('pg3').feature('surf1').set('rangeactualminmax',
[6.930233436572695 1.225720492312875E8]);
model.result('pg3').set('renderdatacached', false);
model.result('pg3').set('allowtableupdate', true);
model.result('pg3').set('renderdatacached', true);
model.result.table.create('evl3', 'Table');
model.result.table('evl3').comments('Interactive 3D values');
model.result.table('evl3').name('Evaluation 3D');
model.result.table('evl3').addRow([22.99894427431682 -8.915856664213026
38.794939558605634 2778661.3566767545]);
model.result('pg3').set('edgecolor', 'black');
model.result('pg3').set('legendpos', 'right');
model.result('pg3').set('solnum', '96');
model.result('pg3').run;
model.result('pg3').feature('surf1').set('colortable', 'Rainbow');
```

```
model.result('pg3').feature('surf1').set('rangecoloractive', 'on');
model.result('pg3').feature('surf1').set('rangecolormax', '40000000');
model.result('pg3').set('allowtableupdate', false);
model.result('pg3').set('title', 'ND(96)=0.94875 Surface: von Mises
stress (N/m<sup>2</sup>)');
model.result('pg3').feature('surf1').set('rangeunit', 'N/m^2');
model.result('pg3').feature('surf1').set('rangedatamin',
6.930233436572695);
model.result('pg3').feature('surf1').set('rangedatamax',
1.225720492312875E8);
model.result('pg3').feature('surf1').set('rangedataactive', 'off');
model.result('pg3').feature('surf1').set('rangeactualminmax',
[6.930233436572695 1.225720492312875E8]);
model.result('pg3').set('renderdatacached', false);
model.result('pg3').set('allowtableupdate', true);
model.result('pg3').set('renderdatacached', true);
model.result('pg3').feature('surf1').set('wireframe', 'off');
model.result('pg3').feature('surf1').set('colortablesym', 'off');
model.result('pg3').feature('surf1').set('colortablerev', 'off');
model.result('pg3').feature('surf1').set('inheritheightscale', 'on');
model.result('pg3').feature('surf1').set('inheritdeformscale', 'on');
model.result('pg3').feature('surf1').set('inheritrange', 'on');
model.result('pg3').feature('surf1').set('inheritcolor', 'on');
model.result('pg3').run;
model.result('pg3').run;
model.result('pg3').set('legendpos', 'bottom');
model.result('pg3').set('frametype', 'material');
model.result('pg3').set('edgecolor', 'white');
model.result('pg3').set('allowtableupdate', false);
model.result('pg3').set('title', 'ND(96)=0.94875 Surface: von Mises
stress (N/m<sup>2</sup>)');
model.result('pg3').feature('surf1').set('rangeunit', 'N/m^2');
model.result('pg3').feature('surf1').set('rangedatamin',
6.930233436572695);
model.result('pg3').feature('surf1').set('rangedatamax',
1.225720492312875E8);
model.result('pg3').feature('surf1').set('rangedataactive', 'off');
model.result('pg3').feature('surf1').set('rangeactualminmax',
[6.930233436572695 1.225720492312875E8]);
model.result('pg3').set('renderdatacached', false);
model.result('pg3').set('allowtableupdate', true);
model.result('pg3').set('renderdatacached', true);
model.result('pg3').set('edgecolor', 'black');
model.result.export.create('img1', 'Image2D');
model.result.export('img1').set('unit', 'px');
model.result.export('img1').set('height', '600');
model.result.export('img1').set('width', '800');
model.result.export('img1').set('lockratio', 'off');
model.result.export('img1').set('resolution', '96');
model.result.export('img1').set('size', 'manual');
model.result.export('img1').set('antialias', 'on');
model.result.export('img1').set('title', 'on');
model.result.export('img1').set('legend', 'on');
```

```
model.result.export('img1').set('logo', 'on');
model.result.export('img1').set('options', 'off');
model.result.export('img1').set('fontsize', '9');
model.result.export('img1').set('customcolor', [1 1 1]);
model.result.export('img1').set('background', 'color');
model.result.export('img1').set('qualitylevel', '92');
model.result.export('img1').set('qualityactive', 'off');
model.result.export('img1').set('imagetype', 'png');
model.result.export('img1').set('axes', 'on');
model.result.export('img1').set('pngfilename',
'Z:\Documents\Thesis\COMSOL\four_point_balanced_V3_redo.png');
model.result.export('img1').run;
model.result.export('img1').set('options', 'off');
model.result('pg3').run;
model.result('pg3').run;
model.result('pg3').set('legendpos', 'left');

model.name('four_point_balanced_V3.mph');

model.result('pg3').run;
model.result.report.create('rpt1', 'Report');
model.result.report('rpt1').set('level', 'complete');
model.result.report('rpt1').feature.create('tp1', 'TitlePage');
model.result.report('rpt1').feature.create('toc1', 'TableOfContents');
model.result.report('rpt1').feature.create('sec1', 'Section');
model.result.report('rpt1').feature('sec1').set('source', 'custom');
model.result.report('rpt1').feature('sec1').set('heading', 'Global
Definitions');
model.result.report('rpt1').feature('sec1').feature.create('sec1',
'Section');
model.result.report('rpt1').feature('sec1').feature('sec1').set('source
', 'firstchild');
model.result.report('rpt1').feature('sec1').feature('sec1').set('headin
g', 'Parameters');
model.result.report('rpt1').feature('sec1').feature('sec1').feature.cre
ate('param1', 'Parameter');
model.result.report('rpt1').feature.create('sec2', 'Section');
model.result.report('rpt1').feature('sec2').set('source', 'custom');
model.result.report('rpt1').feature('sec2').set('heading', 'Model 1
(mod1)');
model.result.report('rpt1').feature('sec2').feature.create('sec1',
'Section');
model.result.report('rpt1').feature('sec2').feature('sec1').set('source
', 'custom');
model.result.report('rpt1').feature('sec2').feature('sec1').set('headin
g', 'Definitions');
model.result.report('rpt1').feature('sec2').feature('sec1').feature.cre
ate('sec1', 'Section');
model.result.report('rpt1').feature('sec2').feature('sec1').feature('se
c1').set('source', 'custom');
model.result.report('rpt1').feature('sec2').feature('sec1').feature('se
c1').set('heading', 'Coordinate Systems');
```

```
model.result.report('rpt1').feature('sec2').feature('sec1').feature('se
c1').feature.create('sec1', 'Section');
model.result.report('rpt1').feature('sec2').feature('sec1').feature('se
c1').feature('sec1').set('source', 'firstchild');
model.result.report('rpt1').feature('sec2').feature('sec1').feature('se
c1').feature('sec1').set('heading', 'Boundary System 1');
model.result.report('rpt1').feature('sec2').feature('sec1').feature('se
c1').feature('sec1').feature.create('csys1', 'CoordinateSystem');
model.result.report('rpt1').feature('sec2').feature('sec1').feature('se
c1').feature('sec1').feature('csys1').set('noderef', 'sys1');
model.result.report('rpt1').feature('sec2').feature.create('sec2',
'Section');
model.result.report('rpt1').feature('sec2').feature('sec2').set('source
', 'firstchild');
model.result.report('rpt1').feature('sec2').feature('sec2').set('headin
g', 'Geometry 1');
model.result.report('rpt1').feature('sec2').feature('sec2').feature.cre
ate('geom1', 'Geometry');
model.result.report('rpt1').feature('sec2').feature('sec2').feature('ge
om1').set('noderef', 'geom1');
model.result.report('rpt1').feature('sec2').feature.create('sec3',
'Section');
model.result.report('rpt1').feature('sec2').feature('sec3').set('source
', 'custom');
model.result.report('rpt1').feature('sec2').feature('sec3').set('headin
g', 'Materials');
model.result.report('rpt1').feature('sec2').feature('sec3').feature.cre
ate('sec1', 'Section');
model.result.report('rpt1').feature('sec2').feature('sec3').feature('se
c1').set('source', 'firstchild');
model.result.report('rpt1').feature('sec2').feature('sec3').feature('se
c1').set('heading', 'Material 1');
model.result.report('rpt1').feature('sec2').feature('sec3').feature('se
c1').feature.create('mat1', 'Material');
model.result.report('rpt1').feature('sec2').feature('sec3').feature('se
c1').feature('mat1').set('noderef', 'mat1');
model.result.report('rpt1').feature('sec2').feature.create('sec4',
'Section');
model.result.report('rpt1').feature('sec2').feature('sec4').set('source
', 'custom');
model.result.report('rpt1').feature('sec2').feature('sec4').set('headin
g', 'Solid Mechanics (solid)');
model.result.report('rpt1').feature('sec2').feature('sec4').feature.cre
ate('phys1', 'Physics');
model.result.report('rpt1').feature('sec2').feature('sec4').feature('ph
ys1').set('noderef', 'solid');
model.result.report('rpt1').feature('sec2').feature.create('sec5',
'Section');
model.result.report('rpt1').feature('sec2').feature('sec5').set('source
', 'firstchild');
model.result.report('rpt1').feature('sec2').feature('sec5').set('headin
g', 'Mesh 1');
```

```
model.result.report('rpt1').feature('sec2').feature('sec5').feature.cre
ate('mesh1', 'Mesh');
model.result.report('rpt1').feature('sec2').feature('sec5').feature('me
sh1').set('noderef', 'mesh1');
model.result.report('rpt1').feature.create('sec3', 'Section');
model.result.report('rpt1').feature('sec3').set('source', 'custom');
model.result.report('rpt1').feature('sec3').set('heading', 'Study 1');
model.result.report('rpt1').feature('sec3').feature.create('std1',
'Study');
model.result.report('rpt1').feature('sec3').feature('std1').set('nodere
f', 'std1');
model.result.report('rpt1').feature('sec3').feature.create('sec1',
'Section');
model.result.report('rpt1').feature('sec3').feature('sec1').set('source
', 'custom');
model.result.report('rpt1').feature('sec3').feature('sec1').set('headin
g', 'Solver Configurations');
model.result.report('rpt1').feature('sec3').feature('sec1').feature.cre
ate('sec1', 'Section');
model.result.report('rpt1').feature('sec3').feature('sec1').feature('se
c1').set('source', 'firstchild');
model.result.report('rpt1').feature('sec3').feature('sec1').feature('se
c1').set('heading', 'Solver 1');
model.result.report('rpt1').feature('sec3').feature('sec1').feature('se
c1').feature.create('sol1', 'Solver');
model.result.report('rpt1').feature('sec3').feature('sec1').feature('se
c1').feature('sol1').set('noderef', 'sol1');
model.result.report('rpt1').feature.create('sec4', 'Section');
model.result.report('rpt1').feature('sec4').set('source', 'custom');
model.result.report('rpt1').feature('sec4').set('heading', 'Results');
model.result.report('rpt1').feature('sec4').feature.create('sec1',
'Section');
model.result.report('rpt1').feature('sec4').feature('sec1').set('source
', 'custom');
model.result.report('rpt1').feature('sec4').feature('sec1').set('headin
g', 'Data Sets');
model.result.report('rpt1').feature('sec4').feature('sec1').feature.cre
ate('sec1', 'Section');
model.result.report('rpt1').feature('sec4').feature('sec1').feature('se
c1').set('source', 'firstchild');
model.result.report('rpt1').feature('sec4').feature('sec1').feature('se
c1').set('heading', 'Solution 1');
model.result.report('rpt1').feature('sec4').feature('sec1').feature('se
c1').feature.create('dset1', 'DataSet');
model.result.report('rpt1').feature('sec4').feature('sec1').feature('se
c1').feature('dset1').set('noderef', 'dset1');
model.result.report('rpt1').feature('sec4').feature.create('sec2',
'Section');
model.result.report('rpt1').feature('sec4').feature('sec2').set('source
', 'custom');
model.result.report('rpt1').feature('sec4').feature('sec2').set('headin
g', 'Derived Values');
```

```
model.result.report('rpt1').feature('sec4').feature('sec2').feature.cre
ate('sec1', 'Section');
model.result.report('rpt1').feature('sec4').feature('sec2').feature('se
c1').set('source', 'firstchild');
model.result.report('rpt1').feature('sec4').feature('sec2').feature('se
c1').set('heading', 'Surface Integration 1');
model.result.report('rpt1').feature('sec4').feature('sec2').feature('se
c1').feature.create('num1', 'DerivedValues');
model.result.report('rpt1').feature('sec4').feature('sec2').feature('se
c1').feature('num1').set('noderef', 'int1');
model.result.report('rpt1').feature('sec4').feature.create('sec3',
'Section');
model.result.report('rpt1').feature('sec4').feature('sec3').set('source
', 'custom');
model.result.report('rpt1').feature('sec4').feature('sec3').set('headin
g', 'Tables');
model.result.report('rpt1').feature('sec4').feature('sec3').feature.cre
ate('sec1', 'Section');
model.result.report('rpt1').feature('sec4').feature('sec3').feature('se
c1').set('source', 'firstchild');
model.result.report('rpt1').feature('sec4').feature('sec3').feature('se
c1').set('heading', 'Table 1');
model.result.report('rpt1').feature('sec4').feature('sec3').feature('se
c1').feature.create('mtbl1', 'Table');
model.result.report('rpt1').feature('sec4').feature('sec3').feature('se
c1').feature('mtbl1').set('noderef', 'tbl1');
model.result.report('rpt1').feature('sec4').feature('sec3').feature.cre
ate('sec2', 'Section');
model.result.report('rpt1').feature('sec4').feature('sec3').feature('se
c2').set('source', 'firstchild');
model.result.report('rpt1').feature('sec4').feature('sec3').feature('se
c2').set('heading', 'Table 2');
model.result.report('rpt1').feature('sec4').feature('sec3').feature('se
c2').feature.create('mtbl1', 'Table');
model.result.report('rpt1').feature('sec4').feature('sec3').feature('se
c2').feature('mtbl1').set('noderef', 'tbl2');
model.result.report('rpt1').feature('sec4').feature('sec3').feature.cre
ate('sec3', 'Section');
model.result.report('rpt1').feature('sec4').feature('sec3').feature('se
c3').set('source', 'firstchild');
model.result.report('rpt1').feature('sec4').feature('sec3').feature('se
c3').set('heading', 'Evaluation 3D');
model.result.report('rpt1').feature('sec4').feature('sec3').feature('se
c3').feature.create('mtbl1', 'Table');
model.result.report('rpt1').feature('sec4').feature('sec3').feature('se
c3').feature('mtbl1').set('noderef', 'evl3');
model.result.report('rpt1').feature('sec4').feature.create('sec4',
'Section');
model.result.report('rpt1').feature('sec4').feature('sec4').set('source
', 'custom');
model.result.report('rpt1').feature('sec4').feature('sec4').set('headin
g', 'Plot Groups');
```

```
model.result.report('rpt1').feature('sec4').feature('sec4').feature.cre
ate('sec1', 'Section');
model.result.report('rpt1').feature('sec4').feature('sec4').feature('se
c1').set('source', 'firstchild');
model.result.report('rpt1').feature('sec4').feature('sec4').feature('se
c1').set('heading', '1D Plot Group 2');
model.result.report('rpt1').feature('sec4').feature('sec4').feature('se
c1').feature.create('pg1', 'PlotGroup');
model.result.report('rpt1').feature('sec4').feature('sec4').feature('se
c1').feature('pg1').set('noderef', 'pg2');
model.result.report('rpt1').feature('sec4').feature('sec4').feature.cre
ate('sec2', 'Section');
model.result.report('rpt1').feature('sec4').feature('sec4').feature('se
c2').set('source', 'firstchild');
model.result.report('rpt1').feature('sec4').feature('sec4').feature('se
c2').set('heading', 'Stress (solid)');
model.result.report('rpt1').feature('sec4').feature('sec4').feature('se
c2').feature.create('pg1', 'PlotGroup');
model.result.report('rpt1').feature('sec4').feature('sec4').feature('se
c2').feature('pg1').set('noderef', 'pg3');
model.result.report('rpt1').set('htmlprint', 'on');
model.result.report('rpt1').set('format', 'docx');
model.result.report('rpt1').set('docxfilename',
'Z:\Documents\Thesis\COMSOL\four_point_balanced_V3');
model.result.dataset('dset1').run;

model.view.remove('view2');

model.result('pg2').run;
model.result('pg3').run;
model.result.report('rpt1').run;
model.result.report('rpt1').set('disableimages', 'on');
model.result.report('rpt1').set('level', 'brief');
model.result.report('rpt1').set('docxfilename',
'Z:\Documents\Thesis\COMSOL\four_point_balanced_V3');
model.result.report('rpt1').run;
model.result.report('rpt1').set('docxfilename',
'Z:\Documents\Thesis\COMSOL\four_point_balanced_V3');
model.result.dataset('dset1').run;

model.view.remove('view2');

model.result('pg2').run;
model.result('pg3').run;
model.result.report('rpt1').run;
model.result.report.create('rpt2', 'Report');
model.result.report('rpt2').set('level', 'brief');
model.result.report('rpt2').feature.create('tp1', 'TitlePage');
model.result.report('rpt2').feature.create('toc1', 'TableOfContents');
model.result.report('rpt2').feature.create('sec1', 'Section');
model.result.report('rpt2').feature('sec1').set('source', 'custom');
```

```
model.result.report('rpt2').feature('sec1').set('heading', 'Global
Definitions');
model.result.report('rpt2').feature('sec1').feature.create('sec1',
'Section');
model.result.report('rpt2').feature('sec1').feature('sec1').set('source
', 'firstchild');
model.result.report('rpt2').feature('sec1').feature('sec1').set('headin
g', 'Parameters');
model.result.report('rpt2').feature('sec1').feature('sec1').feature.cre
ate('param1', 'Parameter');
model.result.report('rpt2').feature.create('sec2', 'Section');
model.result.report('rpt2').feature('sec2').set('source', 'custom');
model.result.report('rpt2').feature('sec2').set('heading', 'Model 1
(mod1)');
model.result.report('rpt2').feature('sec2').feature.create('sec1',
'Section');
model.result.report('rpt2').feature('sec2').feature('sec1').set('source
', 'custom');
model.result.report('rpt2').feature('sec2').feature('sec1').set('headin
g', 'Definitions');
model.result.report('rpt2').feature('sec2').feature('sec1').feature.cre
ate('sec1', 'Section');
model.result.report('rpt2').feature('sec2').feature('sec1').feature('se
c1').set('source', 'custom');
model.result.report('rpt2').feature('sec2').feature('sec1').feature('se
c1').set('heading', 'Coordinate Systems');
model.result.report('rpt2').feature('sec2').feature('sec1').feature('se
c1').feature.create('sec1', 'Section');
model.result.report('rpt2').feature('sec2').feature('sec1').feature('se
c1').feature('sec1').set('source', 'firstchild');
model.result.report('rpt2').feature('sec2').feature('sec1').feature('se
c1').feature('sec1').set('heading', 'Boundary System 1');
model.result.report('rpt2').feature('sec2').feature('sec1').feature('se
c1').feature('sec1').feature.create('csys1', 'CoordinateSystem');
model.result.report('rpt2').feature('sec2').feature('sec1').feature('se
c1').feature('sec1').feature('csys1').set('noderef', 'sys1');
model.result.report('rpt2').feature('sec2').feature.create('sec2',
'Section');
model.result.report('rpt2').feature('sec2').feature('sec2').set('source
', 'firstchild');
model.result.report('rpt2').feature('sec2').feature('sec2').set('headin
g', 'Geometry 1');
model.result.report('rpt2').feature('sec2').feature('sec2').feature.cre
ate('geom1', 'Geometry');
model.result.report('rpt2').feature('sec2').feature('sec2').feature('ge
om1').set('noderef', 'geom1');
model.result.report('rpt2').feature('sec2').feature.create('sec3',
'Section');
model.result.report('rpt2').feature('sec2').feature('sec3').set('source
', 'custom');
model.result.report('rpt2').feature('sec2').feature('sec3').set('headin
g', 'Materials');
```

```
model.result.report('rpt2').feature('sec2').feature('sec3').feature.cre
ate('sec1', 'Section');
model.result.report('rpt2').feature('sec2').feature('sec3').feature('se
c1').set('source', 'firstchild');
model.result.report('rpt2').feature('sec2').feature('sec3').feature('se
c1').set('heading', 'Material 1');
model.result.report('rpt2').feature('sec2').feature('sec3').feature('se
c1').feature.create('mat1', 'Material');
model.result.report('rpt2').feature('sec2').feature('sec3').feature('se
c1').feature('mat1').set('noderef', 'mat1');
model.result.report('rpt2').feature('sec2').feature.create('sec4',
'Section');
model.result.report('rpt2').feature('sec2').feature('sec4').set('source
', 'custom');
model.result.report('rpt2').feature('sec2').feature('sec4').set('headin
g', 'Solid Mechanics (solid)');
model.result.report('rpt2').feature('sec2').feature('sec4').feature.cre
ate('phys1', 'Physics');
model.result.report('rpt2').feature('sec2').feature('sec4').feature('ph
ys1').set('noderef', 'solid');
model.result.report('rpt2').feature('sec2').feature.create('sec5',
'Section');
model.result.report('rpt2').feature('sec2').feature('sec5').set('source
', 'firstchild');
model.result.report('rpt2').feature('sec2').feature('sec5').set('headin
g', 'Mesh 1');
model.result.report('rpt2').feature('sec2').feature('sec5').feature.cre
ate('mesh1', 'Mesh');
model.result.report('rpt2').feature('sec2').feature('sec5').feature('me
sh1').set('noderef', 'mesh1');
model.result.report('rpt2').feature.create('sec3', 'Section');
model.result.report('rpt2').feature('sec3').set('source', 'custom');
model.result.report('rpt2').feature('sec3').set('heading', 'Study 1');
model.result.report('rpt2').feature('sec3').feature.create('std1',
'Study');
model.result.report('rpt2').feature('sec3').feature('std1').set('nodere
f', 'std1');
model.result.report('rpt2').feature.create('sec4', 'Section');
model.result.report('rpt2').feature('sec4').set('source', 'custom');
model.result.report('rpt2').feature('sec4').set('heading', 'Results');
model.result.report('rpt2').feature('sec4').feature.create('sec1',
'Section');
model.result.report('rpt2').feature('sec4').feature('sec1').set('source
', 'custom');
model.result.report('rpt2').feature('sec4').feature('sec1').set('headin
g', 'Data Sets');
model.result.report('rpt2').feature('sec4').feature('sec1').feature.cre
ate('sec1', 'Section');
model.result.report('rpt2').feature('sec4').feature('sec1').feature('se
c1').set('source', 'firstchild');
model.result.report('rpt2').feature('sec4').feature('sec1').feature('se
c1').set('heading', 'Solution 1');
```

```
model.result.report('rpt2').feature('sec4').feature('sec1').feature('se
c1').feature.create('dset1', 'DataSet');
model.result.report('rpt2').feature('sec4').feature('sec1').feature('se
c1').feature('dset1').set('noderef', 'dset1');
model.result.report('rpt2').feature('sec4').feature.create('sec2',
'Section');
model.result.report('rpt2').feature('sec4').feature('sec2').set('source
', 'custom');
model.result.report('rpt2').feature('sec4').feature('sec2').set('headin
g', 'Derived Values');
model.result.report('rpt2').feature('sec4').feature('sec2').feature.cre
ate('sec1', 'Section');
model.result.report('rpt2').feature('sec4').feature('sec2').feature('se
c1').set('source', 'firstchild');
model.result.report('rpt2').feature('sec4').feature('sec2').feature('se
c1').set('heading', 'Surface Integration 1');
model.result.report('rpt2').feature('sec4').feature('sec2').feature('se
c1').feature.create('num1', 'DerivedValues');
model.result.report('rpt2').feature('sec4').feature('sec2').feature('se
c1').feature('num1').set('noderef', 'int1');
model.result.report('rpt2').feature('sec4').feature.create('sec3',
'Section');
model.result.report('rpt2').feature('sec4').feature('sec3').set('source
', 'custom');
model.result.report('rpt2').feature('sec4').feature('sec3').set('headin
g', 'Tables');
model.result.report('rpt2').feature('sec4').feature('sec3').feature.cre
ate('sec1', 'Section');
model.result.report('rpt2').feature('sec4').feature('sec3').feature('se
c1').set('source', 'firstchild');
model.result.report('rpt2').feature('sec4').feature('sec3').feature('se
c1').set('heading', 'Table 1');
model.result.report('rpt2').feature('sec4').feature('sec3').feature('se
c1').feature.create('mtbl1', 'Table');
model.result.report('rpt2').feature('sec4').feature('sec3').feature('se
c1').feature('mtbl1').set('noderef', 'tbl1');
model.result.report('rpt2').feature('sec4').feature('sec3').feature.cre
ate('sec2', 'Section');
model.result.report('rpt2').feature('sec4').feature('sec3').feature('se
c2').set('source', 'firstchild');
model.result.report('rpt2').feature('sec4').feature('sec3').feature('se
c2').set('heading', 'Table 2');
model.result.report('rpt2').feature('sec4').feature('sec3').feature('se
c2').feature.create('mtbl1', 'Table');
model.result.report('rpt2').feature('sec4').feature('sec3').feature('se
c2').feature('mtbl1').set('noderef', 'tbl2');
model.result.report('rpt2').feature('sec4').feature('sec3').feature.cre
ate('sec3', 'Section');
model.result.report('rpt2').feature('sec4').feature('sec3').feature('se
c3').set('source', 'firstchild');
model.result.report('rpt2').feature('sec4').feature('sec3').feature('se
c3').set('heading', 'Evaluation 3D');
```

```
model.result.report('rpt2').feature('sec4').feature('sec3').feature('se
c3').feature.create('mtbl1', 'Table');
model.result.report('rpt2').feature('sec4').feature('sec3').feature('se
c3').feature('mtbl1').set('noderef', 'evl3');
model.result.report('rpt2').feature('sec4').feature.create('sec4',
'Section');
model.result.report('rpt2').feature('sec4').feature('sec4').set('source
', 'custom');
model.result.report('rpt2').feature('sec4').feature('sec4').set('headin
g', 'Plot Groups');
model.result.report('rpt2').feature('sec4').feature('sec4').feature.cre
ate('sec1', 'Section');
model.result.report('rpt2').feature('sec4').feature('sec4').feature('se
c1').set('source', 'firstchild');
model.result.report('rpt2').feature('sec4').feature('sec4').feature('se
c1').set('heading', '1D Plot Group 2');
model.result.report('rpt2').feature('sec4').feature('sec4').feature('se
c1').feature.create('pg1', 'PlotGroup');
model.result.report('rpt2').feature('sec4').feature('sec4').feature('se
c1').feature('pg1').set('noderef', 'pg2');
model.result.report('rpt2').feature('sec4').feature('sec4').feature.cre
ate('sec2', 'Section');
model.result.report('rpt2').feature('sec4').feature('sec4').feature('se
c2').set('source', 'firstchild');
model.result.report('rpt2').feature('sec4').feature('sec4').feature('se
c2').set('heading', 'Stress (solid)');
model.result.report('rpt2').feature('sec4').feature('sec4').feature('se
c2').feature.create('pg1', 'PlotGroup');
model.result.report('rpt2').feature('sec4').feature('sec4').feature('se
c2').feature('pg1').set('noderef', 'pg3');
model.result.report('rpt2').set('disableimages', 'on');
model.result.report('rpt2').set('docxfilename',
'Z:\Documents\Thesis\COMSOL\four_point_balanced_V32');
model.result.dataset('dset1').run;

model.view.remove('view2');

model.result('pg2').run;
model.result('pg3').run;
model.result.report('rpt2').run;
model.result.report('rpt2').set('docxfilename',
'Z:\Documents\Thesis\COMSOL\four_point_balanced_V32');
model.result.dataset('dset1').run;

model.view.remove('view2');

model.result('pg2').run;
model.result('pg3').run;
model.result.report('rpt2').run;
model.result.export.create('data1', 'Data');
model.result.export('data1').set('filename', 'balanced_export');
model.result.export('data1').run;
```

```
model.result.export('data1').set('transpose', 'off');
model.result.report('rpt2').set('level', 'intermediate');
model.result.report('rpt2').set('docxfilename',
'Z:\Documents\Thesis\COMSOL\four_point_balanced_V32');
model.result.report('rpt2').run;
model.result.report('rpt2').set('level', 'complete');
model.result.report('rpt2').set('docxfilename',
'Z:\Documents\Thesis\COMSOL\four_point_balanced_V32');
model.result.report('rpt2').run;
model.result.report('rpt2').set('docxfilename',
'Z:\Documents\Thesis\COMSOL\four_point_balanced_V32');
model.result.report('rpt2').run;
model.result.report('rpt2').set('docxfilename',
'Z:\Documents\Thesis\COMSOL\four_point_balanced_V32');
model.result.report('rpt2').run;

out = model;
```

Bibliography

1. Fulcher, B.A., *Evaluation of systems containing negative stiffness elements for vibration and shock isolation*, in *Mechanical Engineering*. 2012, M.S. Thesis, The University of Texas at Austin: Austin, TX.
2. Fulcher, B.A., Shahan, D.W., Haberman, M.R.*, et al.*, *Analytical and experimental investigation of buckled beams as negative stiffness elements for passive vibration and shock isolation systems.* Journal of Vibration and Acoustics, 2014. **136**: p. 031009.
3. Correa, D.M., Klatt, T.D., Cortes, S.A.*, et al.*, *Negative stiffness honeycombs for recoverable shock isolation.* Solid Freeform Fabrication Symposium, 2014: p. 702–713.
4. Qiu, J., Lang, J.H. and Slocum, A.H., *A centrally-clamped parallel-beam bistable mems mechanism*. in *Micro Electro Mechanical Systems*. 2001: Interlaken, Switzerland: IEEE: p. 353–356.
5. Seepersad, C., Janet, A., McDowell, D. and Mistree, F., *Robust design of cellular materials with topological and dimensional imperfections.* Journal of Mechanical Design, 2006. **128**: p. 1285–1297.
6. Yamashita, M. and Gotoh, M., *Impact behavior of honeycomb structures with various cell specifications—numerical simulation and experiment.* International Journal of Impact Engineering, 2005. **32**: p. 618–630.
7. Gibson, L.J. and Ashby, M.F., *Cellular Solids: Structure and Properties*. 1999, Cambridge University Press: Cambridge, UK.
8. Hayes, A., Wang, A., Dempsey, B.M.*, et al.*, *Mechanics of linear cellular alloys.* Mechanics of Materials, 2004. **36**: p. 691–713.
9. Hou, B., Ono, A., Abdennadher, S.*, et al.*, *Impact behavior of honeycombs under combined shear-compression. Part i: Experiments.* International Journal of Solids and Structures, 2011. **48**: p. 687–697.
10. Timoshenko, S.P. and Gere, J.M., *Theory of Elastic Stability*. 1989, New York, NY: Dover Publications.
11. Alabuzhev, P., *Vibration Protecting and Measuring Systems with Quasi-zero Stiffness*. 1989, USA: Hemishpere Publishing Corporation.
12. Qiu, J., Lang, J.H. and Slocum, A.H., *A curved-beam bistable mechanism.* Journal of Microelectomechanical Systems, 2004. **13**: p. 137–146.
13. Lee, J., Lee, M., Jang, W.*, et al.*, *Bi-stable planar polysilicon microactuators with shallow arch-shaped leaf springs*. in *Proc. SPIE Conference on Micromachined Devices and Components*. 1999: p. 274–279.
14. Dellmann, L., Noell, W., Marxer, C.*, et al.*, *4x4 matrix switch based on mems switches and integrated waveguides.* Proc. Solid-State Sensors Actuators, 2001. **2**: p. 1332–1335.
15. Correa, D.M., Klatt, T., Cortes, S.*, et al.*, *Negative stiffness honeycombs for recoverable shock isolation.* Rapid Prototyping Journal, 2014. **21**: p. 193–200.

16. Budynas, R.G. and Nisbett, J.K., *Mechanical Engineering Design*. 8th ed. 2008, New York, NY: McGraw-Hill.
17. *Euler-bernoulli beam theory*. 2014 [cited 2015 1/22/2015]; Available from: http://en.wikipedia.org/wiki/Euler%E2%80%93Bernoulli_beam_theory.
18. Bodner, S.R., *Unified plasticity for engineering application*. Mathematical concepts and methods in science and engineering, ed. Miele, A. 2002, New York, NY: Kluwer Academic/ Plenum.
19. Symonds, P.S. and Jones, N., *Impulsive loading of fully clamped beams with finite plastic deflections and strain-rate sensitivity.* International Journal of Mechanical Science, 1972. **144**: p. 49–46.
20. Naida, A.A., *Evaluating large plastic strains in shock-loaded beams.* Prikladnaya Mekhanika, 1986. **22**: p. 66–71.
21. Barlat, F., Glazov, M.V., Brem, J.C.*, et al.*, *A simple model for dislocation behavior, strain and strain rate hardening evolution in deforming aluminum alloys.* International Journal of Plasticity, 2002. **18**: p. 919–939.
22. Estrin, Y. and Kubin, L.P., *Local strain hardenting and nonuniformity of plastic deformation.* Acta Metal, 1986. **34**: p. 2455–2464.
23. Baker, W.E., Togami, T.C. and Weydert, J.C., *Static and dynamic propeties of high-density metal honeycombs.* International Journal of Impact Engineering, 1998. **21**: p. 149–163.
24. Zhao, H. and Gary, G., *Crushing behaviour of aluminum honeycombs under impact loading.* International Journal of Impact Engineering, 1998. **21**: p. 827–836.

Vita

Ken Bostwick was born and raised in San Diego, CA. He received his Bachelor's Degree from Brigham Young University in Provo, UT in 2013. In 2013 he was admitted to the Acoustics program at The University of Texas at Austin to receive a Master's Degree. While a student at UT Austin he enlisted in the United States Navy and upon completion of his Master's Degree he received his commission as an officer in the United States Navy.

Permanent email: kenbostwick@gmail.com

This thesis was typed by Kenneth Bostwick.